A Study of the Effects of Discharge Characteristics on Ignition Performance in a Spark Ignition Engine

火花点火機関の着火特性に放電特性が及ぼす影響に関する研究

August 2022

CHEN QINGCHU

Graduate School of

Science and Engineering

CHIBA UNIVERSITY

（千葉大学審査学位論文）

A Study of the Effects of Discharge Characteristics on Ignition Performance in a Spark Ignition Engine

火花点火機関の着火特性に放電特性が及ぼす影響に関する研究

August 2022

CHEN QINGCHU

Graduate School of

Science and Engineering

CHIBA UNIVERSITY

TABLE OF CONTENTS

ABSTRACT

In recent years, due to global environmental concerns and a shortage of energy resources, internal combustion engines must adopt novel combustion that achieves high thermal efficiency and low exhaust gas emissions. As spark-ignition engines are fueled with gasoline continue to be the primary power system for light-duty vehicles. There is a continued need to improve the thermal efficiency and decrease the SI engine's exhaust emissions. In order to meet these demands, advanced combustion technologies like highly boosted and lean or dilute combustion have been employed in the spark-ignition engine, which has increased the challenges of ignition control since ignition is the trigger of the combustion, developing a next-generation spark ignition system is strongly required for the spark-ignition engine.

First of all, understanding the process of the initial flame kernel growth during the ignition is important. Most of the researchers use schlieren photography to capture the initial flame during the ignition process. However, it had been found that in this method, it is hard to distinguish between the preheated zone and initial flame, even under no fuel conditions, the preheated zone could still be detected by the schlieren imaging method. Therefore, this study uses a high-speed infrared camera to detect the initial flame because most combustion products, like CO, CO_2, and H_2O, absorb specific infrared wavelengths and radiate the infrared when the components become hot. Infrared images have provided a more accurate way of measuring the initial flame and being able to analyze quantitatively.

After that, a new simultaneous visualization method by a high-speed infrared camera (FLIR X6900sc) and a conventional high-speed camera (Photron SA-X) has been proposed to obtain deeper insights into the ignition process in a constant volume combustion chamber (CVCC), the influence of discharge channel behaviors on the initial flame formation could be investigated by this method. Results show that short-cut and restrike are two kinds of discharge channel shortening behaviors that affect early flame overlap and growth, short-cut shortening behavior is better than restrike shortening behavior for the flame development and enlarges the early flame during the discharge duration.

In addition, to found out a suitable ignition strategy under different ignition conditions, the ignition performance is studied with various mixture dilutions, flow conditions, and discharge characteristics under the CVCC. Two types of ignition coils that have the same discharge energy were analyzed in particular. The results show that extending discharge duration is more helpful in improving the ignition performance under the increasing dilution ratio compared with the enhanced discharge current at the

same discharge energy. However, the discharge current plays a more vital role in perfecting the ignition performance under the increasing local flow velocity than the discharge duration.

Finally, the results of the CVCC experiment imitated the engine conditions, it needs to be confirmed in the actual engine conditions. Hence, the engine test is carried out on a single-cylinder of JUKE four-stroke SI gasoline engine with EGR technology to confirm the results in the CVCC. Results have demonstrated that increasing the EGR rate needs to advance the ignition timing for obtaining the lowest cycle-to-cycle variations, knocking is the obstacle to advancing the ignition timing further when under the low EGR rate conditions; when increasing the EGR rate to the EGR limit, misfire becomes the obstacle to enlarging the ignition advanced timing. Meanwhile, when focusing on the same ignition energy, prolonging the discharge duration has more benefits to improving the engine performance under low flow conditions, while the discharge current plays a more vital role in perfecting the engine performance than the discharge duration under the high flow condition.

NOMENCLATURE

AC	Alternating current
A/F	Air-fuel ratio
ATDC	After the top dead center
BSFC	Brake-specific fuel consumption
CAD	Crank angle degree
CA10	Crank angle timing for 10% mass fraction burn
CCV	Cycle-to-cycle variations
CDI	Capacitive discharge ignition
CI	Compression ignition (CI).
CO	Carbon monoxide
CO_2	Carbon dioxide
COV	Coefficient of Variation
CVCC	Constant volume combustion chamber
DC	Direct current
ECU	Electronic control unit
EGR	Exhaust Gas Recirculation
fps	Frames per second
GDI	Gasoline direct injection
HC	Hydrocarbon compounds
ICEs	Internal combustion engines
IG	Ignition timing
IGBT	Insulated gate bipolar transistor
IMEP	Indicated mean effective pressure
IR	Infrared radiation
MBT	Minimum advance for best torque
MFB1	Mass fraction burn of 1 percent
NA	Natural aspirated engine
NOx	Nitrogen oxide
O_2	Oxygen

PIV	Particle image velocimetry
PLIF	Plane laser induced florescence
PM	Particulate matter
RF	Radio-frequency
ROHR	Rate of heat release
SI	spark ignition
TCI	Transistorized coil ignition
TDC	Top dead center
VOIS	Variable output ignition system
WLTP	Worldwide Harmonized Light Vehicle Test Procedure
η	Thermal efficiency
k	Specific heat ratio
ε	Compression ratio

Chapter 1 Introduction

1.1 Background

In recent years, the burden of traditional resources and environmental concerns demand high efficiency and low emissions in internal combustion engines (ICEs) for on-road vehicle applications. In addition to the increasing electrification of vehicles, forecasts show a worldwide increase in the number of combustion engines being produced. With hybridization growing apace, at least 75 % of the 120 million new registrations expected in 2030 will be for vehicles based on combustion engines, most of the gasoline engines. Europe, Japan, China, and the United States continue to introduce strict automotive exhaust emissions regulations and CO_2 emission limits [1]. In China, new emission standards (China VI – Emission Standard) for light-duty vehicles were announced, and all new vehicles should meet it at the start of 2020 [2]. Under Worldwide Harmonized Light Vehicle Test Procedure (WLTP), CO, THC, NOx, and PM should be reduced by 50%, 50%, 40%, and 33%, respectively, compared to China VI – Emission Standard. It announced that National VIa Emission Standard is equivalent to European VI Standard, and National VIb has higher requirements than European VI Standard, becoming one of the most stringent automotive exhaust emission standards in the world. These have brought new challenges and requirements to the development of engine technologies, especially for emissions-reducing and economic improvement. The future global CO_2 emission regulations and fuel consumption for passenger vehicles are summarized in Figure 1-1 [3]. The proposed target of CO_2 emission values of the EU will decrease quickly and will reach 67 g/km in 2030. This means that the EU plans to shrink CO_2 emission by about 30% by 2030 compared to the CO_2 emission value in 2020. It requires a reduction in the fuel consumption of the engine.

In addition to the increasing electrification of vehicles, forecasts show a worldwide increase in the number of combustion engines being produced. With hybridization growing apace, at least 75 % of the 120 million new registrations expected in 2030 will be for vehicles based on combustion engines, most of the gasoline engines. Thus, internal combustion engines are still accepted to remain a major part of the modern vehicle market in the foreseeable future. All of these indicate that continued investigation of advanced internal combustion engine techniques to improve fuel efficiency and reduce emissions is meaningful and important.

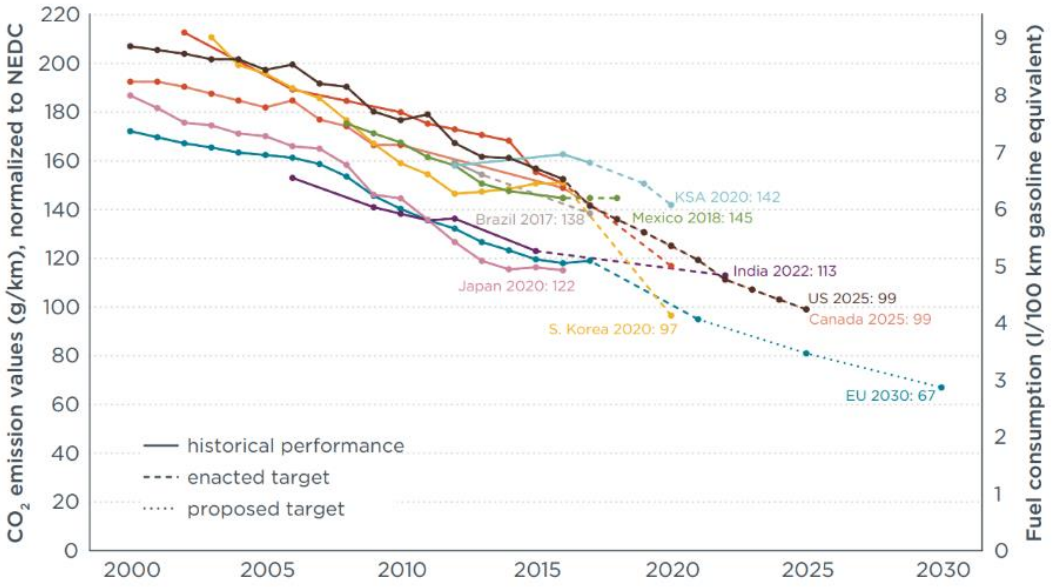

Figure 1-1. Global CO_2 emission and fuel consumption regulations for passenger vehicles [3]

1.2 Challenges to the ignition system of SI engines

Improving the fuel economy while meeting strict emission standards is the focus of engine research. More and more advanced technologies have been continuously developed and applied in internal combustion engines, such as a new way of burning (homogeneous charge compression ignition, lean burn), exhaust gas recirculation (EGR), new types of injection (port injection, direct injection, dual-injection, new kind of injector, etc.), alternative fuels, and engine downsizing, and turbocharging [4-9]. These advanced combustion technologies had increased the challenges of ignition control in SI engines.

1.2.1 Lean burn and EGR

Lean burn is developed base on stoichiometric combustion, when the fuel and air are mixed according to the theoretical air-fuel ratio of the complete chemical reaction, the in-cylinder combustion belongs to stoichiometric combustion; when adding excess air based on the theoretical air-fuel ratio, the combustion belongs to lean burn. According to formula 1-1, η stands for the thermal efficiency, k stands for the specific heat ratio, and ε is the compression ratio of the engine [10]. The engine thermal efficiency can be increased by increasing the specific heat ratio k, and the lean mixture results

in a higher specific heat ratio. Besides, the excess air of lean combustion is conducive to completing the combustion, and at the same time, the combustion temperature is lower than that of stoichiometric combustion [11], which reduces the heat transfer loss to the cylinder wall, meanwhile, lower combustion temperature can suppress knocking [12], which is beneficial to the improvement of compression ratio. In addition, lean combustion can effectively reduce throttle loss by increasing the throttle valve opening [13] and reducing gas consumption by cooperating with the intake air boost. On the other hand, since lean combustion can reduce the combustion temperature, it is beneficial to reduce NOx generation. With the increase in the air-fuel ratio, the NOx emission level shows a gradually decreasing trend [14]. However, the lean burn reduces the combustion speed due to the lower combustion temperature, which brings a lot of challenges to the ignition system for igniting the mixture under such conditions.

$$\eta = 1 - \frac{1}{\varepsilon^{k-1}} \tag{1-1}$$

EGR is another technology to change the specific heat ratio, this technology allows the burned exhaust gas to be recirculated back into the intake manifold, and mixed with the fresh air in the next cycle to burn in the engine cylinder. Specifically, it can be divided into two methods: internal EGR and external EGR. Figure 1-2 shows the gas exchange of the internal EGR, the internal EGR [15] has a simple structure by adjusting the valve timing to increase the residual exhaust gas coefficient, but it is difficult to achieve precise control of the EGR rate. External EGR [16] includes low-pressure loop EGR and high-pressure loop EGR, as shown in Figure 1-3a, in low-pressure loop EGR, Exhaust gas goes into the turbine at first, and then into the compressor together with fresh air; while in the high-pressure loop EGR of Figure 1-3b, in this structure, exhaust gas is from the upstream of turbine to the downstream of compressor or of the intercooler. However, such a high-pressure loop EGR must ensure that turbine upstream pressure is sufficiently higher than boost pressure.

Exhaust gas recirculation technologies, either internal EGR or external EGR have introduced CO_2 and other gases into the combustion chamber, which consider an efficient way to improve engine performance. On the one hand, the mixture can be diluted, and the specific heat ratio of the mixture in the cylinder can be increased by means of CO_2, etc., on the other hand, the diluted mixture reduced the combustion reaction speed and reaction temperature [14], which result in suppressing knocking and reducing NOx emissions. EGR technologies also lessen the throttling of intake air at part loads, which lowers the pumping loss of engine gas exchange cycling; Lean or dilute combustion improves

the potential thermal efficiency by increasing isentropic exponent and reducing heat loss because of the lowered combustion temperature [17] [18]. However, as the EGR ratio or dilution level increases, it may be difficult to maintain the combustion at its optimal location for the best fuel efficiency, which will also deteriorate cycle-to-cycle variations due to the partial burning [19]. Lean and dilute combustion is regarded as an effective way to improve the fuel efficiency for SI engines [20]. However, the excessive air dilution reduces the opportunities for forming an ignitable composition in the vicinity of the spark gap; the air dilution reduces the flame propagation speed, which makes ignition more difficult.

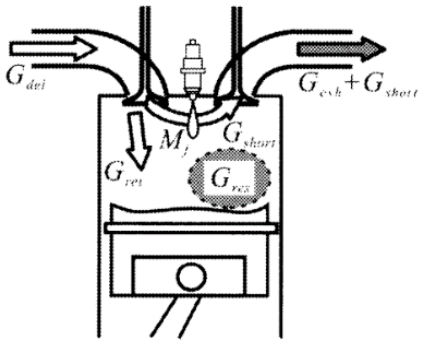

Figure 1-2 gas exchange of the internal EGR [15]

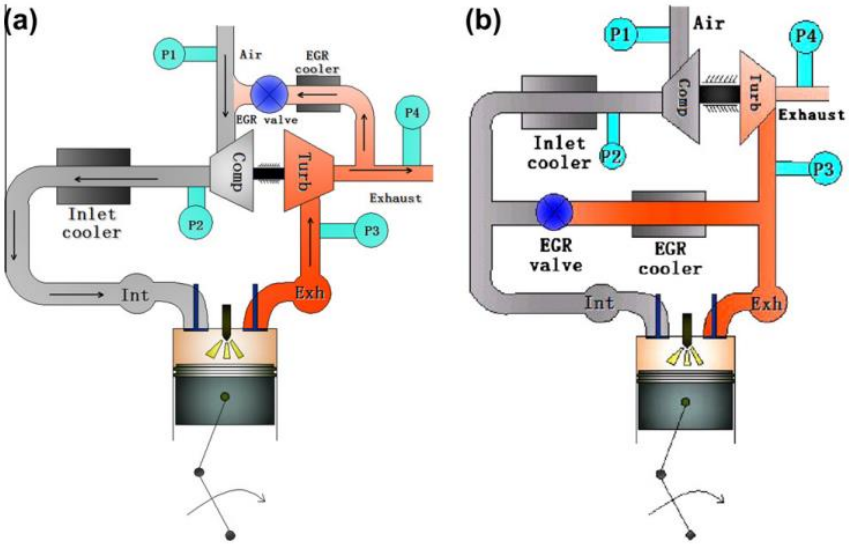

Figure 1-3 Low pressure (a) and high pressure (b) of external EGR [16]

1.2.2 New types of injection

New types of injectors and injection methods have been developed to improve engine performance. By these methods, gasoline direct injection (GDI) has been proved to improve thermal efficiency and reduce emissions (HC and NOx) as shown in Figure 1-4 [21,22]. However, GDI engines also have challenges of knock and particulate matter (PM) [23]. Thus, new technologies were developed for better application of GDI engines. Multi-hole injectors were designed for use in direct-injection gasoline engines. A V-type intersecting hole nozzle was designed and studied using X-ray and three-fluid methods [24-26]. Results showed that non-cavitating internal flow improved the discharge coefficients of V-type intersecting hole nozzles. Spray-guided parts were designed and used to improve the stratified strategy in GDI engines [27,28].

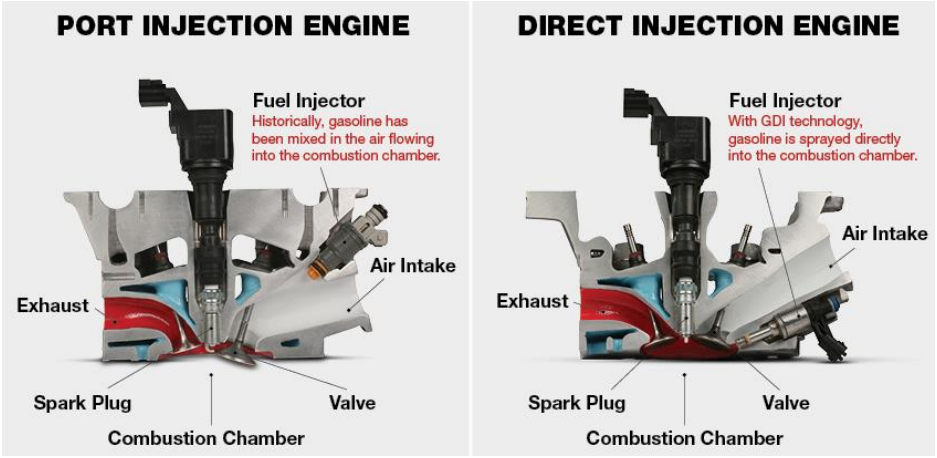

Figure1-4. Port Injection Engines versus Direct Injection Engines [22]

1.2.3 Alternative fuels

Due to the crises of environmental degradation and lack of fossil fuels, alternative fuels were also studied and applied in internal combustion engines [29]. Figure 1-5 shows the primary energy sources, including fossil and regenerative energy, such as biomass, solar, and wind. A part of them can be produced by absorbing CO_2 from the environment [30]. Alternative fuels are environmentally friendly to help ease the oil shortage and allow CO_2 to reach balance in the atmosphere. In addition, it is also beneficial to improve engine efficiency and reduce exhaust emissions. Gong [31] has applied methanol

to port injection and direct injection engines. It proved that it was effective to extend the lean-burn range and improve the high indicated mean effective pressure (IMEP) by using methanol added with hydrogen. Due to the higher low heating value, faster combustion speed, and lower knock occurrence properties of methanol, it is beneficial to increase the compression ratio and engine efficiency [32]. Ethanol is a renewable, domestically produced transportation fuel. Whether used in low-level blends, such as E10 (10% ethanol, 90% gasoline), E15 (10.5% to 15% ethanol), or E85 (flex fuel), ethanol helps reduce emissions [33]. However, ethanol gasoline is corrosive to a certain extent, it will dissolve the long-term precipitation jelly in the oil circuit and bring it into the cylinder, resulting in a carbonization reaction at high temperature, and forming new carbon deposits, which also challenges the ignition system.

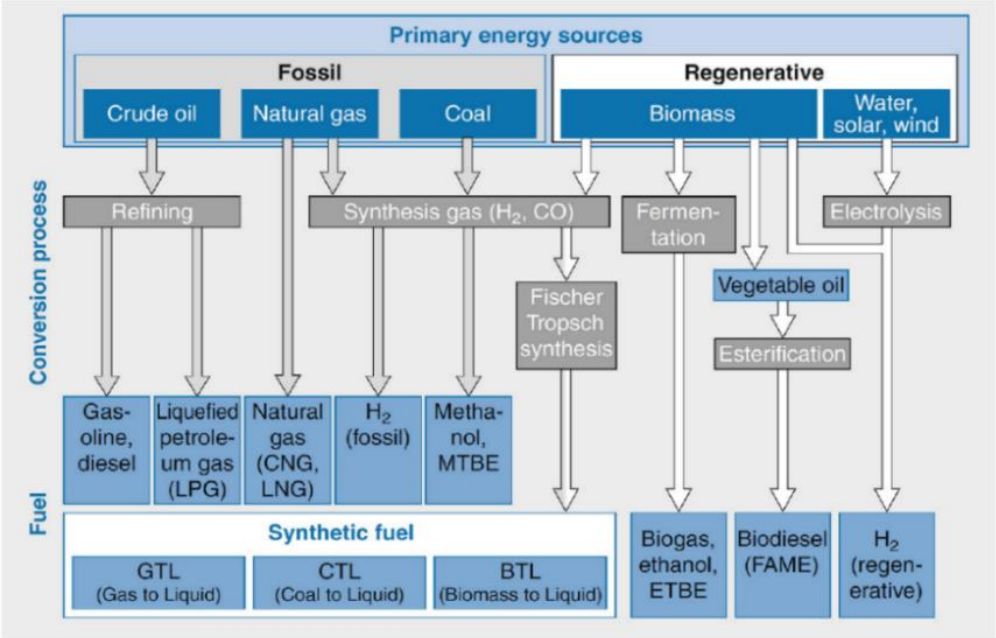

Figure 1-5. Manufacturing paths of fossil and regenerative fuels [30]

1.2.4 Engine downsizing,

Downsizing was introduced to decrease the engine capacity for decades, as shown in Figure 1-6, such as turbocharged engines [34]. This allows reduces engine size and weight greatly both gasoline engines and diesel engines. Due to turbocharging system utilization, Engine downsizing did not deteriorate the performance of the engine, and loss the engine power. The engine downsizing technique

has become a kind of widely accepted technology for engine fuel consumption improvement and CO_2 emissions reduction, especially in turbocharged engines [35]. The reduction in greenhouse CO_2 resulting from downsizing engines is an effective method to meet the stringent emission regulations of global vehicles compared to large-size engines [36]. Nevertheless, the engine downsizing has demanded compacting the engine components and parts, which also challenges the ignition system to simplify for the SI engines.

Figure 1-6 Engine downsizing [34]

1.2.5 Turbocharging

Turbocharging techniques are widely applied to spark ignition (SI) engines. When under stoichiometric combustion of turbocharged gasoline engines, the engine output power is based on the air supplied by the intake system. While with a turbocharged system, the intake pressure is boosted to higher than atmospheric pressure, thereby increasing intake air density and the air mass flow rate. Under stoichiometric operation conditions, more air means more fuel injection in the cylinder to increase the engine power directly for a given engine displacement [37]. As usual, the engine output power is in proportion to the amount of air, and for naturally aspirated (NA) engines, it depends on the engine displacement. Turbocharging allows for reducing the required engine displacement for required engine power by boosting the intake pressure compared to conventional naturally aspirated engines [38]. Nevertheless, Turbocharging techniques have increased the intake the air mass flow rate, which also brings challenges to reliably generating a flame kernel under such high mass flow conditions for the ignition system.

A high-performance ignition system is demanded four requirements: a high ignition voltage to break

down the gap between the plug electrodes; a high energy storage capacity to create a spark kernel of sufficient size to be reliable; a low source impedance or steep voltage rise; sufficient duration of the voltage pulse to ensure ignition. Therefore, the spark plug life is the other challenge as the discharge energy and duration increase. The erosion of electrodes comes in two ways. one aspect is sputtering, which is caused by the high voltage at the breakdown; Another is the oxidization, which is caused by the thermal plasma during the discharge, energy stored in the parasite capacitors will dump into the plasma if the arc channel forms, leading to severe electrode erosion. [39-42].

Due to the challenges mentioned above, the development of a next-generation spark ignition system is greatly needed to meet these challenges for SI engines.

1.3 Fundamental of the ignition process in SI engines

Ignition is the trigger for the combustion in the SI engine. The electrical discharge produced between the spark plug electrodes by the ignition system after the compression stroke in the SI engines, the air mixture in the vicinity of the spark plug is initiated by the high-temperature plasma, which forms the initial flame kernel. Typically, the ignition duration will sustain several milliseconds for the initial flame kernel to develop into a self-sustaining flame and propagate downstream. Therefore, the process of ignition can be divided into three phases: the breakdown phase, the arc phase, and the glow phase [39].

1.3.1 Breakdown phase

The process of a breakdown following the mechanism as shown in Figure 1-7, free electrons travel from the cathode to the anode and collide with the neutral gas molecules under the strong electric field between the two electrodes. The ionization of the neutral gas is promoted when the voltage exceeds a static breakdown threshold, producing a corona discharge, as a form of non-equilibrium plasma. When the voltage further increases to a dynamic breakdown threshold, an electron avalanche occurs and thus the equilibrium plasma is formed [43]. The breakdown phase is characterized by a high voltage (maximum at 10kv), peak current (maximum at 200A), and extremely short duration (within 10ns) [39]. The discharge plasma glows because the electron energy and number density are high enough to generate visible light by excitation collisions.

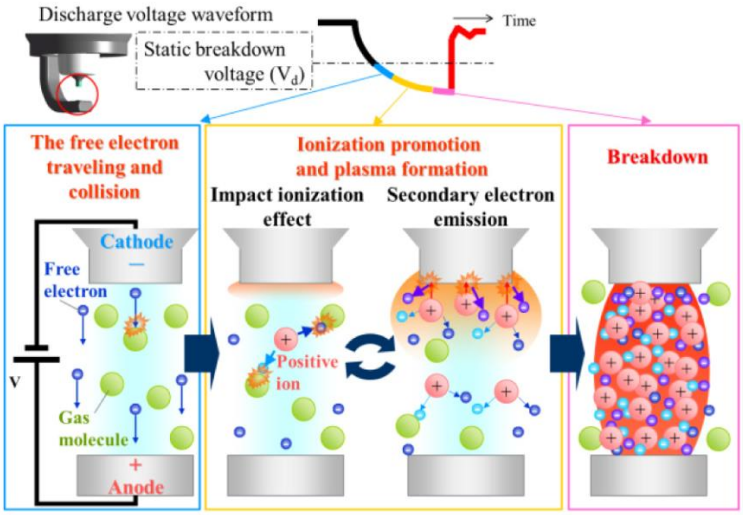

Figure 1-7. Schematic of the breakdown phase [44]

1.3.2 Arc phase

After the end of the breakdown phase, the arc phase will follow immediately. During the arc phase, the ignition energy stored inside the cable and coil capacitances is released within several microseconds, the temperature will up to about 6000 K at the center of discharge plasma [41], and the voltage of the arc phase is lower than the breakdown phase. The arc phase is maintained by the numerous electrons emitted from the cathode surface, the thermionic emission produced an amount of molten hot spots resulting in electrode erosion.

1.3.3 Glow phase

The glow phase is always followed after the end of the arc phase, as the decreasing of discharge current and discharge voltage. However, the glow phase usually sustains for several milliseconds, and the voltage drop between the spark plug gap is typically 300 to 500 V [41]. It is the longest phase during the ignition, most of the ignition energy will release during the glow phase. Due to the long-last duration, the length of the discharge channel is affected by the flow field. For instance, the discharge channel will stretch with the flow crossing, and the discharge channel will shorten when the flow intensity is strong enough, short-cut and restrike shorten behaviors may occur across the spark

plug gap [44].

1.4 Advanced Ignition Techniques

Based on the mentioned above, the role of the ignition is to open a pathway to deliver the energy into the gas mixture and to generate the flame kernel. due to the glow phase being the most energy release duration during the ignition process, more and more advanced ignition techniques have been developed and applied to optimize the glow phase via the different forms of the energy supply. There are several kinds of promising ways of the follow-up energy supply that have been studied recently, which include capacitive discharge, radio-frequency energy discharge, laser ignition, and resistive discharge.

1.4.1 The capacitive discharge

A capacitive discharge method has employed a capacitor coupled with the capacitive discharge ignition (CDI) system. As shown in Figure 1-8, the difference between the conventional ignition system and the capacitive discharge ignition system had been shown clearly. The left of Figure1-8(b) stands for the CDI system, which added the CDI module and directly connected to the spark plug unit via the discharge cables. In the CDI system, there is a tertiary circuit to create the ionized plasma kernel using a high-voltage capacitor, which includes a piezoelectric ceramic material [46].

Kwonse et al. [46-48] have investigated the capacitive discharge ignition on the discharge channel formation and initial flame propagation. Results have shown that CDI improved the flame propagation process by dielectric breakdown strength offered from capacitor-discharge, and improved the initial flame kernel growth between the spark plug gap. Koji et al. [49] investigated a newly developed plasma jet igniter in a combustion chamber, results show that the maximum combustion pressure increases and the burning period decrease with increasing the cavity volume. Sung et al. [50] analyzed the multi-spark capacitor discharge ignition system to improve the ignitability under the lean burn condition, results of the engine test with capacitor discharge ignition system showed about 10% extension of lean limit and a 5% increase of brake thermal efficiency than the single spark ignition system. Shui Yu et al. [51] compared the results of ignition flame kernel initiated between the pure inductive discharges and capacitive-coupled discharges. It can be seen from the early ignition flame images that the capacitive discharge ignition methods produced larger flame kernels than the inductive

discharge ignition methods under both stoichiometric and lean mixture conditions.

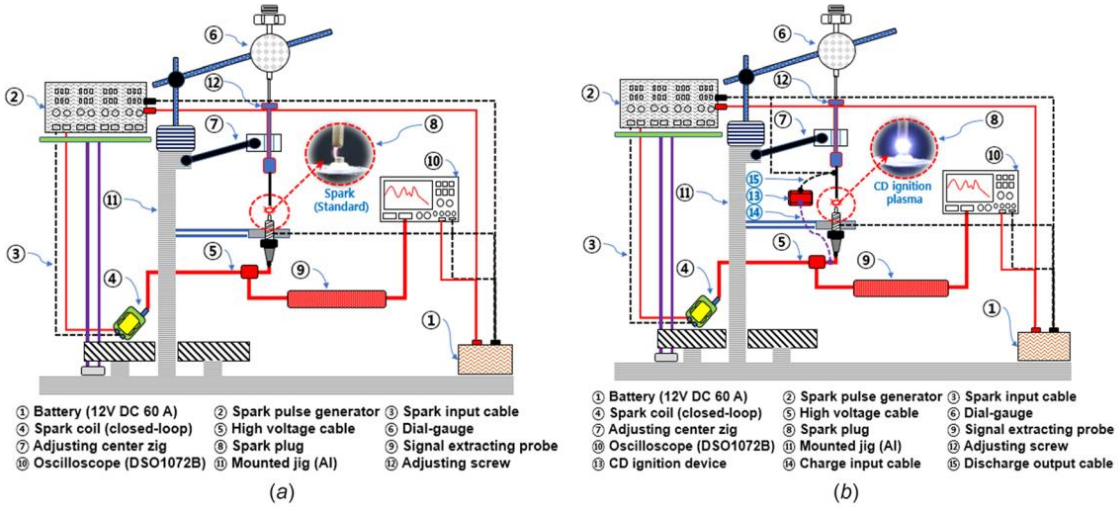

Figure 1-8. Schematic diagrams of (a) conventional ignition and (b) capacitive discharge ignition (CDI) systems [46]

1.4.2 Radio-frequency energy discharge

There are two major methods to apply radio-frequency (RF) energy discharge during the ignition process, one is the RF spark ignition, and another is the RF corona ignition.

Nishiyama et al. [52] developed an ignition system employing a standard ignition coil for breakdown and adding a high-frequency coil for supplying current into the formed plasma kernel. As shown in Figure 1-9 of the schematic of the RF spark ignition system. The frequency of the alternating current ranged from kHz to MHz orders. The voltage amplitude was higher than the resistive discharge voltage but could be lower than the breakdown threshold. The standard ignition coil contributed about 30mJ ignition energy, while the high-frequency coil supplemented 120mJ. The ignition system was evaluated by the engine tests conducted at 0.4 MPa IMEP and 2000 r/min with 20% EGR. Results indicated that the initial combustion period and IMEP were strongly correlated. Therefore, the stable, short initial combustion period led to a high IMEP and less combustion fluctuation. Heise et al. [53] have developed a high-frequency electrical resonance-based ignition concept to replace the conventional ignition systems. This concept employs an alternative method of generating high voltages, using inductors and capacitors trimmed such that the supplied energy steadily increases the output voltage. The high-frequency ignition system was evaluated on a direct injection gasoline engine and compared with a multi-charge ignition system. results show that over the EGR range up to 20%

at light loads no significant difference was observed between the HFIS and the multi-charge ignition system, while the HFIS offered a lower misfire tendency at 25% EGR.

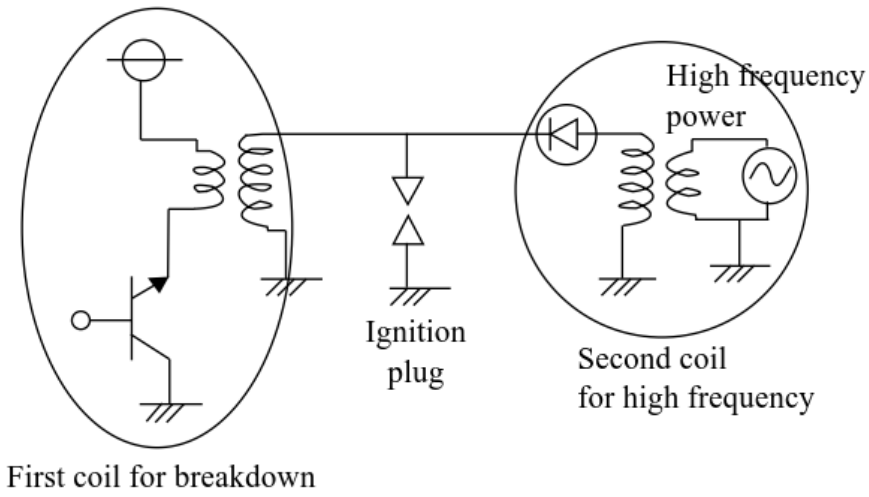

Figure 1-9. Schematic of RF spark ignition system[52]

The RF corona ignition technique has raised much attention in recent years, for the corona discharge uses a strong electric field to generate a plasma beam at the tip of a single electrode, which is released from the tip of the electrode [54]. Figure 1-10 shows a corona discharge plasma channel and its high-frequency voltage and current signals. [55]. It can be seen from Figure 1-10 that corona discharge is a kind of volume discharge, and the coverage of the plasma channel is large, which is conducive to the formation of a large initial fire nucleus [56]. In addition, the power discharge tip has no ground electrode, which can effectively reduce the heat loss to the electrode. Figure 1-11 is an implementation circuit of AC corona discharge [55]. The DC voltage is converted into AC voltage through a two-transistor circuit, which is initially boosted and supplied to the primary coil (300-500V AC) and then ignited. The coil generates a higher voltage alternating current, and the frequency of the alternating voltage is determined by the frequency of the control signal of the two-transistor logic circuit. Corona discharge mainly relies on the RLC series resonant circuit in the secondary coil, where C is the parasitic capacitance. When the operating frequency is close to the RLC resonant frequency, an ideal voltage amplitude (5-15kV) can be generated at the electrode tip. Burrows et al. [57] had also researched the RF corona ignition, it indicated that the increase of gas density significantly suppressed the corona discharge. Bellenoue et al. [58] compared the ignition abilities between the spark plug and

corona ignition, results showing that corona ignition results in faster combustion and a higher lean limit, it demonstrated that corona ignition can ignite in quiescent extremely lean conditions which cannot be realized using more powerful spark plug ignition.

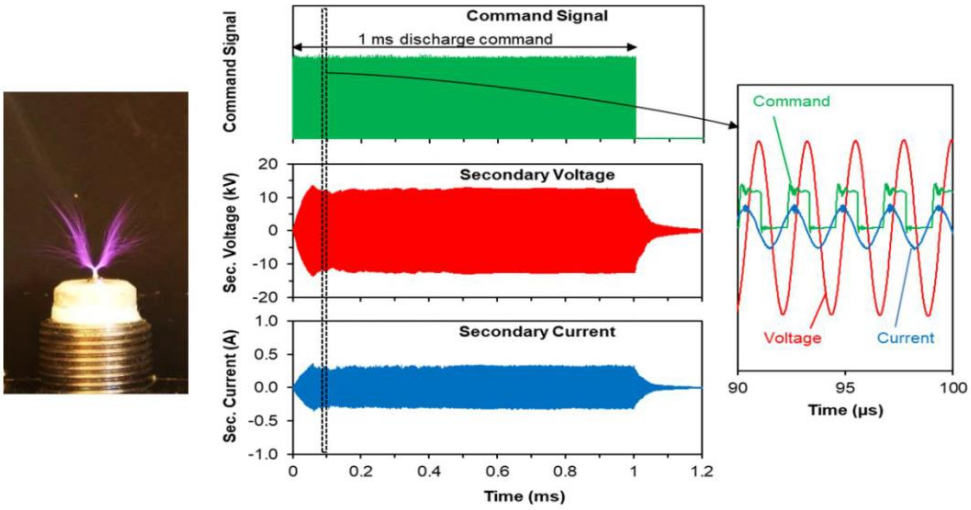

Figure 1-10. RF corona ignition[55]

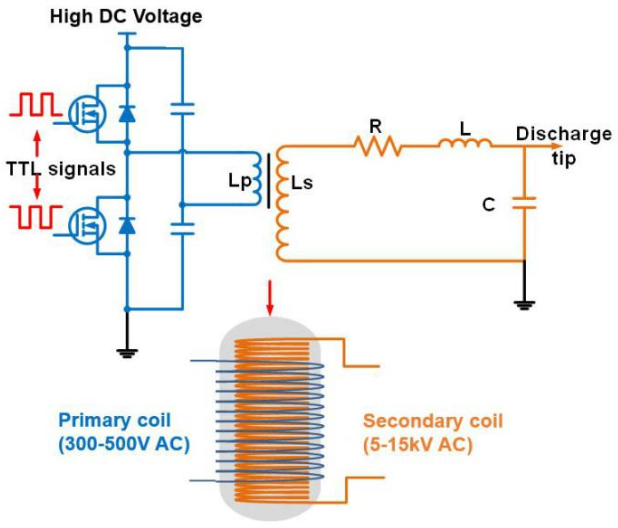

Figure 1-11. Schematic of corona discharge system[55]

1.4.3 Laser ignition

Laser ignition is a non-contact ignition method. Figure 1-12 shows the comparison between laser ignition spark plug and traditional spark plug [59]. Since the laser ignition source is not in direct contact with the surrounding metal, it can reduce the heat loss to the electrode of spark plugs and other devices in the early stage of ignition, which maximizes the use of ignition energy in the mixture. Takahashi et al. [60] investigated the possibilities of advanced laser ignition in a natural gas engine, it demonstrated that the lean burn limit is extended using laser ignition, especially for multi-point laser ignition. However, considering the reliability, cost and other issues, laser ignition technology has not been popularized.

Figure 1-12 Comparison of laser ignition and traditional spark plugs [59]

1.4.4 Resistive discharge

Resistive discharge is a kind of transistorized coil ignition (TCI), TCI technology is currently the most mature and common ignition method. The schematic diagram of the TCI device structure is shown in Figure 1-13. When the insulated gate bipolar transistor (IGBT) is turned on, the power supply charges the primary coil of the ignition coil. When the IGBT is turned off, a strong induced current is generated in the secondary coil due to electromagnetic induction. The breakdown has occurred when the voltage at the spark plug gap exceeds a static breakdown threshold, and a plasma channel is formed at the gap [61]. The TCI ignition method can control the ignition time and charging time by controlling

the on-time and off time of the IGBT, and the charging time directly affects the discharge energy of the spark plug. In a conventional inductive ignition system, the majority of spark energy is deposited through the resistive discharge [19]. Due to the extremely short duration of the breakdown phase, the energy cannot be depleted, therefore, a subsequent resistive discharge has occurred after the breakdown phase, the ignition system resistance, and the turn-ratio of the coil transformer affect the resistive discharge energy.

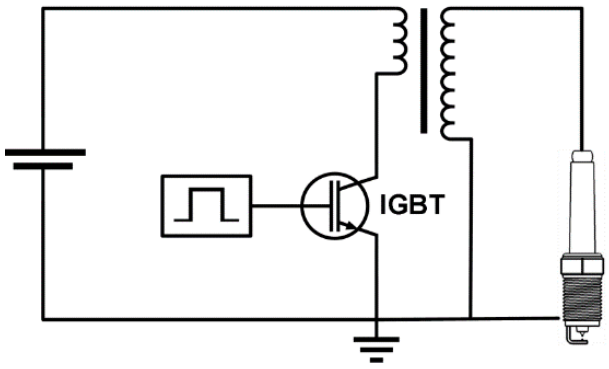

Figure 1-13 Schematic of transistorized coil ignition system [62]

Due to the resistive discharge being the most mature and common ignition method, plenty of research has been carried out to improve the ignition system basic on this method. Alger et al. [63-65] have developed a continuous discharge strategy in SI engines, as shown in Figure 1-14, this method uses two ignition coils to deliver the energy to a single spark plug in a multi-charge mode, with one ignition coil energizing during the dwell of the other. Therefore, a long-duration continuous resistive discharge can be created. This discharge strategy resulted in a larger improvement in burn rate and stability than the one coil in multi-strike mode. The high-energy continuous discharge ignition system has a significant expansion in the dilution tolerance of the engine. Which enabled an improvement in fuel consumption through typical dilution mechanisms - a reduction in knock, pumping work, and heat transfer.

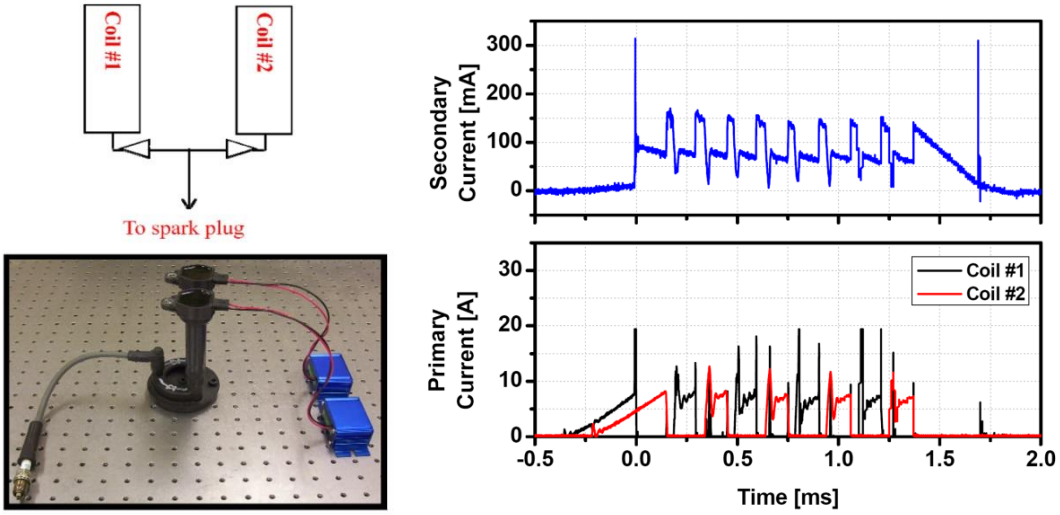

Figure 1-14 Schematic and discharge current of the ignition system [63]

Figure 1-15 [66] shows a new rail plug ignition concept, it is a high-energy ignition system and adds a follow-on circuit to provide a high current (of the order of 100 A) after breakdown for accelerating the plasma down the rails. The results show that rail plugs have a very strong arc phase that can ensure the ignition of very dilute mixtures in a natural gas engine.

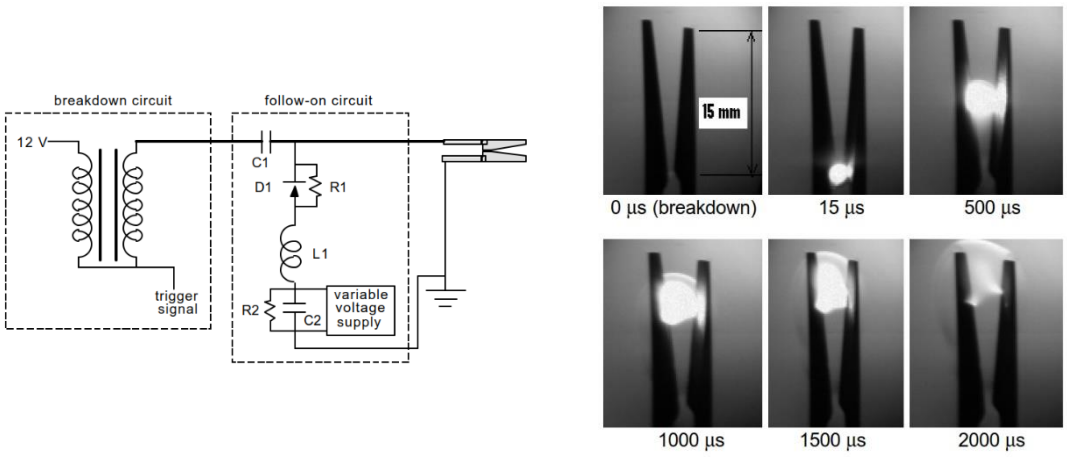

Figure 1-15 Schematic and images of the new rail plug ignition [66]

Yu xiao [67] has proposed a boosted current ignition system, as shown in Figure 1-16, it can change

the current duration, current timing offset, and current level. The effect of discharge current level and discharge duration on the combustion has been studied in a single-cylinder engine, results show that increasing the discharge current result in a shorter ignition delay and higher combustion stability. However, this boosted current spark strategy also change ignition energy, so that, the results can be explained by the difference in the ignition energy.

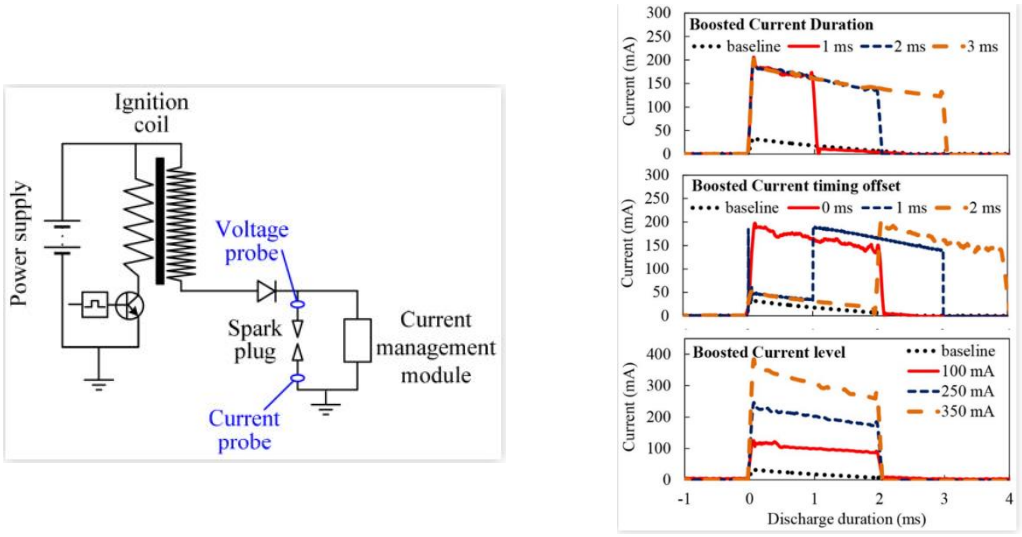

Figure 1-16 Configurations of the spark ignition system and waveforms of the boosted discharge current [67]

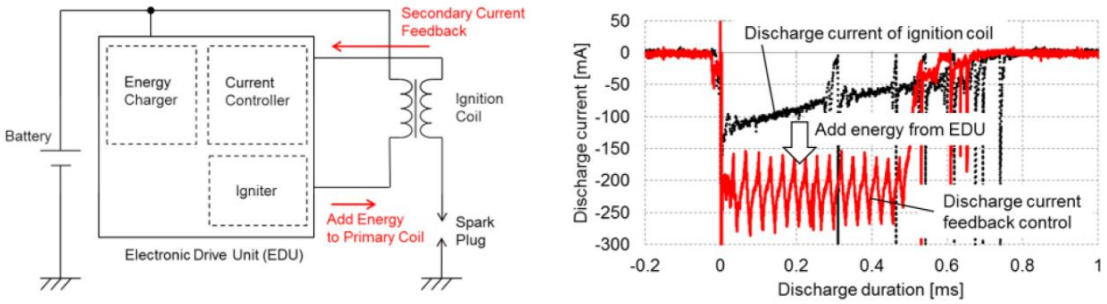

Figure 1-17 Discharge control ignition system configuration [68]

As shown in Figure 1-17, Naoto [68] employed a variable control device of discharge current instead

of the conventional ignition system, and they suggested that ideally, the ignition system should control the discharge current according to engine conditions.

Dongwon Jung [69] [70] et al. increased the discharge energy by combining ten spark coils to improve the stability of the lean limit in the SI engine. Figure 1-18 [70] shows the schematic of a high-energy inductive ignition system. Results indicated that increased discharge energy of ten spark coils achieve the lean limit at λ=1.9 and with a thermal efficiency of 16.5% improvement.

As shown in Figure 1-19 [71]. Chen et al. developed a Variable Output Ignition System (VOIS) to control the ignition energy, duration, and phasing of two ignition coils per cylinder on a gasoline engine. Test results show that the spark plug gap size is the dominant factor impacting the EGR limit and combustion stability under the two engine conditions examined. small gap size has a lower EGR limit than the large gap size plug.

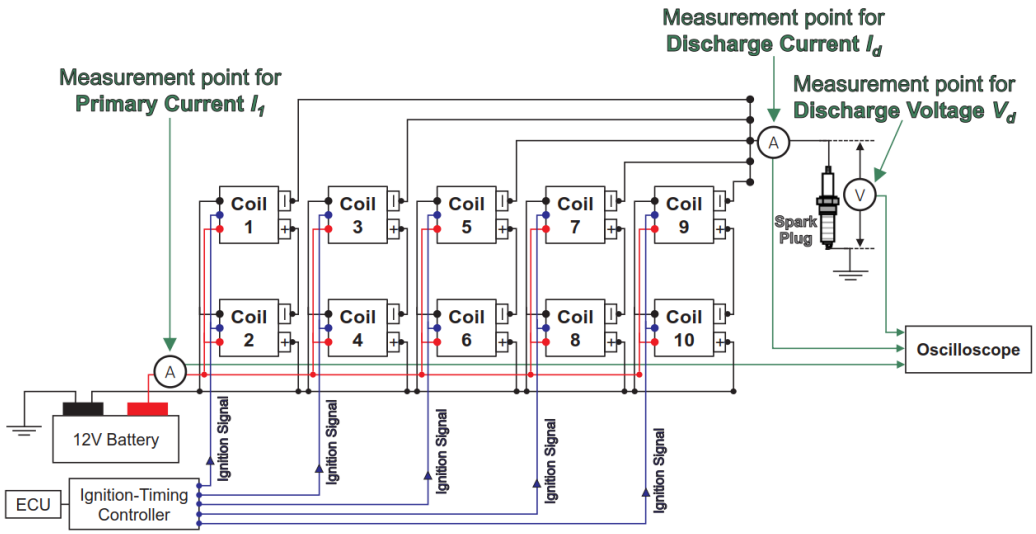

Figure 1-18 Schematic of high-energy inductive ignition system [70]

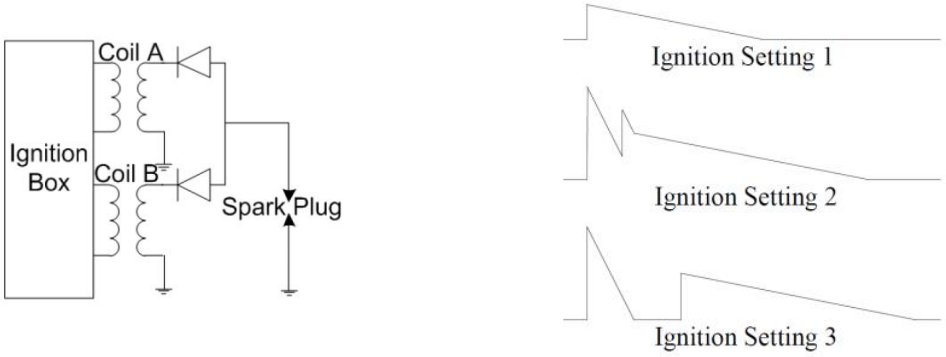

Figure 1-19 Schematic and the current setting of the VOIS ignition system [71]

1.5 Visualization method

In order to get a deeper insight into the ignition process, the visualization experiment has to conduct to capture the images during the ignition process. Usually, the test is conducted in engines and combustion chambers, engines including the optical engines and the borescope method in normal engines.

Dahms [72-75] has studied the ignition process in an optical engine, as shown in Figure 1-20, Dahms uses the CN*-radical emission imaging method during the ignition process. It has presented a new ignition model which contains the sub-grid scale turbulent velocity and mixture-fraction fluctuations, the model suggested that the ignition is a three-stage process. first is the spark channel formation, second is the spherical flame kernel formation and propagation, and third is the flame kernel development. results show that the local mixture ignitability is determined by a local Karlovitz-number criterion and influenced strongly along the spark channel. Peterson et al. [76-78] use an optical engine with the method of high-speed PLIF and PIV to analyze the spatial and temporal evolution of the fuel distribution and flow velocity on flame kernel development to better understand the nature of poor burning cycles at each dilution level. It is important to note that mixture conditions found in misfiring and partially burning cycles are within the ignitability range and fall within the general population of all cycles. Martinez et al. [79] [80] used an optical engine to investigate the flame propagation under lean conditions, as shown in Figure 1-22, the optical window is from the bottom of the cylinder in this optical engine. Results demonstrated increased flame distortion and center movement from the location of the spark plug compared to the stoichiometric case; engine stability decreased as the lean

flammability limit was approached.

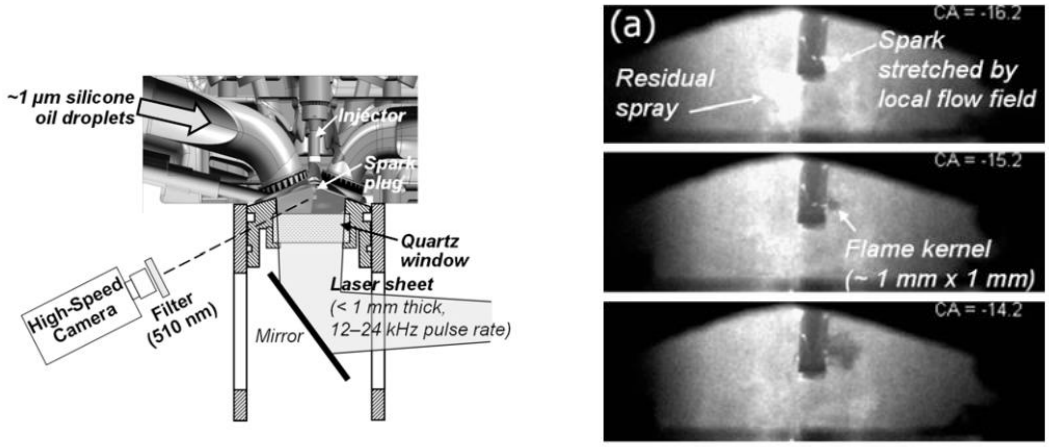

Figure 1-20 Single-cylinder optical SG engine and images [72]

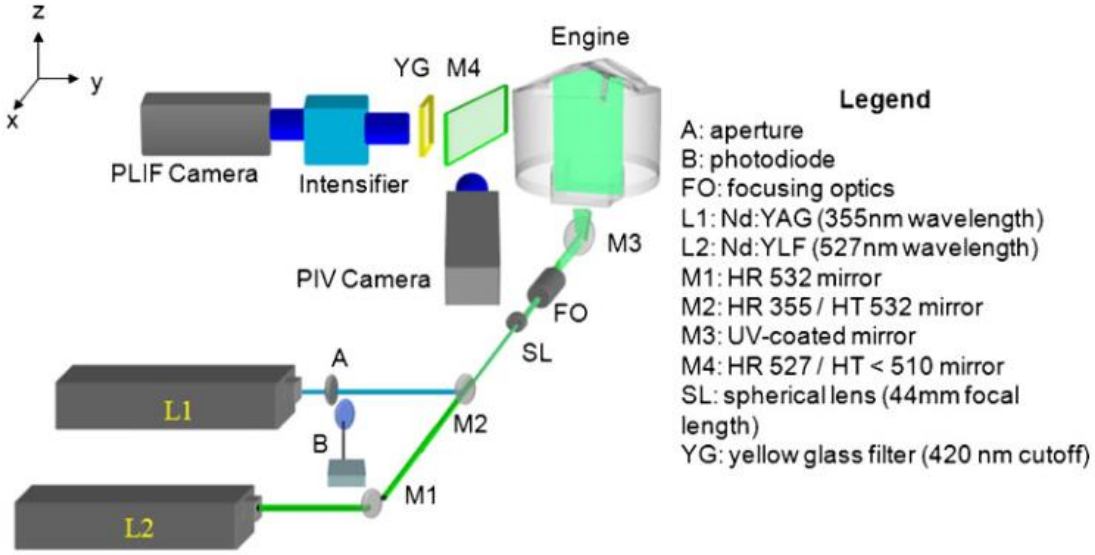

Figure 1-21 Optical setup for combined PIV-PLIF experiments [76]

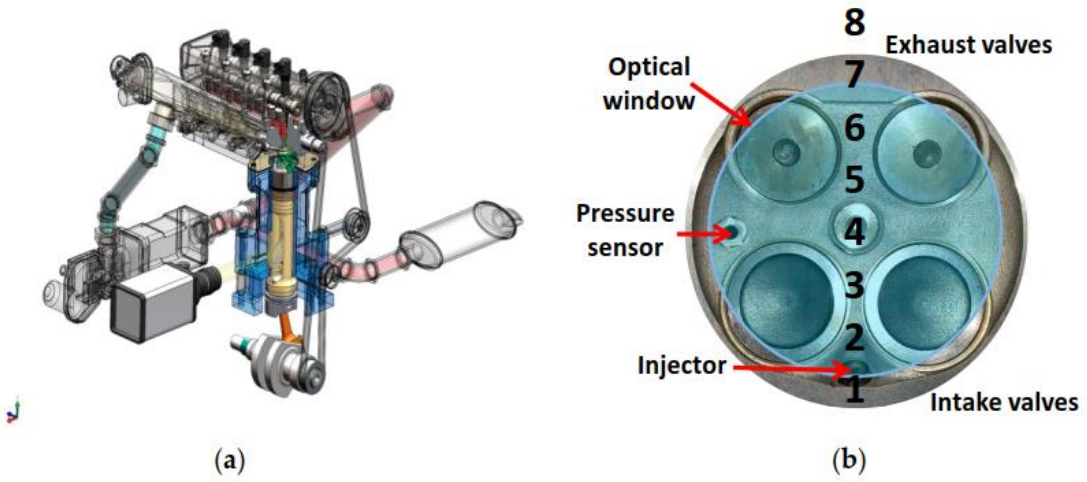

Figure 1-22 Schematic representation of (a) the experimental setup and (b) bottom field of view of the combustion chamber [79]

In Figure 1-23, Jeffrey et al. [81] [82] used a direct injection optical engine to introduce a novel approach for the calculation of equivalent spherical flame radius for analysis of flame speed and stretch. And investigate the flow conditions in the vicinity of the spark plug during the ignition timing by an optical engine, flow field measurement by particle imaging velocimetry. It is observed that the flow motion near the spark plug varies significantly from cycle to cycle and can change direction from the bulk tumble flow near the time of ignition, especially when the ignition timing is late in the cycle at low tumble conditions. Wang et al. [83] changed the spark plug direction to study the effect of spark plug orientation on the initial flame formation. experiments conducted by using two kinds of spark plugs and selecting four directions, results revealed that the crossflow direction results in the largest and fastest growing initial flame kernel; the 0-degree index direction leads to the flame kernel convected onto the spark plug electrode, which produces the smallest and slowest growing flame kernel. Badawy et al. [84] used the optical engine to study the effects of spark plug gap on flame kernel growth and engine performance by the method of PLIF, as shown in Figure 1-24, the optical view is equipped with a triangular window that can capture the images around the spark plug, as a result, the flame kernel growth area increases with the spark plug gap increases, meanwhile, the engine performance increases slightly due to the reduction in cyclic fluctuation as the spark plug gap increases. Philipp et al. [85] used a single-cylinder optical engine to investigate the flame formation and propagation through the method of PIV and OH* flame imaging. As shown in Figure 1-25, this

research used two cameras to set up the optical method. The analysis here revealed that the combustion-phasing cycle-to-cycle variations (CCV) are established by the time of the notional laminar-to-turbulent flame transition that occurs by CA10, measured here from the flame-image growth. therefore, the ignition process is the crucial factor affecting the cycle-to-cycle variations. Atsushi et al. [86] used a conventional ignition system to investigate the flow velocity and discharge channel behavior in an optical SI engine. They also used two cameras to capture the images simultaneously (as shown in Figure 1-26) and observed that higher flow velocities increase the discharge channel stretching length and decrease the ignition delay.

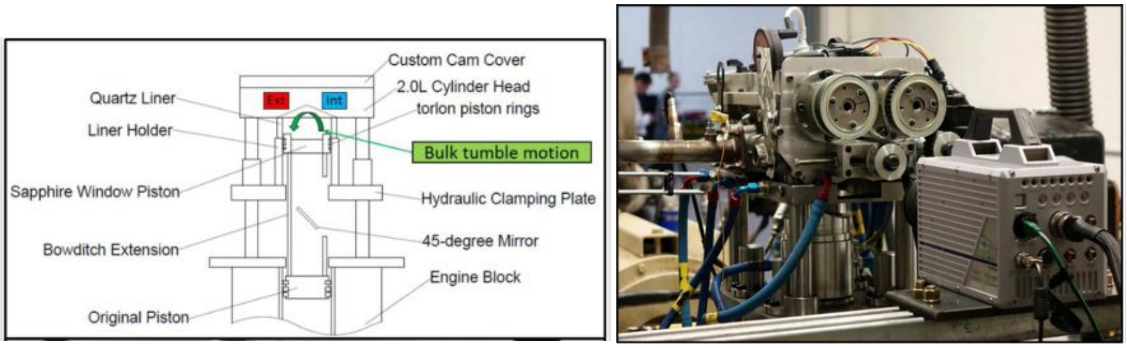

Figure 1-23 Single cylinder direct injection optical engine [81]

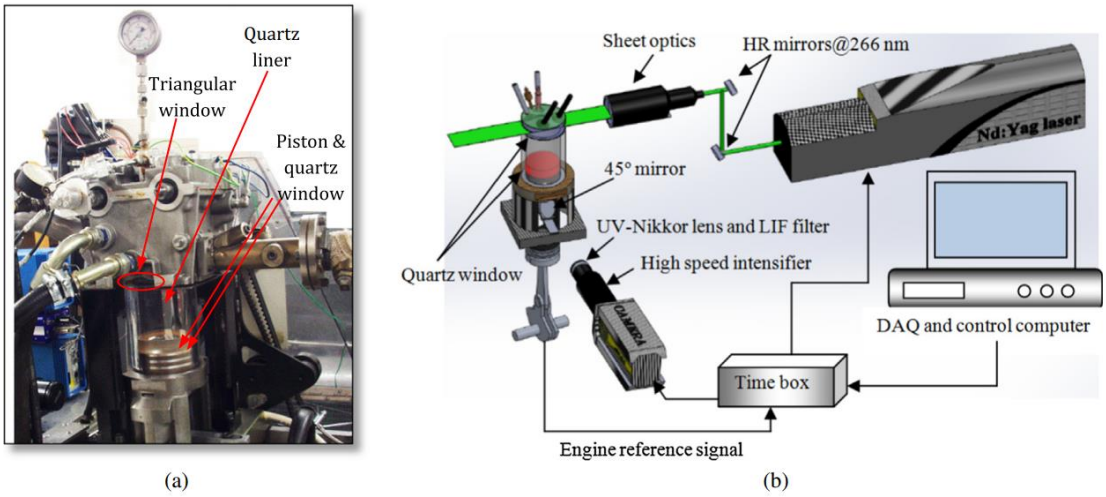

Figure 1-24 The experimental system (a) Optical accesses of the single-cylinder engine, (b) schematic diagram of the PLIF setup [84]

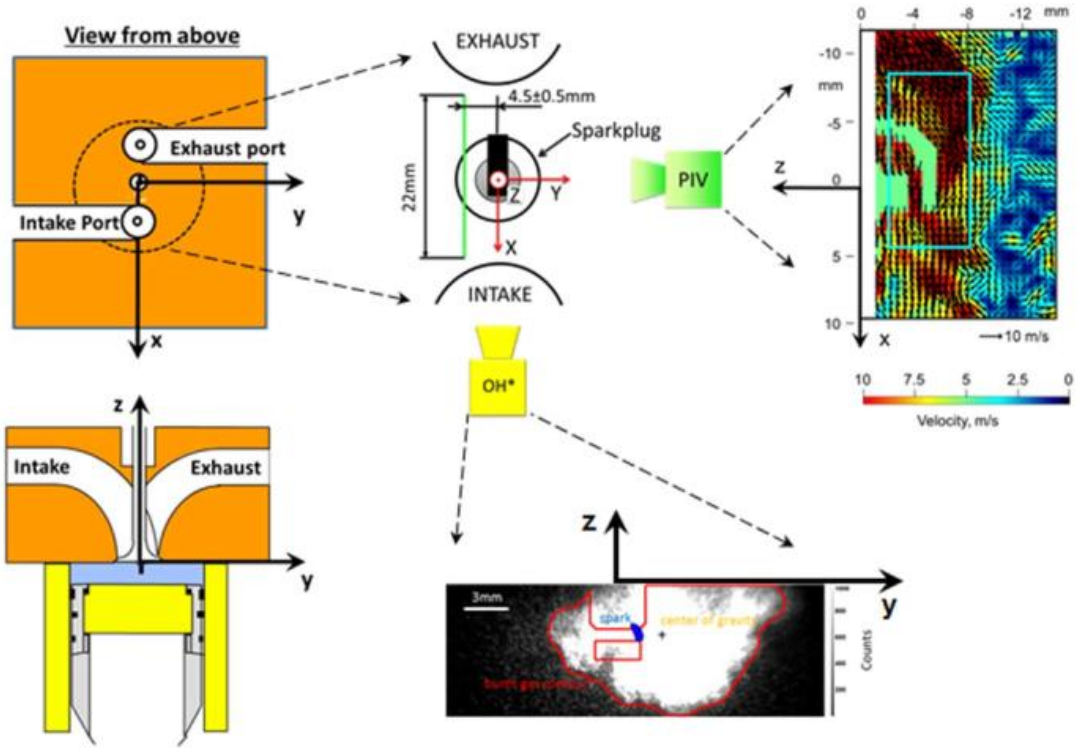

Figure 1-25 TCC-III engine geometry, fields-of-view for optical measurements and sample OH* and PIV velocity flow field images. [85]

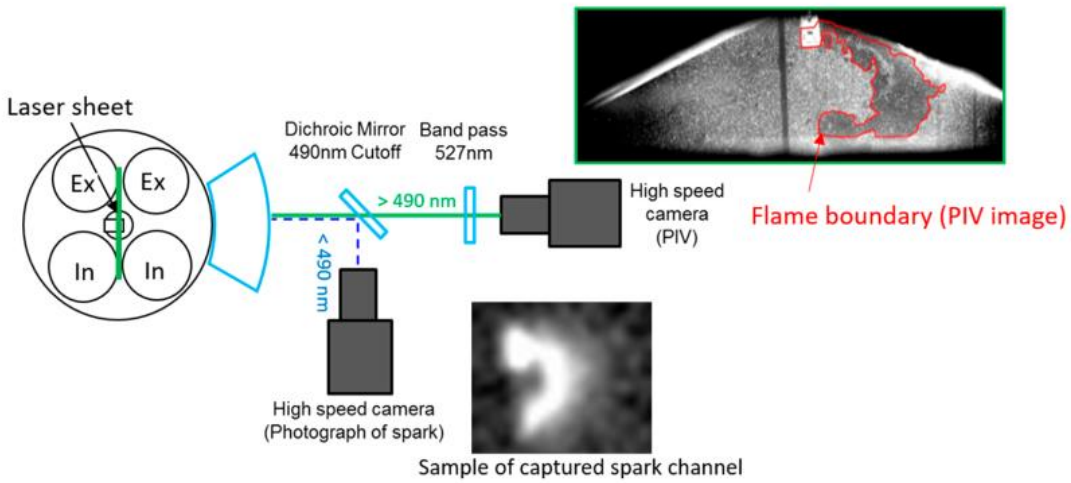

Figure 1-26 Simultaneous setup for PIV/flame imaging and high-speed spark imaging, together with their sample raw images. [86]

Considering that the optical engine usually has a seal problem, the operation of the optical engine is usually under low speed and low load [81] [87]. Therefore, the Borescope is another method for getting the optical accessibly. This method needs to modify the engine for adding the borescope at the cylinder head. Sick et al. [88-90] used two high-speed infrared (IR) cameras with borescopes access to one cylinder of an HD NG engine, as illustrated in the re 1-27, the borescope had been mounted at the cylinder head of the engine. The effect of the ignition system on the early flame-kernel development and cycle-to-cycle variability (CCV) was investigated. The water emission of IR yielded as the initial flame kernel area in the test, three kinds of ignition systems with the energy of 65mJ, 140mJ, and 300mJ were carried out to investigate the effect of ignition energy on the flame kernel growth. results show that a higher ignition energy system has a lower cyclic variation compared to a 65mJ igniter under the lean or EGR diluted condition. Image-based metrics also revealed that early flame kernels located further from the head yielded better combustion, showing that borescope IR imaging can provide guidance for future engine design. Seima et al. [91] used a customized ignition system with 20 ignition coils to improve the operation lean limit at the excess air ratio of 2.1 in a single-cylinder high-compression ratio engine. The borescope optical measurements were conducted to capture the images around the spark plug in the cylinder. Figure 1-28 has shown the in-cylinder image around the spark plug through the borescope. Oryoji et al. [92] [93] investigated the ignition phenomena using an endoscope to realize the in-cylinder optical measurement. It demonstrated that the initial combustion period correlated with spark stretch before the 1st restrike and spark-stretch rate.

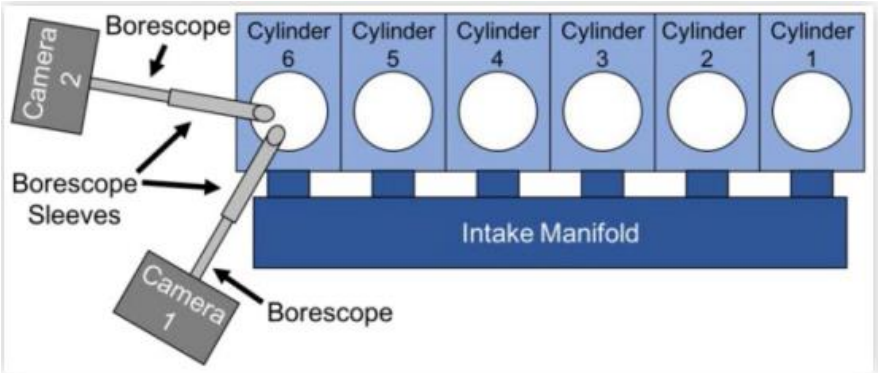

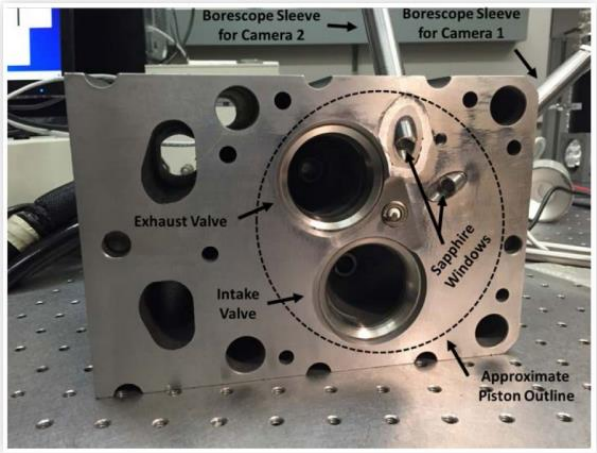

Figure 1-27 The experimental setup used with the production engine. [88]

Figure 1-28 Experimental setup and the view of the in-cylinder around the spark plug. [91]

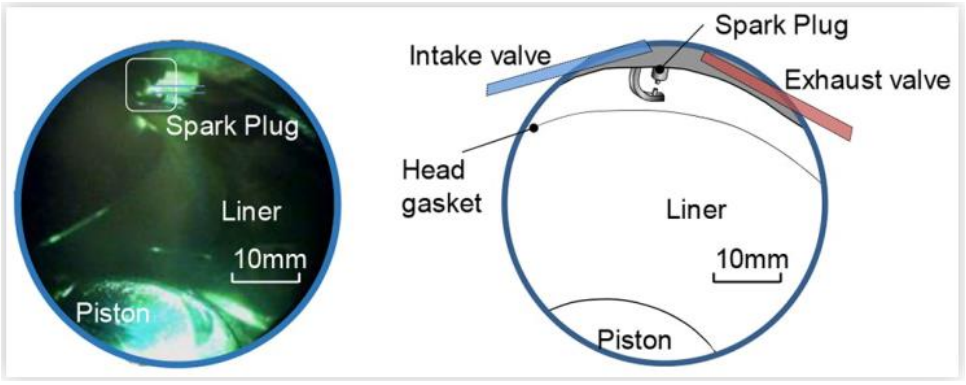

Figure 1-29 In-cylinder optical measurement area measured with the high-speed camera through borescope. [92]

In addition, due to the limit of the engine bench test, the initial flame formation during the ignition process still had not been studied very well. Moreover, the in-cylinder ambient environment parameters, such as gas flow velocity, gas composition, and ambient pressure et al., are challenging to separate and analyze independently due to the complexity of such parameter interactions. On the other hand, the mixture concentration in the vicinity of the spark plug is not always the same at every firing cycle, and under the actual engine bench test, the ignition swing also will alter the indicating parameters of engine performance. While the experiments in a constant volume combustion chamber (CVCC) help fill in the gap in this aspect. First of all, several studies have been conducted in the combustion chamber under static conditions. In Lee's study [94], as shown in Figure 1-30, the time-resolved current and voltage measurements of a spark discharge for a standard inductive automotive spark system were carried out in a combustion chamber. Spark duration was found to decrease as pressure and spark gap size were increased. Yu et al. [95] also carried out the experiment in a combustion chamber under the static condition, as shown in Figure 1-31, the relationship between spark discharge characteristics and different inductive spark ignition circuit parameters has been investigated in this research. The extracted secondary circuit resistance indicates that the ion channels which formed during the spark discharge would become more resistive as the back pressure increases. In Figure 1-32 [47], Kim's studies [46-48] have investigated the effects of the discharge method on ignition performance under the static condition.

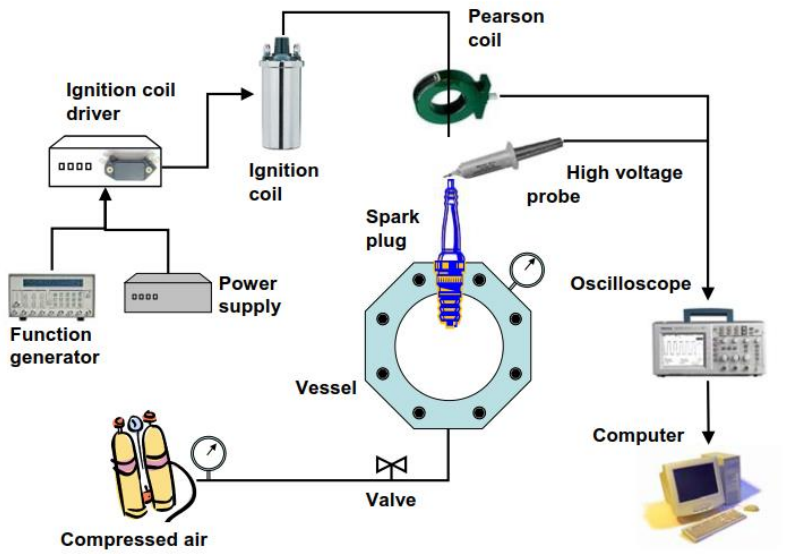

Figure 1-30 Schematic of the experimental setup. [94]

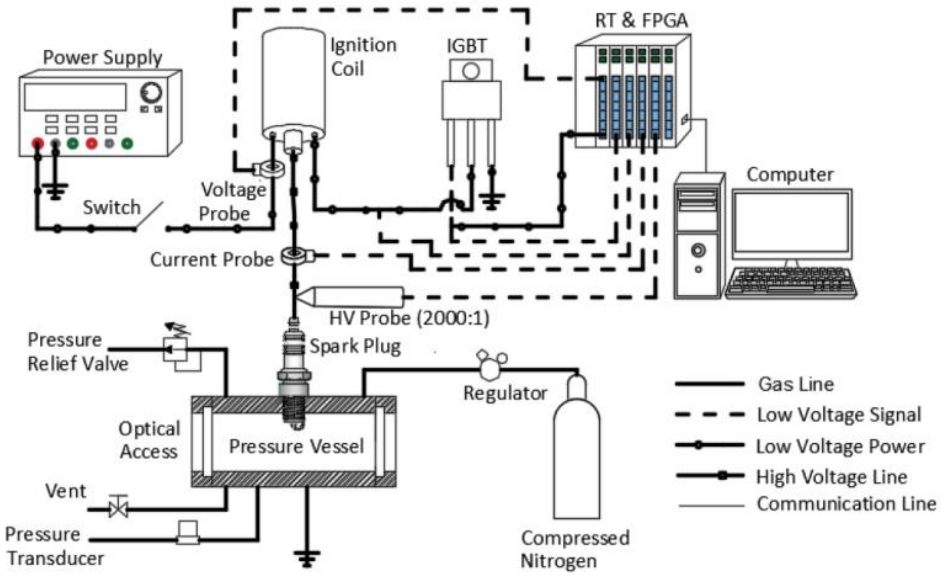

Figure 1-31 Experimental setup schematics. [95]

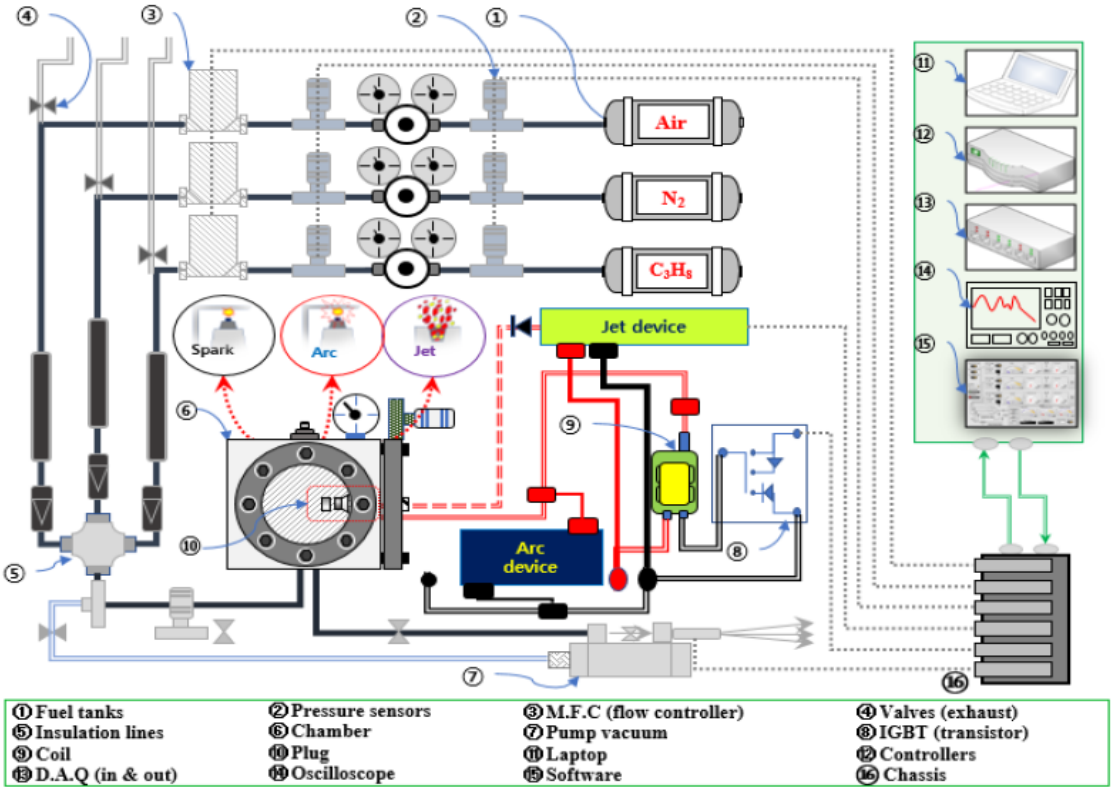

Figure 1-32 Schematic diagram of the static combustion system used in the experiment. [47]

Due to the static condition can only form the sphericity flame, as shown in Figure 1-33 [47], which is not imitated the in-cylinder conditions fully, other studies have considered the flow conditions and equipped the fan to generate the flow in the combustion chamber. In the re 1-34, Zhang et al. [96] used a combustion chamber equipped with a shrouded fan to investigate the ignition performance of a two-strike discharge ignition system under the flow condition, the effect of delay time between two strikes on the combustion has been also studied. Results demonstrated that the turbulent flow has the effect of wrinkling the initial flame kernel into several separate smaller sized flames.

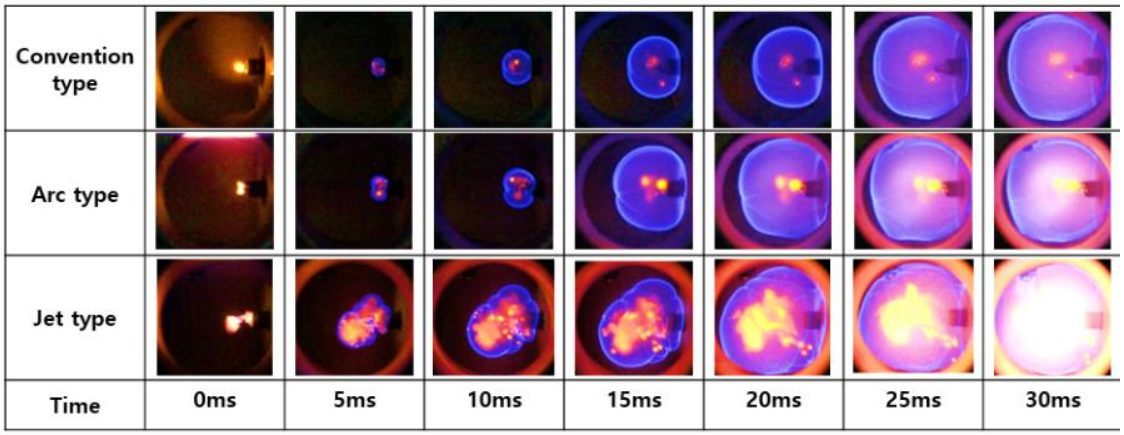

Figure 1-33 The sphericity flame in the combustion chamber under static conditions. [47]

With the development of the experimental method, the discharge channel behaviors under the flow conditions have been studied in recent years. In Shiraishi's research [97] [98], the discharge channel formation was studied under different flow velocities and gas pressure in a combustion chamber, as shown in Figure 1-35[98], the flow was generated by the fan installed at the combustion chamber. Results indicated that the discharge channel stretching follows the gas flow velocity closely under relatively high gas pressure, there is a strong correlation between the maximum spark channel length before the first restrike and the average discharge current until 1ms after the onset of discharge. Raising the discharge current makes it possible to lengthen the time to the first restrike and to increase the spark channel length. Schneider et al. [99] investigated the effect of the discharge current level and profile, and flow velocity on the discharge channel formation, results showed that a higher current stabilizes the discharge channel and increases the maximum elongation of the discharge channel.

Sayama et al. [100-105] focus on the discharge channel shorten behaviors, it had developed the model of discharge channel shorten behaviors, which has illustrated the fundamental reason for discharge channel shorten behaviors. Chang et al. [106] investigated the effect of excess air ratio on discharge channel shorten behaviors, and results have shown that combustible mixture makes the short-cut easy to occur and prevented restrike events. Whereas, the changes of initial flame formation owing to the discharge channel behaviors are not well understood. As shown in Figure 1-36 [107], Zhenyi Yang [107-109] et al. used the schlieren photography method to investigate the initial flame formation. The results indicated that an attached flame kernel could be formed by either increasing the discharge current or prolonging the discharge duration under the flow velocity of 25m/s.

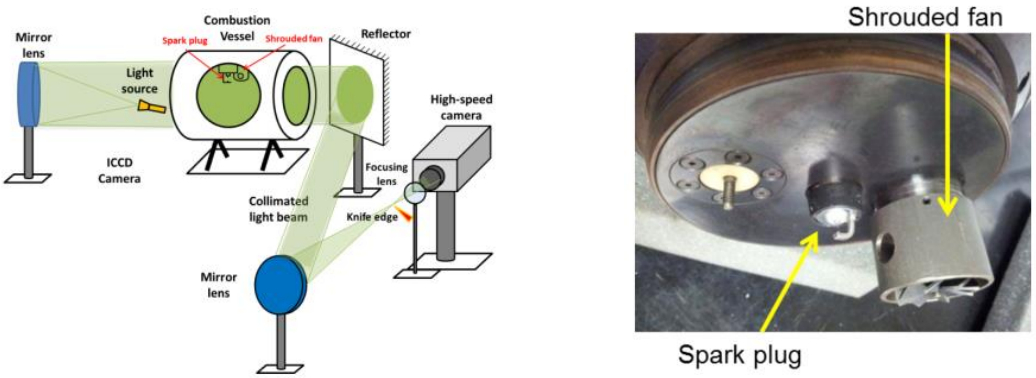

Figure 1-34 Experimental setup equipped with a shrouded fan. [96]

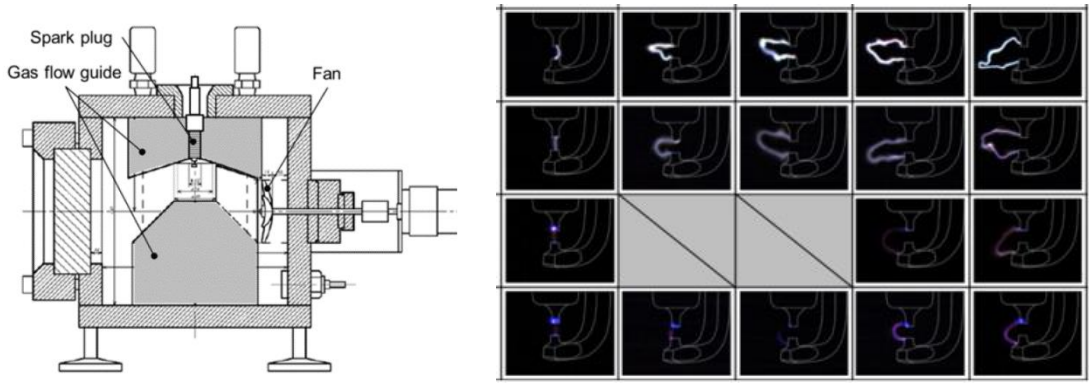

Figure 1-35 Experimental setup and the images of the discharge channel. [98]

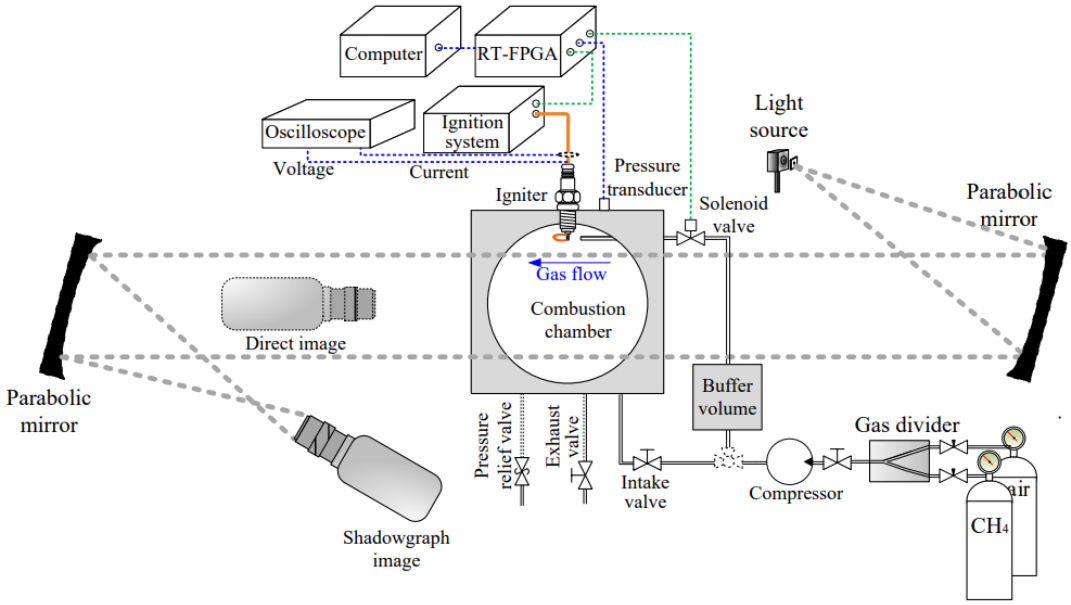

Figure 1-36 Schematic diagram of the optical combustion chamber test platform.[107]

1.6 Objectives of the thesis

Ignition systems are crucial for the future high efficiency clean spark-ignition engines, understanding the process of ignition and developing the advanced discharge strategies are both of great importance for developing the next generation ignition system. the main objectives of this work are shown as follows.

(1) For a better understanding of the ignition process, the simultaneous visualization by a high-speed infrared camera (FLIR X6900sc) and a conventional high-speed camera (FASTCAM SA-X) is built up to obtain deeper insights into the ignition process in a constant volume combustion chamber (CVCC).

(2) Study the effects of discharge strategies on the discharge channel behaviors and the initial flame formation during the ignition process by the simultaneous visualization method.

(3) Investigate the effects of discharge strategies on the ignition performance under different flow and dilute conditions.

(4) To confirm the suitable discharge strategies in the engine conditions, understanding the impacts of ignition performance on the EGR limit of the engine operation.

1.7 Outline of the thesis

The outlines of this thesis are shown as follows: Firstly, Chapter 1 introduces the background of this research, meanwhile, the challenges of the ignition system and the fundamentals and types of ignition techniques are also introduced. The experimental setup of CVCC is shown in Chapter 2, including constant volume combustion chamber (CVCC), ignition system, and a new simultaneous visualization method. Then, the visualization method is applied in the CVCC experiments. The effect of discharge current and discharge duration on the discharge channel behaviors and early flame formation are investigated by the simultaneous visualization method. In chapter 3, the impact of discharge characteristics on ignition performance under different diluted and flow conditions are studied. In addition, in order to confirm the results of CVCC in the actual engine conditions, the engine test is carried out on a four-stroke SI gasoline engine, the results of engine operation performance with different ignition coils under different flow conditions are shown in Chapter 4. Finally, the conclusions and future prospects are proposed in Chapter 5.

Reference

1. European Union. Worldwide Emission Standards and Related Regulations - Passenger Cars / Light and Medium Duty Vehicles. Cont Futur Motion 2019:210 pages.
2. Wang J, Wu Q, Liu J, et al. Vehicle emission and atmospheric pollution in China: problems, progress, and prospects. PeerJ. 2019;7:e6932. Published 2019 May 16. doi:10.7717/peerj.6932
3. Yang Z, Bandivadekar A. Light-duty vehicle greenhouse gas and fuel economy standards[J]. ICCT report, 2017.
4. An Y, Jaasim M, Raman V, et al. Homogeneous charge compression ignition (HCCI) and partially premixed combustion (PPC) in compression ignition engine with low octane gasoline[J]. Energy, 2018, 158: 181-191.
5. Bendu H, Murugan S. Homogeneous charge compression ignition (HCCI) combustion: Mixture preparation and control strategies in diesel engines[J]. Renewable and Sustainable Energy Reviews, 2014, 38: 732-746.
6. Yasuo MORIYOSHI TK. Recent Progress in HCCI Combustion for a Practical Usage as a Gasoline Engine. J Automot Saf Energy 2012;3:105 — 115. doi:10.3969/j.issn.1674-8484.2012.02.002.
7. Park C, Kim S, Kim H, et al. Stratified lean combustion characteristics of a spray-guided combustion system in a gasoline direct injection engine[J]. Energy, 2012, 41(1): 401-407.
8. M. Bunce, et al., The Effects of Turbulent Jet Characteristics on Engine Performance Using a Pre-Chamber Combustor, SAE Technical Paper, 2014
9. F.A. Rodrigues Filho, et al.E25 stratified torch ignition engine performance, CO_2 emission and combustion analysis Energy Convers. Manage., 115 (2016), pp. 299-307
10. J. B. Heywood, “Internal combustion engines fundamentals”, Mc Graw Hill, ISBN 0-07-100499-8, 1988.
11. ZHANG G, Mu S, DENG K, QU S. Development and application of low concentration minegas engine. CIMAC 2013, NO.62.
12. WANG Z, LIU H, REITZ R D. Knocking combustion in spark-ignition engines[J]. Progress in Energy and Combustion Science, 2017, 61:78-112.
13. TSUBOI S, MIYOKAWA S, MATSUDA M, et al. Influence of spark discharge characteristics on ignition and combustion process and the lean operation limit in a spark ignition engine. Applied Energy, 2019, 250:617-32.

14. LI T, YIN T, WANG B. A phenomenological model of knock intensity in spark-ignition engines[J]. Energy Conversion and Management, 2017, 148:1233-47.
15. Masahide T., Yoshio T. Study of Internal EGR Control Using Variable Valve Timing. Marine Engineering, 2004, Vol 39, No 10, pp:706-712. DOI: 10.5988/jime.39.706.
16. Wei H, Zhu T, Shu G, et al. Gasoline engine exhaust gas recirculation–a review[J]. Applied energy, 2012, 99: 534-544.
17. Alger, T., et al.: Cooled exhaust-gas recirculation for fuel economy and emissions improvement in gasoline engines, International Journal of Engine Research, 12.3, p.252-264 (2011).
18. Alger, Terrence, et al.: The role of EGR in PM emissions from gasoline engines, SAE International Journal of Fuels and Lubricants, 3.1, p. 85-98 (2010).
19. Ming Zheng, et al: Advanced Ignition Systems for Future Clean Combustion Engines: Review. Journal Automotive Safety and Energy, Vol. 6, No. 4. 2015
20. Zhu, H., Wang, L., Yang, Z., Liang, L. et al., Investigation of Flame Detachment Effect during Early Flame Development in a Swirl Flow Field, SAE Technical Paper 2021-01-0482, 2021, https://doi.org/10.4271/2021-01-0482.
21. Zhao F, Lai M C, Harrington D L. Automotive spark-ignited direct-injection gasoline engines[J]. Progress in energy and combustion science, 1999, 25(5): 437-562.
22. SN PLUS & LSPI – What You Need to Know, https://www.tyreeoil.com/news/sn-plus-amp-lspi-what-you-need-to-know
23. Shuai S, Ma X, Li Y, et al. Recent progress in automotive gasoline direct injection engine technology[J]. Automotive Innovation, 2018, 1(2): 95-113.
24. Mitroglou N, Nouri J M, Yan Y, et al. Spray structure generated by multi-hole injectors for gasoline direct-injection engines[R]. SAE Technical Paper, 2007.
25. Leng X, Jin Y, He Z, et al. Numerical study of the internal flow and initial mixing of diesel injector nozzles with V-type intersecting holes[J]. Fuel, 2017, 197: 31-41.
26. Leng X, Jin Y, He Z, et al. Effects of V-type intersecting hole on the internal and near field flow dynamics of pressure atomizer nozzles[J]. International Journal of Thermal Sciences, 2018, 130: 183-191.
27. Tang Y, Deng W, Liu B, et al. The new Changan inline 4-cylinder 1.6 L gasoline naturally aspirated GDI engine[R]. SAE Technical Paper, 2018.
28. Park C, Kim S, Kim H, et al. Stratified lean combustion characteristics of a spray-guided combustion system in a gasoline direct injection engine[J]. Energy, 2012, 41(1): 401-407.

29. Bae C, Kim J. Alternative fuels for internal combustion engines[J]. Proceedings of the Combustion Institute, 2017, 36(3): 3389-3413.
30. Agarwal A K. Biofuels (alcohols and biodiesel) applications as fuels for internal combustion engines[J]. Progress in energy and combustion science, 2007, 33(3): 233-271.
31. Gong C, Li Z, Yi L and Liu F. Comparative study on combustion and emissions between methanol port-injection engine and methanol direct-injection engine with H2-enriched port-injection under lean-burn conditions. Energy Conversion and Management. 2019; 200: 112096.
32. Verhelst S, Turner J W G, Sileghem L, et al. Methanol as a fuel for internal combustion engines[J]. Progress in Energy and Combustion Science, 2019, 70: 43-88.
33. Moriarty, K. Handbook for Handling, Storing, and Dispensing E85 and Other Ethanol-Gasoline Blends[B], 2013-09-01
34. Shapur talks about the downsides of the downsizing trend on engines for India. Is downsizing dead? https://www.autocarindia.com/auto-blogs/is-downsizing-dead-410640
35. Patil C, Varade S, Wadkar S. A review of engine downsizing and its effects[J]. International Journal of Current Engineering and Technology, 2017, 7(7): 319-324.
36. Clenci A C, Descombes G, Podevin P, et al. Some aspects concerning the combination of downsizing with turbocharging, variable compression ratio, and variable intake valve lift[J]. Proceedings of the Institution of Mechanical Engineers, Part D: Journal of Automobile Engineering, 2007, 221(10): 1287-1294.
37. Isenstadt A, German J, Dorobantu M, et al. Downsized, boosted gasoline engines[J]. The international council on clean transportation, 2016.
38. Wirth M, Mayerhofer U, Piock W F, et al. Turbocharging the DI gasoline engine[J]. SAE transactions, 2000: 146-155.
39. J. B. Heywood, “Internal combustion engines fundamentals”, Mc Graw Hill, ISBN 0-07-100499-8, 1988.
40. Yu S, Zheng M. Future gasoline engine ignition: A review on advanced concepts. International Journal of Engine Research. 2021;22(6):1743-1775. doi:10.1177/1468087420953085
41. Maly RR and Herweg R. Spark ignition and combustion in four-stroke gasoline engines. In: Arcoumanis C and Kamimoto T (eds) Flow and combustion in reciprocating engines, experimental fluid mechanics. Berlin: Springer, 2008.
42. Nishioka S, Hanashi K and Okabe S. Super ignition spark plug with wear resistive electrode. SAE technical paper 2008-01-0092, 2008.

43. ZHENG, Ming; SHUI, Y. U. Advanced ignition systems for future clean combustion engines. Journal of Automotive Safety and Energy, Vol. 6, No. 04 pp: 295-313 2015
44. Y. Abe, A. Sugiura, K. Doi, M. Shibata, N. Yokoo, K. Nakata, “Study of ignition system for demand voltage reduction”, SAE Technical Paper 2015-01-0777, 2015, doi: 10.4271/2015-01-0777.
45. Zhu, Hua, Spark Energy and Transfer Efficiency Analyses on Various Transistor Coil Ignition Systems (2018). Electronic Theses and Dissertations of University of Windsor. 7456.
46. Kim, K., Askari, O. Understanding the effect of capacitive discharge ignition on plasma formation and flame propagation of air–propane mixture. Journal of Energy Resources Technology, (2019). 141(8).12
47. Choe, M. S., Kim, K. S., Choi, D. S. Study on flame propagation characteristics according to new ignition-source in a constant volume combustion chamber. In Defect and Diffusion Forum (2019). Vol. 391, pp. 142-151. Trans Tech Publications Ltd.12
48. Kim, K. S., Lee, K. T., Choe, M. S., Choi, D. S. Understanding of the Spark Effect of Electron Collision by a Capacitive Discharge Ignition in a Constant Volume Combustion Chamber. International Journal of Automotive Technology, (2020), 21(1), 249-257.12
49. Yoshida, K., Shoji, H., Tanaka, H. Performance of newly developed plasma jet igniter. SAE transactions, 2021-2032.12, (1999)
50. Han, S. B., Choi, K. H., Ra, S. O., Lee, S. J., Lee, J. T. Ignitability and combustion characteristics of the multi spark capacitor discharge ignitor for a lean burn engine (No. 952396). SAE Technical Paper. (1995).
51. Yu, S., Xie, K., Tan, Q., Wang, M., Zheng, M. Ignition improvement of premixed methane-air mixtures by distributed spark discharge (No. 2015-01-1889). SAE Technical Paper. (2015).
52. Nishiyama A, Wachi Y, Ikeda Y, et al. Combustion improvement by using combination of high performance ignition system and microwave plasma system [C]// 8th Int’l Conf Modeling and Diagnostics for Adva Engine Syst, July 23-26, 2012, Fukuoka, Japan.
53. Heise, V., Farah, P., Husted, H., Wolf, E. High frequency ignition system for gasoline direct injection engines (No. 2011-01-1223). SAE Technical Paper. (2011).
54. CHANG J-S, LAWLESS P A, YAMAMOTO T. Corona discharge processes. IEEE Transactions on plasma science, 1991, 19(6): 1152-66.12
55. WANG L. Characterization of Corona Discharge for Ignition Improvement. University of Windsor, 2019.

56. SUESS M, GUENTHNER M, SCHENK M, et al. Investigation of the potential of corona ignition to control gasoline homogeneous charge compression ignition combustion[J]. Proceedings of the Institution of Mechanical Engineers, Part D: Journal of Automobile Engineering, 2012, 226(2): 275-86.
57. Burrows, J., Mixell, K., Reinicke, P. B., Riess, M., Sens, M. Corona ignition-assessment of physical effects by pressure chamber, rapid compression machine, and single cylinder engine testing. In 2nd International Conference on Ignition Systems for Gasoline Engines. (2014, November).
58. Bellenoue, M., Labuda, S., Ruttun, B. and Sotton, J. (2007) spark plug and corona abilities to ignition stoichiometric and lean methane/air mixtures, Combustion Science and Technology, 179:3, pp: 477-496, DOI:10.1080/00102200600637584.
59. PAVEL N, TSUNEKANE M, TAIRA T. All-poly-crystalline ceramics nd: yag/cr4+: yag monolithic micro-lasers with multiple-beam output[J]. Laser Systems for Applications, 2011, 9:59-82.
60. Eiichi T. Hirokazu K. Hirohide F. Advanced ignition technology for the achievement of high thermal efficiency of internal combustion engine. December 2015 Synthesiology 8(4):190-199 DOI: 10.5571/synth.8.4_190
61. Shui Y., Ming Z. Future gasoline engine ignition: A review on advanced concepts. International Journal of Engine Research, 2021;22(6):1743-1775. DOI:10.1177/1468087420953085
62. Huang, S. Study on ignition characteristic and mechanism of lean mixture based on the flexible discharge. Dissertation Submitted to Shanghai Jiao Tong University for the Degree of Doctor, 2021.
63. Alger, T., Gingrich, J., Mangold, B., Roberts, C. (2011). A continuous discharge ignition system for EGR limit extension in SI engines. SAE International Journal of Engines, 4(1), 677-692.
64. Alger, T., Gingrich, J., Roberts, C., Mangold, B., Sellnau, M. (2013). A high-energy continuous discharge ignition system for dilute engine applications. SAE Technical Paper. 2013-01-1628.
65. Gukelberger, R., Alger, T., Gingrich, J., and Mangold, B., Impact of Operating Parameters on Ignition System Energy Consumption, SAE Technical Paper 2014-01-1233, 2014, DOI:10.4271/2014-01-1233.
66. Gao, H., Matthews, R. D., Hall, M. J., Hari, S. From Spark Plugs to Railplugs—The Characteristics of a New Ignition System. SAE transactions, 1546-1556. 2004.

67. Yu, X., Yang, Z., Yu, S., huo, X. et al., Boosted Current Spark Strategy for Lean Burn Spark Ignition Engines, SAE Technical Paper 2018-01-1133, 2018, DOI:10.4271/2018-01-1133.
68. Hayashi, N., Sugiura, A., Abe, Y., Suzuki, K. Development of ignition technology for dilute combustion engines. SAE International Journal of Engines, 10(3), 984-994. 2017.
69. Jung, D., Sasaki, K., Sugata, K., Matsuda, M., Yokomori, T., Iida, N. Combined effects of spark discharge pattern and tumble level on cycle-to-cycle variations of combustion at lean limits of SI engine operation. SAE technical papers, 2017(March).
70. Jung, D., Sasaki, K., Iida, N. Effects of increased spark discharge energy and enhanced in-cylinder turbulence level on lean limits and cycle-to-cycle variations of combustion for SI engine operation. Applied energy, 205, 1467-1477. 2017.
71. Chen, W., Madison, D., Dice, P., Naber, J., Chen, B., Miers, S., Huberts, G. Impact of ignition energy phasing and spark gap on combustion in a homogenous direct injection gasoline SI engine near the EGR limit. SAE technical papers, 2013-01-1630. DOI:10.4271/2013-01-1630.
72. Dahms, R., Fansler, T. D., Drake, M. C., Kuo, T. W., Lippert, A. M., Peters, N. Modeling ignition phenomena in spray-guided spark-ignited engines. Proceedings of the Combustion Institute, 32(2), 2743-2750. 2009. DOI: 10.1016/j.proci.2008.05.052
73. Dahms, R. N., Drake, M. C., Fansler, T. D., Kuo, T. W., Peters, N. Understanding ignition processes in spray-guided gasoline engines using high-speed imaging and the extended spark-ignition model SparkCIMM. Part A: Spark channel processes and the turbulent flame front propagation. Combustion and flame, 158(11), 2229-2244. 2011. DOI: 10.1016/j.combustflame.2011.03.012
74. Dahms, R. N., Drake, M. C., Grover Jr, R. O., Solomon, A. S., Fansler, T. D. Detailed simulations of stratified ignition and combustion processes in a spray-guided gasoline engine using the SparkCIMM/G-equation modeling framework. SAE International Journal of Engines, 5(2), 141-161. 2012.
75. Dahms, R. N., Drake, M. C., Fansler, T. D., Kuo, T. W., Peters, N. Understanding ignition processes in spray-guided gasoline engines using high-speed imaging and the extended spark-ignition model SparkCIMM. Part B: Importance of molecular fuel properties in early flame front propagation. Combustion and flame, 158(11), 2245-2260. 2011. DOI: 10.1016/j.combustflame.2011.04.003

76. Peterson, B., Reuss, D. L., Sick, V. On the ignition and flame development in a spray-guided direct-injection spark-ignition engine. Combustion and Flame, 161(1), 240-255. 2014. DOI: 10.1016/j.combustflame.2013.08.019
77. Peterson, B., Reuss, D. L., Sick, V. High-speed imaging analysis of misfires in a spray-guided direct injection engine. Proceedings of the Combustion Institute, 33(2), 3089-3096. 2011. DOI: 10.1016/j.proci.2010.07.079
78. Peterson, B., & Sick, V. High-speed flow and fuel imaging study of available spark energy in a spray-guided direct-injection engine and implications on misfires. International Journal of Engine Research, 11(5), 313-329. 2010. DOI: 10.1243/14680874JER587
79. Martinez, S., Irimescu, A., Merola, S. S., Lacava, P., Curto-Riso, P. Flame front propagation in an optical GDI engine under stoichiometric and lean burn conditions. Energies, 10(9), 1337. 2017. DOI: 10.3390/en10091337
80. Irimescu, A., Merola, S., and Martinez, S., "Influence of Engine Speed and Injection Phasing on Lean Combustion for Different Dilution rates in an Optically Accessible Wall Guided Spark Ignition Engine," SAE Technical Paper 2018-01-1421, 2018. DOI:10.4271/2018-01-1421.
81. Wang, Y., Zhang, J., Yang, Z., Wang, X., Dice, P., Shahbakhti, M., Huberts, G. Investigation of flow conditions and tumble near the spark plug in a DI optical engine at ignition. SAE Technical Paper 2018-01-0208, 2018, DOI:10.4271/2018-01-0208.
82. Afkhami, B., Wang, Y., Miers, S. A., Naber, J. D. Experimental determination of flame speed and flame stretch using an optically accessible, spark-ignition engine. International Journal of Engine Research, 22(3), 856-872. 2021.
83. Wang, Y., Zhang, J., Wang, X., Dice, P., Shahbakhti, M., Naber, J., Huberts, G. Investigation of Impacts of Spark Plug Orientation on Early Flame Development and Combustion in a DI Optical Engine. SAE International Journal of Engines, 10(3). 2017. doi:10.4271/2017-01-0680
84. Badawy, T., Bao, X., & Xu, H. Impact of spark plug gap on flame kernel propagation and engine performance. Applied Energy, 191, 311–327. 2017.01.059. DOI: 10.1016/j.apenergy.
85. Philipp Schiffmann, Volker Sick, David Reuss. Empirical Investigation of Spark-Ignited Flame-Initiation Cycle-to-Cycle Variability in a Homogeneous-Charge Reciprocating Engine. International Journal of Engine Research, SAGE Publications (UK and US), 2018, 19 (5), pp.491-508. DOI: 0.1177/1468087417720558.

86. Nishiyama, A., et al.: The relationship between in-cylinder flow-field near spark plug areas, the spark behavior, and the combustion performance inside an optical SI engine, Applied Sciences, 9.8, 1545 (2019). DOI:10.3390/app9081545
87. Hokimoto, S., Kuboyama, T., Moriyoshi, Y., Iida, M., Watanabe, T. Analyses of Cycle-to-Cycle Variation of Combustion and In-Cylinder Flow in a Port Injection Gasoline Engine Using PIV and PLIF Techniques. In International Powertrains, Fuels & Lubricants Meeting (No. 2017-01-2213).
88. Mazacioglu, A., Gross, M., Kern, J., Sick, V. Infrared Borescopic Evaluation of High-Energy and Long-Duration Ignition Systems for Lean/Dilute Combustion in Heavy-Duty Natural-Gas Engines. (2018). SAE Technical Paper Series. DOI:10.4271/2018-01-1149
89. Sick, V., Henrion, L., Mazacioglu, A., & Gross, M. (2018). Time-resolved infrared imaging and spectroscopy for engine diagnostics. 2018-06-26
90. Gross, M., Mazacioglu, A., Kern, J., Sick, V. (2018). Infrared Borescopic Analysis of Ignition and Combustion Variability in a Heavy-Duty Natural-Gas Engine. 2018-04-03. DOI: 10.4271/2018-01-0632
91. Tsuboi, S., Miyokawa, S., Matsuda, M., Yokomori, T., Iida, N. Influence of spark discharge characteristics on ignition and combustion process and the lean operation limit in a spark ignition engine. Applied Energy, 250, 617-632. 2019. DOI: 10.1016/j.apenergy.2019.05.036
92. Oryoji, K., Uchise, Y., Akagi, Y., Qingchu, C., Kuboyama, T., Moriyoshi, Y. In-Cylinder Optical Measurement for Analyzing Control Factor of Ignition Phenomena under Diluted Condition. SAE Technical Paper, 2020, No. 2020-01-2048.
93. Kazuhiro, O., Yoshihiko, A., Yoshifumi, U., Yuyu, Z., Tatsuya, K., Yasuo, M. Analysis on control factors of air-fuel ratio limit by using in-cylinder optical measurement. Transactions of the JSME, 2018, Vol 84, No. 863, 1-12.
94. Lee, M. J., Hall, M., Ezekoye, O. A., Matthews, R. D. (2005). Voltage, and energy deposition characteristics of spark ignition systems (No. 2005-01-0231). SAE Technical Paper.
95. Yu, S., Tan, Q., Ives, M., Liu, M., Li, L., Chen, X., Zheng, M. (2016). Parametric analysis of ignition circuit components on spark discharge characteristics (No. 2016-01-1011). SAE Technical Paper. DOI: 10.4271/2016-01-1011
96. Zhang, A., Cung, K., Lee, S. Y., Naber, J., Huberts, G., Czekala, M., Qu, Q. (2013). The impact of spark discharge pattern on flame initiation in a turbulent lean and dilute mixture in a

pressurized combustion vessel. SAE International Journal of Engines, 6(1), 435-446. DOI:10.4271/2013-01-1627.

97. Shiraishi, T., Teraji, A., Moriyoshi, Y. (2015). The effects of ignition environments and discharge waveform characteristics on spark channel formation. Transactions of Society of Automotive Engineers of Japan, 46(2).
98. Shiraishi, T., Teraji, A., & Moriyoshi, Y. (2016). The effects of ignition environment and discharge waveform characteristics on spark channel formation and relationship between the discharge parameters and the EGR combustion limit. SAE International Journal of Engines, 9(1), 171-178. DOI:10.4217/2015-01-1895.
99. Schneider, A., Leick, P., Hettinger, A., Rottengruber, H. (2016). Experimental studies on spark stability in an optical combustion vessel under flowing conditions. In Internationaler Motorenkongress 2016 (pp. 327-348). Springer Vieweg, Wiesbaden.
100. Sayama, S., Kinoshita, M., Mandokoro, Y., Masuda, R., Fuyuto, T. (2018). Modelling on Spark Shortening under High-velocity Flow Conditions (First Report). Transactions of Society of Automotive Engineers of Japan, 49(4).
101. Masuda, R., Sayama, S., Fuyuto, T., Nagaoka, M., Noguchi, Y., Sugiura, A. (2018). Modelling on Spark Shortening under High-velocity Flow Conditions (Second Report). Transactions of Society of Automotive Engineers of Japan, 49(4).
102. Masuda, R., Sayama, S., Fuyuto, T., Nagaoka, M., Sugiura, A., Noguchi, Y. (2018). Application of models of short circuits and blow-outs of spark channels under high-velocity flow conditions to spark ignition simulation (No. 2018-01-1727). SAE Technical Paper. DOI: 10.4271/2018-01-1727.
103. Sayama, S., Kinoshita, M., Mandokoro, Y., Fuyuto, T. (2019). Spark ignition and early flame development of lean mixtures under high-velocity flow conditions: an experimental study. International Journal of Engine Research, 20(2), 236-246. DOI: 10.1177/1468087417748517.
104. Sayama, S., Kinoshita, M., Mandokoro, Y., Masuda, R., Fuyuto, T. (2018). Quantitative Optical Analysis and Modelling of Short Circuits and Blow-Outs of Spark Channels under High-Velocity Flow Conditions (No. 2018-01-1728). SAE Technical Paper. DOI: 10.4271/2018-01-1728.
105. Huang, S., Li, T., Wang, N., Wang, X., Yang, Z., Yu, X., Zheng, M. (2020). Experimental Study on the Characteristics of Short Circuits and Restrikes of Spark Channels (No. 2020-01-1123). SAE Technical Paper. DOI: 10.4271/2020-01-1123.

106. Chang, Y., Li, X., Yu, S., Zheng, M., Xu, M., Effect of discharge current boost on ignition and combustion under cross flow conditions, Combustion and Flame, Vol. 223, (2021), pp. 1-14, DOI: 10.1016/j.combustflame.2020.09.011.
107. Yang, Z., Yu, X., Yu, S., Chen, J., Chen, G., Zheng, M., Ting, D. S. K. (2018, November). Impacts of spark discharge current and duration on flame development of lean mixtures under flow conditions. In Internal Combustion Engine Division Fall Technical Conference (Vol. 51982, p. V001T03A032). American Society of Mechanical Engineers. DOI: 10.1115/ICEF2018-9771.
108. Yang, Z., Yu, X., Zhu, H., Ting, D. S., Zheng, M. (2020). Effect of spark discharge energy scheduling on ignition under quiescent and flow conditions. Proceedings of the Institution of Mechanical Engineers, Part D: Journal of Automobile Engineering, 234(12), 2878-2891. DOI: 10.1177/0954407020915976.
109. Z. Yang, H. Zhu, X. Yu, M. Zheng and D. S. -K. Ting, Spark Plasma in Different Gas Media Under Flow Conditions, in IEEE Transactions on Plasma Science, vol. 48, no. 1, pp. 104-108, Jan. 2020, DOI: 10.1109/TPS.2019.2960154.

Chapter 2 Effects of discharge characteristic on the ignition process

2.1 Constant volume combustion chamber

The experimental study has been carried out in a cubical optically accessible constant volume combustion chamber (CVCC). Due to the limit of the combustion chamber design, many studies [1-5] investigate the ignition process in a combustion chamber under the static condition, thus, only the sphericity flame can be formed, which is not imitated in the in-cylinder conditions fully. However, as shown in Figure 2-1, in this research, the combustion chamber has equipped with a motor at the rear of the chamber, and the rotating speed of the motor can be read and controlled. In Figure 2-2 of the internal structure of the chamber. The CVCC features a pancake internal combustion chamber with a 60 cm3 internal volume. Four pieces of sapphire windows are mounted in the four directions of the cubical CVCC. A commercially available spark plug (NGK DILKAR7C9H) with a 0.9 mm gap between the electrodes is installed at the top of the CVCC. The motor is connected with a fan for generating cross-flow in the chamber, the flow intensity can be varied by controlling the rotating speed of the fan.

Figure 2-3 shows the right and left sides of the combustion chamber with the equipment assembly. On the right side of the chamber, a highly sensitive pressure sensor (Kistler 7061B) is installed at the lower right of the chamber, due to the small volume of the combustion chamber, the slight pressure variation can be detected during the ignition process via this highly sensitive pressure sensor. In addition, the stainless-steel body of the CVCC is equipped with four water pipes for the circulating water, which can keep the temperature of the CVCC by controlling the temperature of the circulating water. On the left side of the chamber, a temperature sensor is installed at the lower left of the chamber, the internal combustion temperature data can be stored during the ignition process. the gas port is designed at the top left of the chamber, it is used to let the mixture gas enter the combustion chamber before the ignition, and exhaust the gas after the combustion.

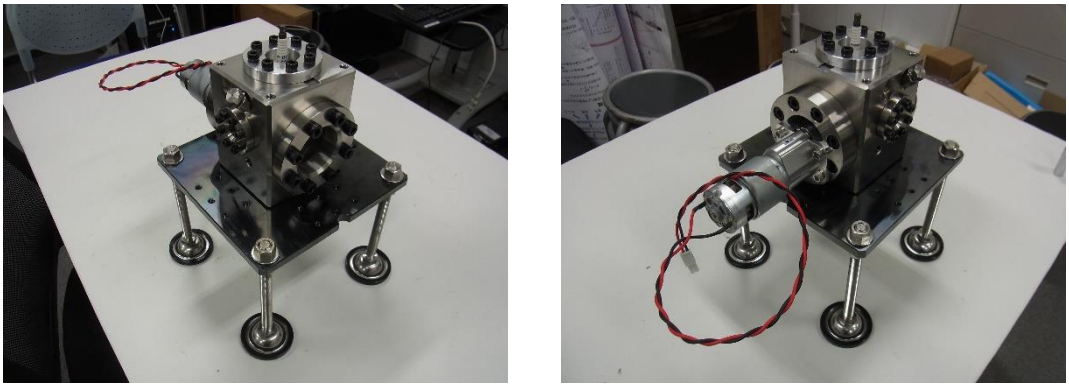

Figure 2-1 The external structure of the constant volume combustion chamber

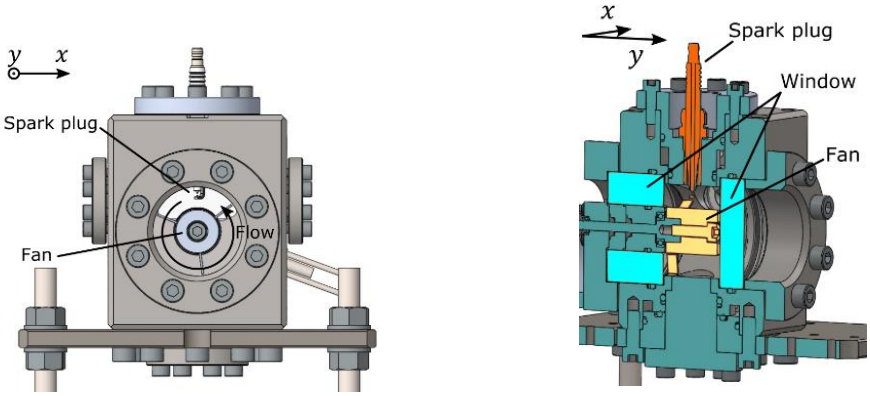

Figure 2-2 The internal structure of the constant volume combustion chamber

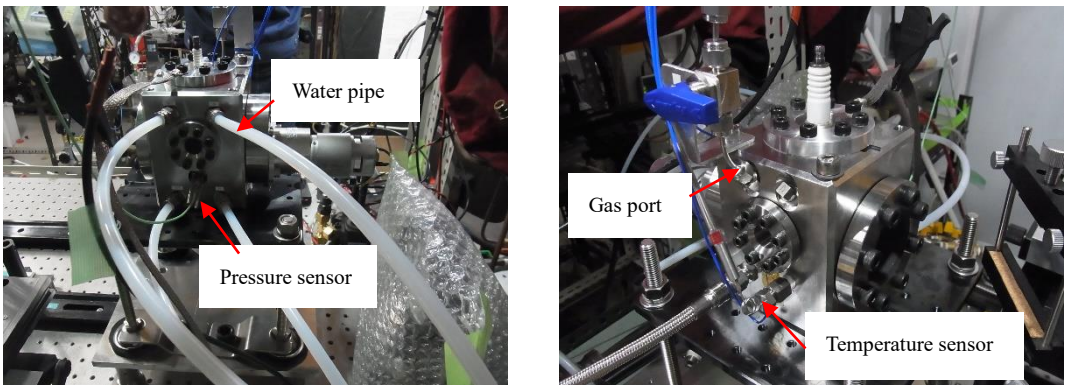

a. Right side b. Left side

Figure 2-3 The Equipment assembly of the constant volume combustion chamber

2.2 Ignition system

2.2.1 Discharge measurement

As shown in Figure 2-4, the ignition system mainly includes an oscilloscope, a high-voltage probe (Tektronix-P6015A), a current probe (Pearson 110A Current Monitors), and a coil. The current probe directly measures the secondary current on the spark plug, and the high-voltage probe measures the secondary voltage on the spark plug electrode cable. The probe characteristics are shown in Table 2-2 and Table 2-3, respectively. The oscilloscope (Tektronix DPO4034B) can record the voltage and current of the entire discharge process, and the ignition energy of different ignition coils can be obtained through integral calculation.

The discharge energy of the ignition coil can be calculated via equation (1), where E stands for the total discharge energy; V is the second discharge voltage; I secondly discharge current; t is the discharge during.

$$E_{total} = \int_0^t v \cdot I \, dt \tag{1}$$

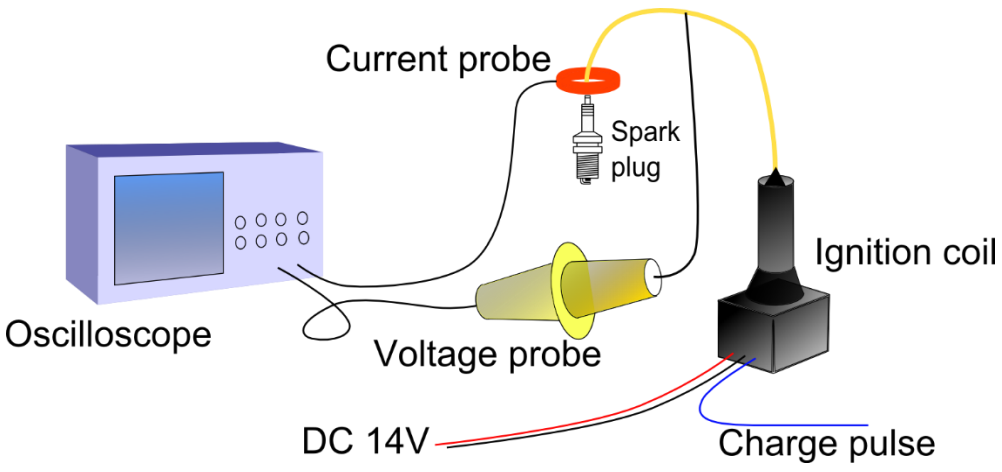

Figure 2-4 Schematic of the discharge waveform measurement

Table 2-2 Specification of the high voltage probe

Maximum input voltage DC + Peak AC Peak pulse	 20 kV 40 kV
Rise time	4.67 ns
Loading	100MΩ / 3 pF
Attenuation	1000: 1 ±3%

Table 2-3 Specification of the current probe

Sensitivity	0.1 V/A +1 / -0 %
Maximum peak current	10 kA
Maximum RMS current	65 A
Rise time	20 ns
Frequency range	1 Hz ~ 20 MHz

2.2.2 Ignition coils

Figure 2-5 shows the appearance of different types of ignition coils, this study tries to use three types of ignition coils to conduct the experiments. The waveform of discharge characteristics for the ignition coils is shown in Figure 2-6. This research takes coil A as the standard coil, coil B as the high current coil, and coil C as the high energy coil. The detailed specifications of the coils are shown in table 1. As described in Table 2-4, coil A and coil B have almost the same ignition energy, and coil C is the highest energy one. However, coil C has almost the same discharge duration as coil A, and coil B is much shorter than coil A and coil C. Coil B and coil C had almost the same discharge current which is much higher than coil A.

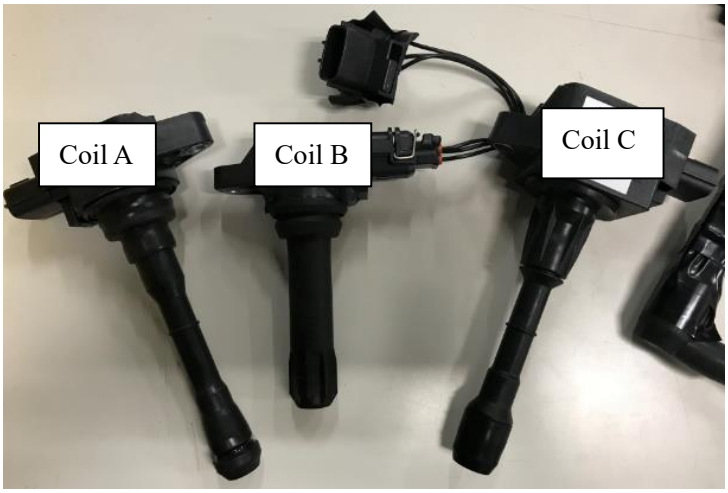

Figure 2-5 Types of ignition coils

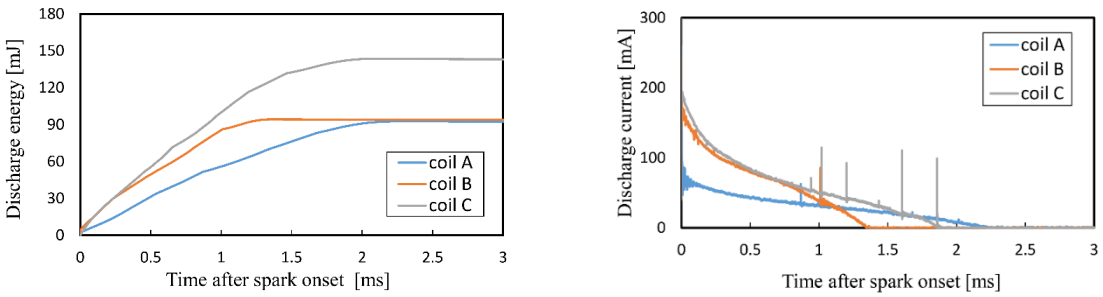

a. Discharge energy b. Discharge current

Figure 2-6. Discharge characteristics of the ignition coils

Table 2-4. Detail specifications of the ignition coils

	Coil A	Coil B	Coil C
Discharge current[mA]	65	170	180
Discharge duration[ms]	2.2	1.3	1.9
Ignition energy[mJ]	95.0	95.0	165.0

2.2.3 Spark plug

As shown in Figure 2-7, the spark plug in this study is a commercially available spark plug (NGK DILKAR7C9H), the specification of the spark plug is described in Table 2-5, and the material of the center electrode is iridium with the diameter of 0.55mm, the thread length of this spark plug is 28.5mm, and the spark plug gap between the discharge electrodes is 0.9mm.

Figure 2-7 Overview of spark plug

Table 2-5 Specification of spark plug

Electrode diameter – material Center electrode	 φ0.55 mm – Iridium
Nominal designation of thread × width across flat	M12 × 12.0 mm
Thread length	28.5 mm
Thermal value	7 (NGK)
Internal resistance	5 kΩ
Spark plug gap	0.9 mm

2.3 Gas mixture and test conditions

2.3.1 Gas mixture production

As shown in Figure 2-8, in order to control the composition of the mixture and reduce the experimental error, a gas mixing chamber was used to make the gas mixture. The chamber was equipped with a fan to stir and mix the gas during the mixture production.

In the test of the constant volume combustion chamber, propane was used as the fuel. According to Figure 2-9, the composition of the gas mixture is set by the experimental conditions. First of all, a vacuum pump was used for removing all the air in the mixture chamber, until it was in a vacuum state; Then, open the valve of the propane tank for letting the propane into the mixing chamber, and the pressure sensor of the mixture chamber controls the gas mass of the propane, and close the valve when the chamber has reached the target pressure; After that, repeat the operation to fill the oxygen and nitrogen into mixing chamber; Finally, close all the valves of the gas tank, keep the mixture chamber stand for 10 minutes and wait for all the gas mix well. Oxygen and nitrogen were used to imitate the air; nitrogen was added to imitate the dilute condition.

Figure 2-8 The gas mixture chamber

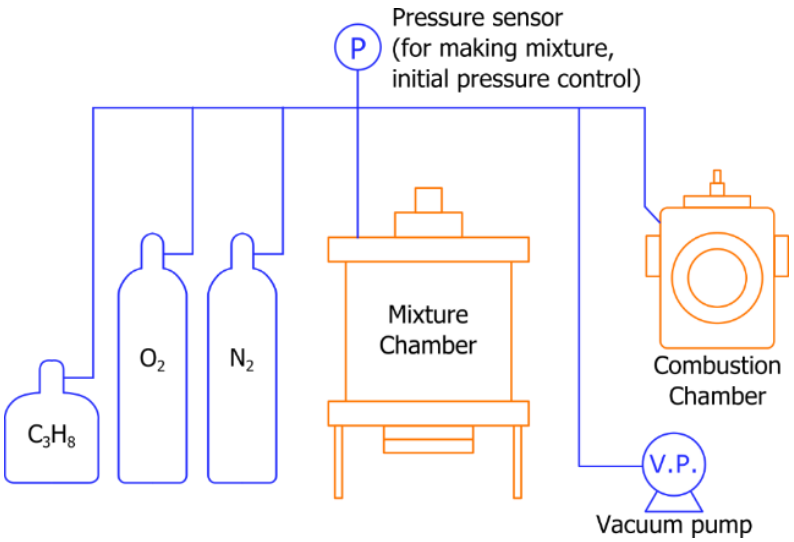

Figure 2-9 schematic of the gas mixture production

2.3.2 Test conditions

Test conditions are listed in Table 2-6. The temperature of the combustion chamber is fixed at 358 K. Air-propane mixture with an equivalence ratio of 0.65 is used in the experiment, because the equivalence ratio of 0.65 is around the lean limit of coil A in the combustion chamber. The initial pressure is constant at 400 kPa for ensuring the initial conditions are consistent before each test, steady flow velocities are 8m/s with an anti-clockwise direction, and the value was calculated by 3-D numerical simulations of CONVERGE software. Each coil will be tested ten times to decrease the experimental error.

Table 2-6. Summary of test conditions

Mixture	3.07% C_3H_8, 15.28%O_2, 81.65%N_2
Equivalence ratio	0.65
Initial temperature	358 K
Initial pressure	400 kPa
Flow velocity	8m/s

2.4 Simultaneous Visualization method

2.4.1 Weakness of the schlieren photography method

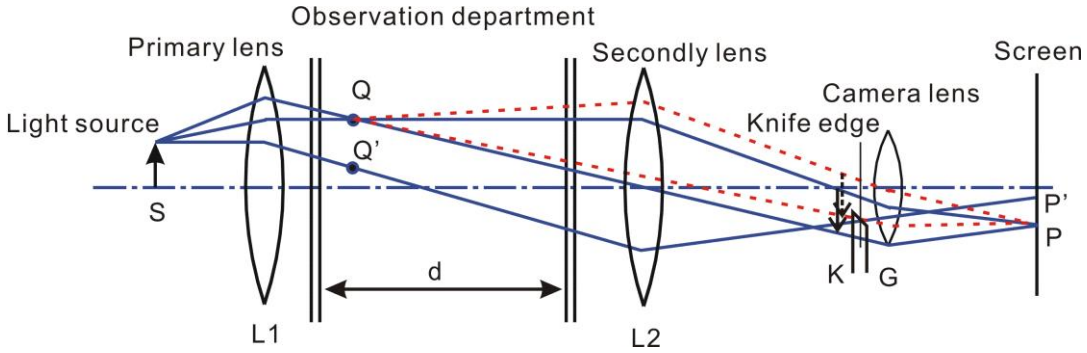

Figure 2-10 Schematics of schlieren method.

Most researchers use high-speed photography to investigate the discharge channel behaviors and the initial flame kernel during the ignition process. The discharge channel is relatively easy to be directly detected by natural imaging since the discharge channel typically emits a visible glow. However, the initial flame kernel is not easy to detect because it is invisible on a visible band [6, 7]. Schlieren photography method is wide to be used to investigate the initial flame kernel in the combustion chamber. The schematics of the schlieren photography method has been shown in Figure 2-10, a light source is set at the focal point before the primary lens, thus, parallel rays pass through the observation department between the primary lens and the second lens, and the image of the light source S is formed at the focal point K of the second lens; Therefore, the camera lens G capture the image of the point Q in the observation unit to the point P on the screen. When the density does not change in the observation department, the light rays passing through Q and the rays passing through Q' are perfectly matched at the focal point K as shown by the solid line, and a clear image of the light source is obtained; When the density gradient of only Q is different from that of other points in the observation department, the light rays passing through Q will be refracted like a dotted line, and the image will be slightly different from the image formed by the light rays passing through Q'. That is to say, variations in refractive index caused by density gradients in the fluid distort the collimated light beam. This distortion creates a spatial variation in the intensity of the light, which can be visualized directly with

a shadowgraph system [8].

However, the schlieren photography method has some weaknesses when applied in the study of ignition. As shown in Figure 2-11, even under no fuel conditions, the preheated zone was still detected by the schlieren imaging [9]. Therefore, this method is hard to distinguish between the preheated zone and initial flame, because the schlieren method visualizes the density gradient in the optical path as a shadow, the preheat zone caused by the discharge channel can be also visualized. As a result, the initial flame will be detected inaccurately.

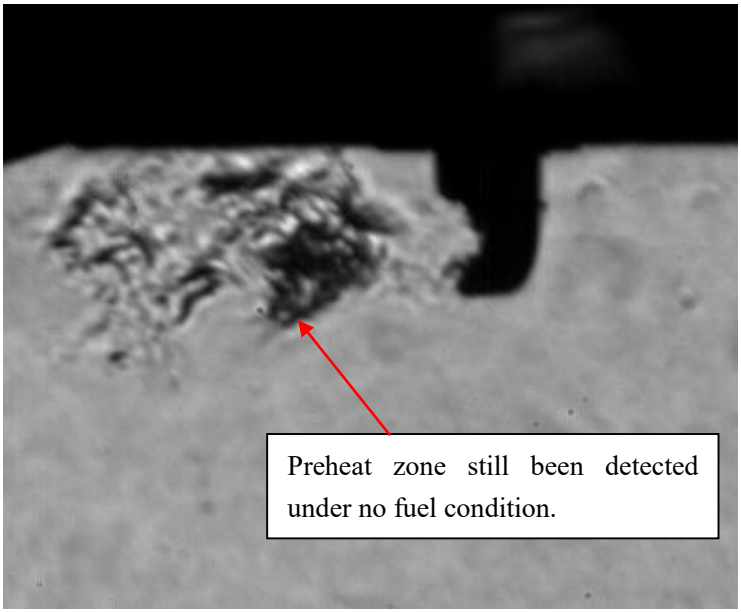

Figure 2-11 schlieren image under the no fuel condition.

2.4.2 Infrared camera

In recent years, the technologies of cooling infrared cameras have been improved and accessible in many fields. Mancaruso [10] et al. applied a high-speed infrared camera to the bottom view of an optical visualization diesel engine to observe the spray combustion of biofuels in the CO_2 and HCs bands. Due to this, it is possible to detect the reaction immediately after SOC of the pilot injection and after the end of visible combustion in the infrared range. Also, it is possible to evaluate the spray evaporation and mixing process, and the combustion evolution after the main injection. In addition, Okabe [11] et al. measure the temperature of spark plugs as an example of applying the near-infrared

region to a spark-ignition engine; The results indicated that the factors of pre-ignition depend on the engine operating conditions.

Therefore, in this study, as shown in Figure 2-12, a high-speed infrared camera was used to detect the initial flame because most of the combustion products, such as carbonic oxide (CO), carbon dioxide (CO_2), and water (H_2O), absorb specific infrared wavelengths and radiate the infrared when the components turn to be hot. The specifications of the infrared camera are shown in Table 2-7 [12], the infrared camera (FLIR X6900sc) is a sensor-cooled infrared camera equipped with an indium antimonide (InSb) element and can store standard 1-inch filters inside. It is possible to shoot at 1000 fps with total pixels (640 * 512 pixels) and at a maximum of about 30000 fps.

a. Front image of the infrared camera b. Rear image of the infrared camera

Figure 2-12 The infrared camera (FLIR X6900sc)

Table 2-7 Specification of the infrared camera [12]

Resolution	640 × 512 pixels
Detector Pitch	25 µm
Spectral Range	1.5 – 5.0 µm
Detector Type	FLIR indium antimonide (InSb)
Dynamic Range	14-bit
Filtering	4-position motorized filter wheel, standard 1-inch filters
Max Frame Rate [Full Window]	1,000 fps
Standard Temperature Range	-20°C to 350°C
Focus method	Manual

Figure 2-13 shows the filters of the infrared camera, there are two kinds of filters prepared in this study, the passed spectral range for the left one is 4675~4765nm, and the right one is 4492.5~4627.5nm. According to the NIST Chemistry WebBook [8], as shown in Figure 2-14 of the infrared radiation (IR) absorbance spectrum, carbonic oxide (CO) has two high absorbances around 4600nm and 4700nm in the spectral range compared with carbon dioxide (CO_2) and water (H_2O). Due to the relatively high absorbance of carbon dioxide, the brightness of CO2 images is accessible to saturation. At the same time, the absorbance of water is too low. Thus, the bandpass 4560 ±135nm filter is utilized in the high-speed infrared camera for capturing the infrared radiation images of carbonic oxide (CO).

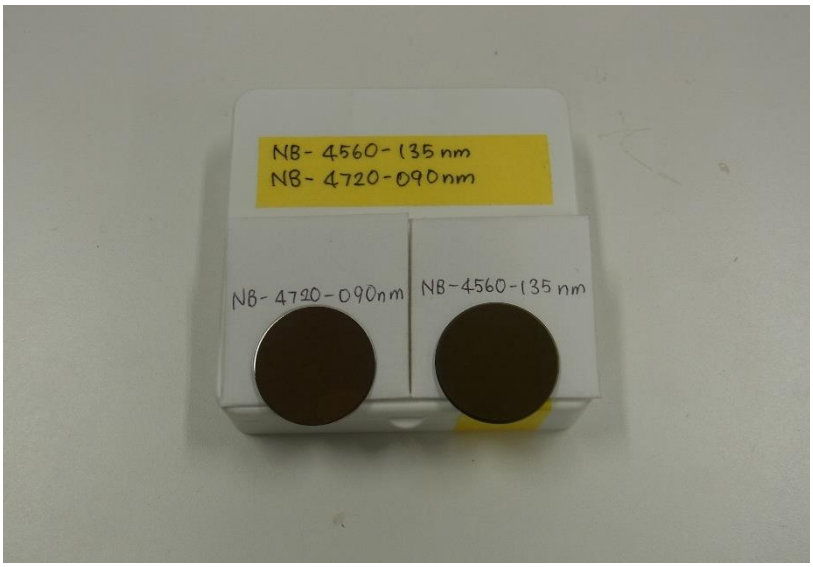

Figure 2-13 filter of the infrared camera

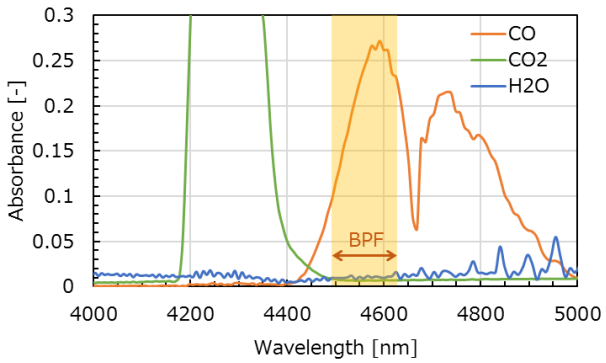

Figure 2-14 IR absorbance spectrum [13]

2.4.3 Normal high-speed camera

A high-speed camera captures momentary movements and short-term high-speed phenomena that cannot be seen by the human eye or a general video camera. In the ignition research, discharge is a very short duration phenomenon, thus, discharge channel behaviors are difficult to capture by the normal speed camera. As a result, high-speed cameras are necessary for capturing the images, and it also required not only to improve shooting speed, but also to improve total performance, including improved sensitivity.

Figure 2-15 shows the high-speed camera of FASTCAM SA-X, this camera is a high-sensitivity camera of the Photron company. The specifications of the high-speed camera are shown in Table 3-2 [9], the frame rate can reach 12,500 frames per second (fps) under the full resolution of 1024 × 1024 pixels, the maximum memory of the camera is 64 GB, which support the camera recorded the images for a long time with the maximum shooting speed of 324,000 fps.

Figure 2-15 High-speed camera (FASTCAM SA-X)

Table 2-8 Specification of the high-speed camera [14]

Resolution	1024 × 1024 pixels
Max Frame Rate [Full resolution]	12,500 fps
Maximum memory	64 GB
Image sensor	C-MOS image sensor
Dynamic Range	36-bit
Maximum shooting speed	324,000 fps
PC connector	Gigabit Ethernet
Image recording format	AVI, BMP, JPEG, TIFF, RAW, etc.
Product dimensions	171 (H) x 160 (W) x 350 (D) mm

2.4.4 Simultaneous visualization setup

As shown in Figure 2-16, A high-speed infrared camera with a 50mm lens and a conventional high-speed camera equipped with an 18-135mm lens were used in this study. In order to capture the images simultaneously for both cameras, a special infrared dichroic mirror is necessary, because two cameras cannot be set in the same direction at the same time, as shown in Figure 2-17, the infrared dichroic mirror is utilized in this study, the dichroic mirror can reflect the ray with 3000~12000nm wavelength and pass the ray with 400~700nm wavelength. Thus, as illustrated on the left of Figure 2-16, the ray of infrared wavelength will be reflected by the dichroic mirror to the infrared camera direction, while the visible wavelength ray will pass the dichroic mirror to the high-speed camera direction.

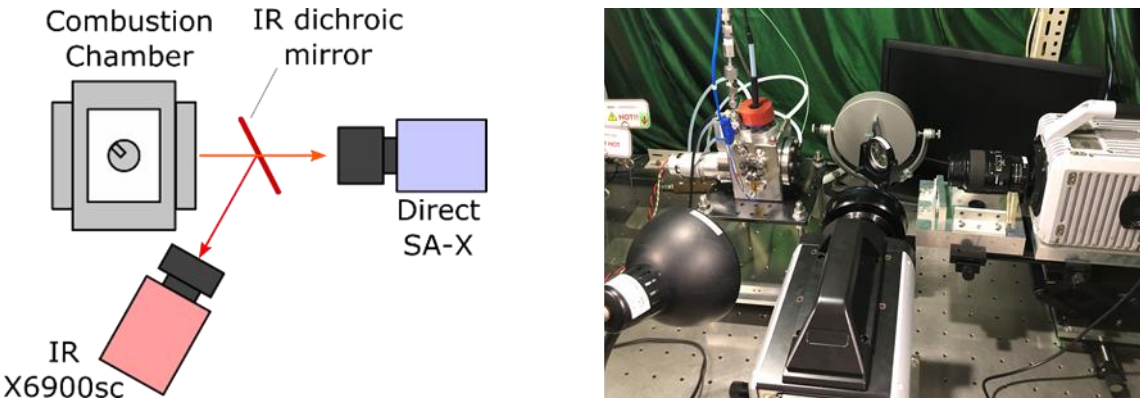

Figure 2-16 Schematics of the simultaneous visualization method

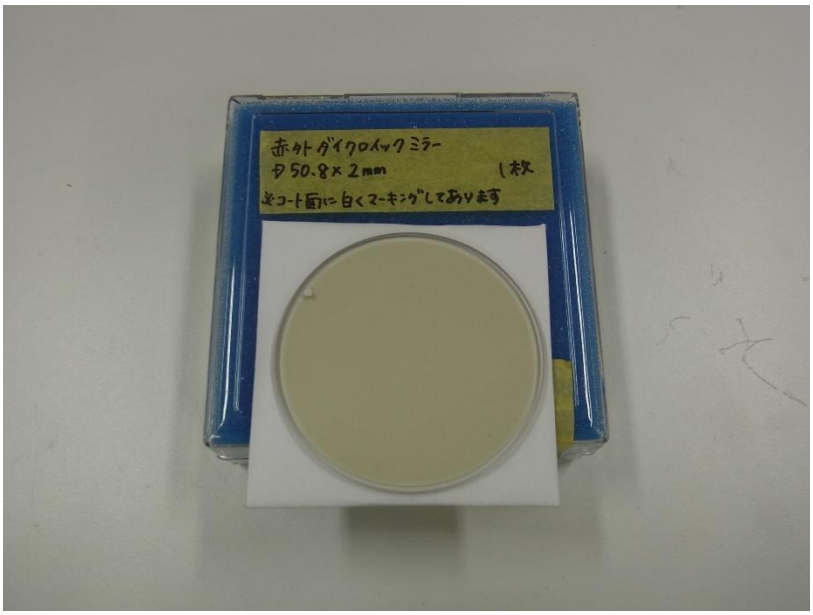

Figure 2-17 The special infrared dichroic mirror

Considering the optical scope and the shooting speed of the cameras, the infrared camera captures the infrared radiation images of carbonic oxide with 5,000 frames per second (fps), meanwhile, the high-speed camera is set up for taking the natural imaging of the discharge channel with 20,000 fps in the visible band. Therefore, to ensure that both cameras capture the images at the same time, the sync adjuster is necessary to control the shooting signal. The sync adjuster control unit is shown in Figure 2-18, which can integrate or divide the input signal with the range from 1/10 to 1, and output the target signal frequency. Figure 2-19 shows the specification of the control signal for the simultaneous visualization. First of all, the trigger signal generator creates the manual signal to the sync adjuster control unit, and then, the sync adjuster unit outputs the adjusted signal to the function generator for the coil charge signal, meanwhile, the adjusted signal is also to the cameras for starting shooting, to ensure that both cameras capture the images at the same time, the shooting signal of the high-speed camera will output to the sync adjuster unit, which integrates the signal into 1/4, and then output the integrated signal to the IR camera. It can ensure that both cameras can shoot in sync and the high-speed camera takes every four images, and the infrared camera takes one image.

Figure 2-20 illustrates the control signal of all the equipment, the cyan line stands for the manual signal, which generates from the trigger signal generator; The blue line of the adjusted signal is created

by the sync adjuster, which is the trigger for three equipment, one is the pressure data recorder of the WE800, the second is the cameras, and the third is the function generator. When receiving the trigger signal for the equipment, WE800 starts to record the pressure data of the combustion chamber, cameras are on standby for shooting the images, function generator creates the signal for the coil charging.

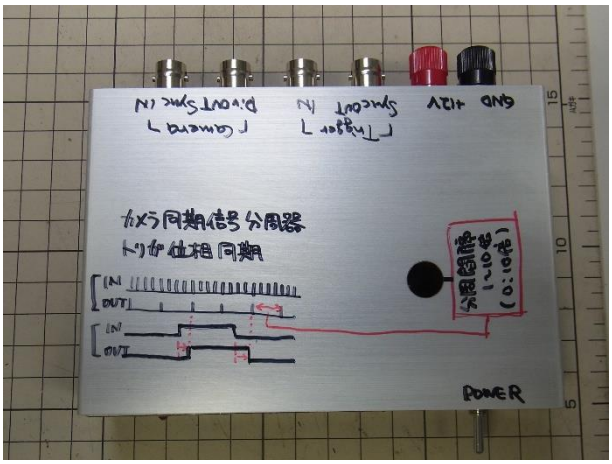

Figure 2-18 The sync adjuster control unit.

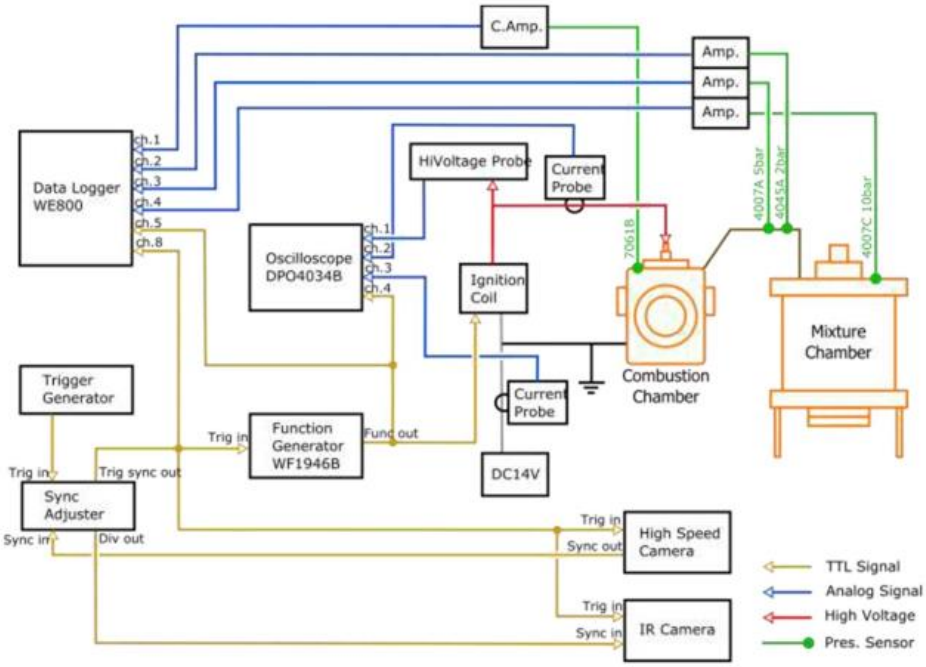

Figure 2-19 The specification of the control signal for the simultaneous visualization

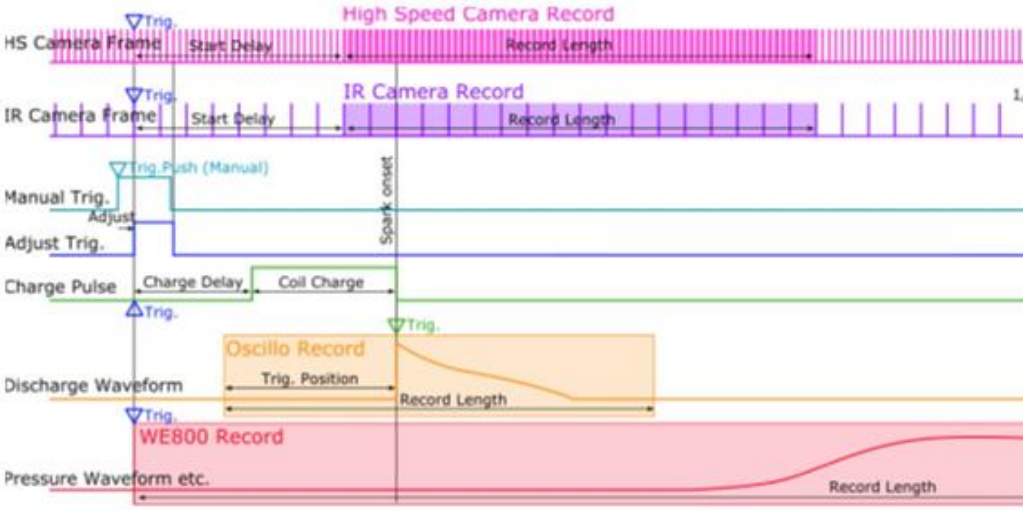

Figure 2-20 The control signal of all the equipment

2.4.5 Simultaneous visualization confirmation

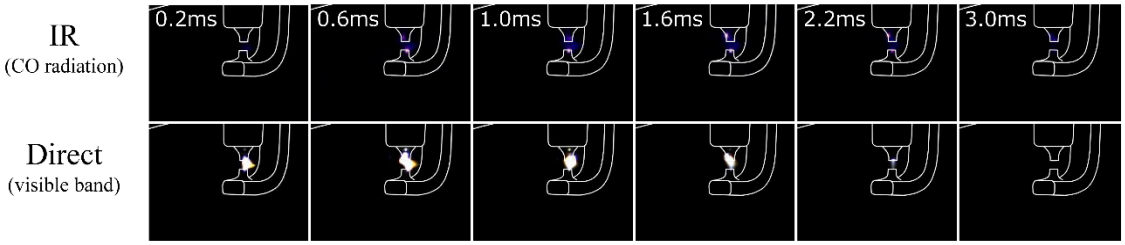

a. With no fuel condition

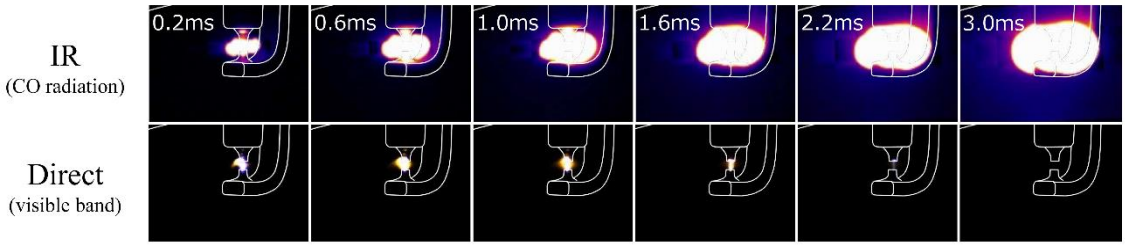

b. With fuel condition

Figure 2-21 Direct and CO radiation images on static fields with/without fuel conditions (top: CO radiation images (aim to detect the initial flame kernel)/ lower: direct images (aim to capture the discharge channel))

In order to confirm whether the preheat zone affects the results of infrared images, the test was conducted under both fuel and no fuel conditions. Under no fuel condition, there was no initial flame kernel generated. Still, the preheat zone will change the temperature in the vicinity of the spark plug via the discharge channel formation. Hence, it is necessary to confirm whether the preheat zone affects the filtered signal in the infrared images or not. Results have been shown in Figure 2-21, the upper part is the no fuel condition, and the lower part is the fuel condition. In each part, the top line is the CO radiation images taken by the infrared camera, and the lower line is the direct images taken by the conventional high-speed camera. The brightness of the initial flame kernel is saturated in the infrared image under fuel conditions, while under the no fuel condition, the brightness of CO radiation is very weak and hardly be confirmed between the spark plug gaps. Figure 2-22 shows the brightness of the infrared images at 1.0ms, the x-axis is the horizontal position centered on the center axis of the spark plug gap, and the y-axis is the brightness of the infrared images. it can be found from the figure, that the brightness of preheat zone can be ignored compared with the brightness of the initial flame kernel.

Thus, it confirmed that the CO radiation images can eliminate the interference of the preheat zone, and detect the area of the initial flame kernel more accurately than the schlieren imaging.

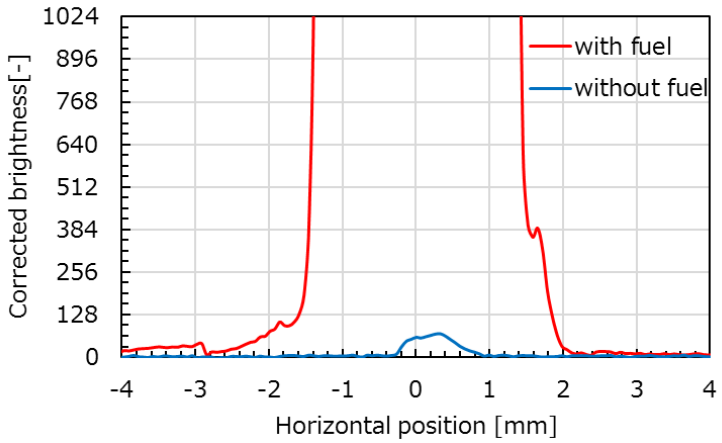

Figure 2-22 The brightness of the infrared images at 1.0ms

2.5 Effect of discharge current

The relationship between the discharge channel and discharge current under flow conditions is investigated. Figure 2-23 shows the direct images of coil A and coil C. For both of the coils, a flow velocity of 8 m/s was taken into consideration and the flow direction was set from right to left. According to the Townsend discharge law [15] [16], the electron avalanche occurs when the discharge voltage exceeds the breakdown voltage across the spark plug gap. Following the breakdown, the discharge channel is formed by electrons and ions. With the higher discharge current level, a higher energy supply of discharge channel between the spark plug gap. According to Figure 2-23, the profile of the discharge channel with low luminosity was shown with the white line, one thing can be noted that the luminosity of the discharge channel is much higher when using coil C at 0.05ms after the breakdown. It can be considered that the discharge channel of coil C has a much higher energy supply due to the higher discharge current, which caused a higher luminosity than that of coil A.

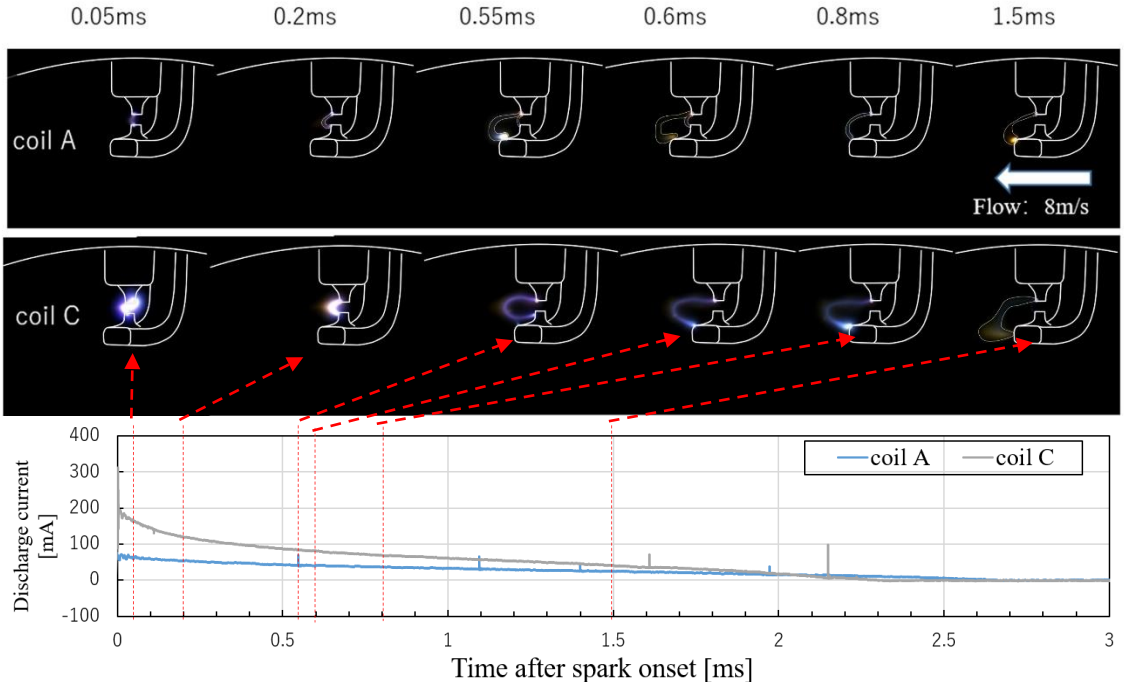

Figure 2-23 Direct shot images on coil A and coil C

Meanwhile, when gas flows through the spark plug gap, the discharge channel expands following

the gas flow. Therefore, the discharge channel is completed through a longer path with higher resistance. Once the gap resistance is too high to maintain the spark channel, restrike occurs with the discharge channel shortening. Unlike the lower discharge current coil, the higher discharge current coil produced a longer channel stretch, by the reason of lower resistance and higher energy supply, because the breakdown voltage is following the Paschen law, which means that breakdown voltage is a function of gas density and spark plug gap size, while these two factors are almost the same in the combustion chamber. Therefore, the higher discharge current coil has a higher energy supply during the discharge, which supports the discharge channel to keep stretching without shortening and increasing the contact area between the discharge channel and the mixture gas. It can be found in Fig. 5 that restrike occurs with respect to coil A at 0.55ms after spark onset, and the original discharge channel dissipated was accompanied by the new channel formed at 0.6ms. In contrast, the discharge channel of coil C kept on extending until 1.6ms and expanding the discharge channel extension length. According to the Kim's research [17], it has studied the relationship between the convection velocity near the spark plug gap and the discharge channel length via a flow apparatus at the ignition timing, a model was developed for assuming the discharge channel length, and the result of equation (1) can evaluate the resistance of the discharge channel during the ignition process. Where R_{spk} means the resistance between the spark plug, L_{spk} is the discharge channel length, i stands for the discharge current, and P is the pressure. As the equation shows that higher discharge current results in a lower resistance when under the same discharge channel length. However, the discharge channel shorten occurs once the resistance is too high to maintain the discharge channel, hence, the higher discharge current will maintain the discharge channel stretch longer due to the lower resistance.

$$R_{spk}(t) = 40.46\, L_{spk}(t)\, i(t)^{-1.32}\, P^{0.51} \quad (1)$$

Figure 2-24 shows all the test results of 1st discharge channel extension length. As the previous paragraph described, the higher discharge current got a higher discharge channel luminosity and kept the discharge channel extending without shortening. It can be found from Figure 2-24 that high current coil C gets a longer 1st discharge channel extension duration under the flow conditions and gets the larger discharge channel extension length compared with lower discharge current coil A. Since almost the 1st discharge channel extension was finished before 1.0ms after breakdown, when investigating the flame area at 1.0ms after breakdown, as Figure 2-25 shows, a larger discharge channel extension length has increased the initial flame area because the initial flame was formed along the discharge

channel. Higher discharge current coil C results in a larger initial flame area than coil A due to the longer discharge channel extension length.

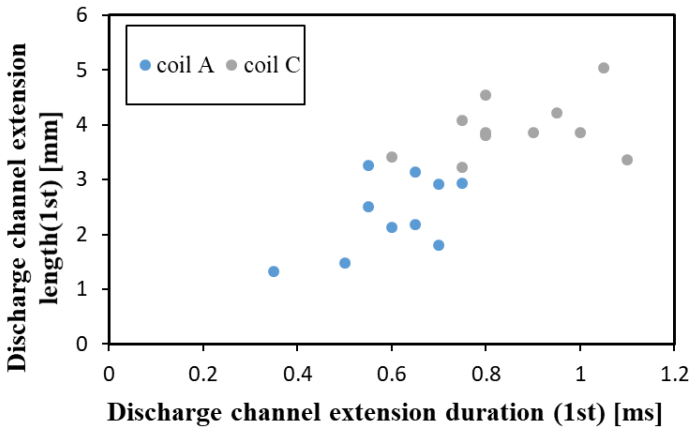

Figure 2-24 Discharge channel extension length of coil A and coil C

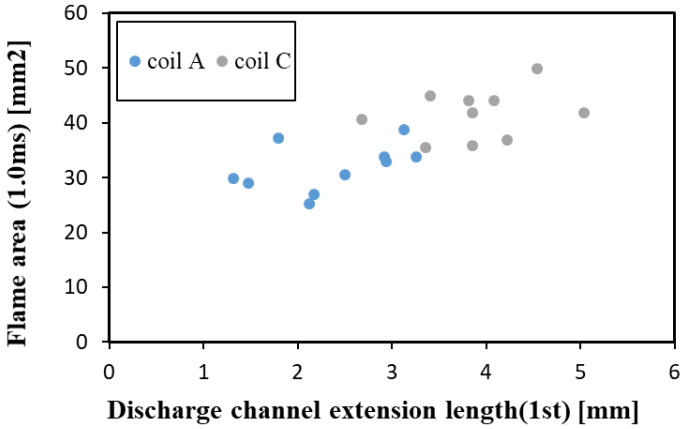

Figure 2-25 Initial flame area at 1.0ms after the breakdown of coil A and coil C

2.6 Effect of discharge duration

Figure 2-26 shows the direct shot images of coil B and coil C, and it can be found that there is not much difference in the discharge channel between coil B and coil C before the 1st short-cut phenomenon (1.05ms). After that, the difference occurred between these two coils, the discharge channel of coil B gradually vanished until 1.6ms, while coil C still has the discharge channel at 1.6ms since coil C has a longer discharge duration which in turn will increase the heating duration of the discharge channel to the mixture gas. Figure 2-27 shows the discharge channel extension length and duration of 1st discharge. The gray points stand for coil C, and the orange points represent coil B. The discharge channel length of 1st discharge for coil B and coil C is almost the same since the discharge current for these two coils is nearly the same. Also, Figure 2-28 shows that the flame area at 1ms for these two coils is at the same level. Owing to the initial flame generated along the discharge channel, according to Figure 2-28, the 1st discharge channel stretch length is almost the same from the range of 3mm to 5mm for the two coils, and the initial flame at 1.0ms also fluctuate around the 40 mm^2, which caused by the same discharge current of these two coils.

Combining the previous results above, the discharge current is the dominant factor in influencing the discharge channel compared with the discharge duration. Since improving the discharge current will increase the discharge channel extension length by keeping the discharge channel extended without restrike, the longer discharge channel enlarged the flame area. While expanding the discharge duration will not change the discharge channel before the 1st discharge, which results in the same flame area generated.

However, the discharge channel cannot extend during the whole ignition process, which means that the discharge channel will shorten during the ignition process. As the initial flame was formed along the discharge channel, discharge channel shortening behaviors will affect the flame formation and development as well. Discharge channel shortening behaviors after 1st discharge channel extension are discussed in the next section.

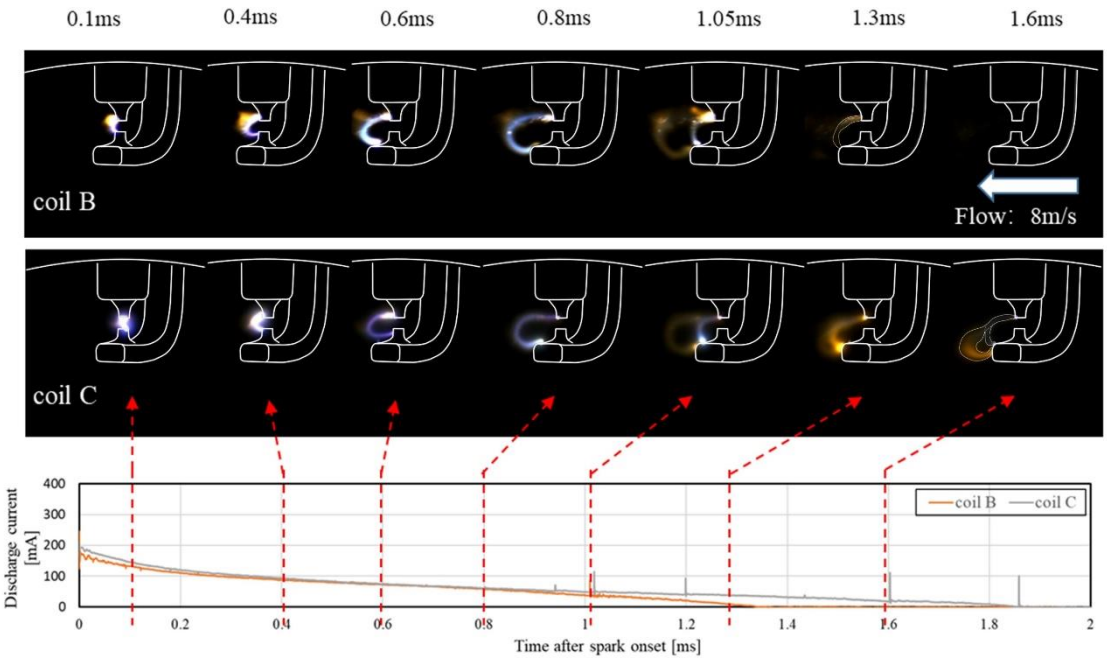

Figure 2-26 Direct shot images of coil B and coil C

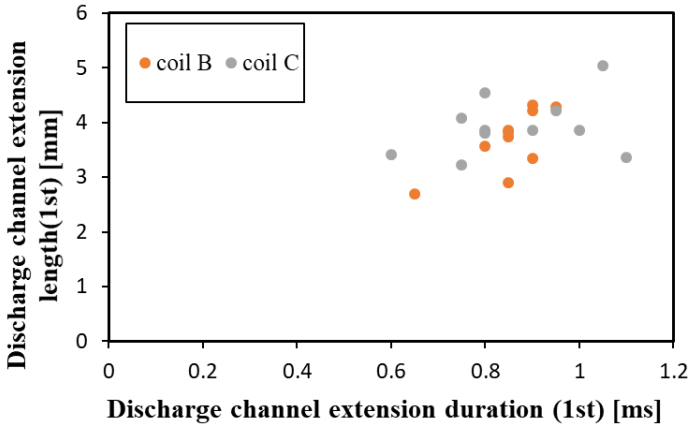

Figure 2-27 Discharge channel extension length of coil B and coil C

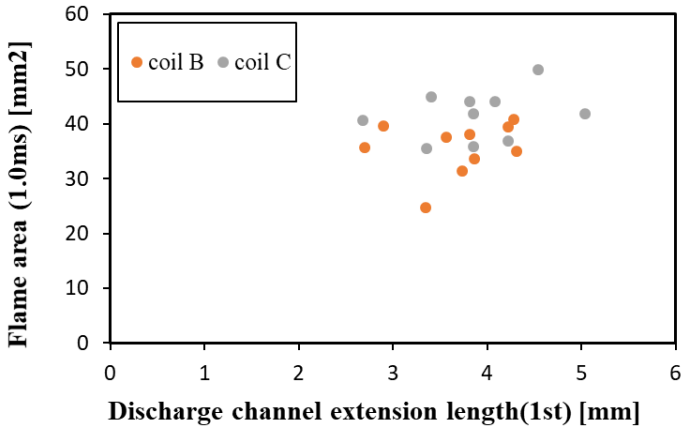

Figure 2-28 Initial flame area at 1.0ms after the breakdown of coil B and coil C

2.7 Effect of discharge channel shortening behaviors

As the previous section found that after the electrical breakdown at the spark plug gap, a discharge channel was formed and stretched downstream with the flow. However, the original discharge channel cannot extend continuously during the whole discharge duration. A short circuit of the discharge channel occurred with the shortening of the original discharge channel. When analyzing the results of high discharge current coil C, two kinds of discharge channel shortening behaviors were found and named restrike and short-cut. Restrike, as shown in Figure 2-29a is used to describe the phenomenon where the short circuit is formed at the spark plug gap while short-cut is as shown in Figure 2-29b. This figure describes the phenomenon where the short circuit is formed inside the original discharge channel circuit. The difference between these two kinds of phenomena is the location and the length of the short circuit at the beginning of the phenomenon where it occurred.

A simultaneous visualization was carried out via a high-speed infrared camera and a normal high-speed camera, and the results are shown in Figure 2-30. Restrike and short-cut are two kinds of phenomena that occur in the discharge channel extension process. It was observed that the initial flame area and its development were affected by the behaviors of the discharge channel.

According to Figure 2-30, two groups of discharge images about the restrike phenomenon and short-cut phenomenon from the high-speed camera are shown. Each group contains two kinds of images. The top one is the CO radiation images taken by the infrared camera, which can reveal the

initial flame zone and the lower images are the direct photographs by the normal high-speed camera. It can be found that after the breakdown, the discharge channel formed at the spark plug gap. Meanwhile, the initial flame was generated along the discharge channel immediately. After that discharge channel stretched as the flow moved downstream, the initial flame was developed with the discharge channel stretch. Since the ignition conditions were almost the same for each test case in the constant volume combustion chamber, there are not many differences between the restrike case and the short-cut case at the beginning of the discharge. However, after 1st discharge channel extension finished and the shortening behavior occurred, the initial flame of two cases with different kinds of discharge channel shorten behaviors was developed in different situations.

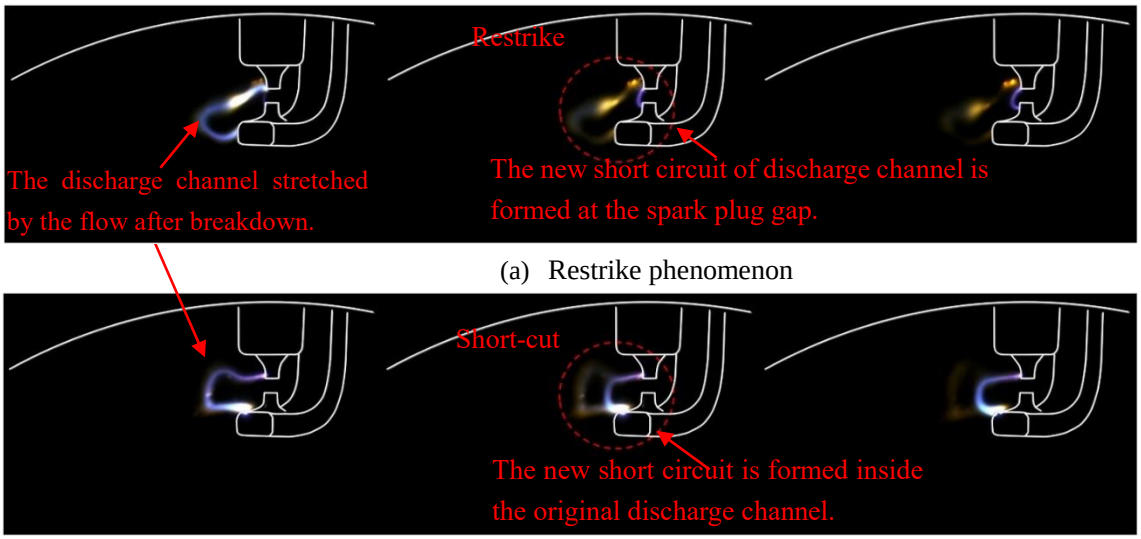

(a) Restrike phenomenon

(b) Short-cut phenomenon

Figure 2-29 Direct shot images on different discharge channel shorten behaviors

According to Figure 2-30a, it can be observed that restrike shortening behavior occurred at 1.0ms after the breakdown and a new initial flame kernel was formed immediately due to the new discharge channel. Then the new initial flame kernel growth moved downstream with the flow, until 1.4ms overlapped with the original flame kernel. Unlike the restrike shortening behavior, according to Figure 2-30b, the short-cut shortening behavior occurred at 0.8ms after breakdown, since the new discharge channel was formed in the middle of the original discharge channel, the new flame kernel was developed near the original flame kernel and overlapped at 1.0ms, which is better for the flame overlap. It demonstrated that the discharge channel shortening behaviors affect the initial flame formation by

the different locations of new flame kernel formation. Compared with the short-cut shortening behavior, the new flame kernel of restrike shorten behavior was formed far away from the original flame kernel, which suppresses the flame development.

Figure 2-31 shows the flame area of the two cases with different shortening behaviors. It revealed that the flame area shows not much of a difference in the early phases of the ignition process. After the shortening behaviors occurred, the difference in the flame area for the two kinds of shortening behaviors appeared. Short-cut shortening behavior resulted in a larger flame area than the restrike shortening behavior. Therefore, one thing can be noted that the short-cut and restrike phenomenon affects the initial flame kernel growth in the discharge period. The reason can be explained that once the discharge channel shortening occurred, the flame kernel that had been generated by the original discharge channel flowed downstream with the flow, while another new flame kernel formed immediately by the re-formed short channel. Therefore, the features of the new discharge channel are essential for flame kernel growth. When the restrike shortening behavior occurs, the new discharge channel starts at the spark plug gap, and the new flame kernel is also formed along with it. Unlike the restrike shortening behavior, when the short-cut shortening behavior occurred, the new flame kernel was generated in the middle of the original discharge channel circuit which led to the development of a new flame that is much closer to the previous flame kernel, which is easier for overlapping with the original flame kernel. Hence, the short-cut is better than the restrike for the flame kernel overlap and enlarges the flame area in the same condition.

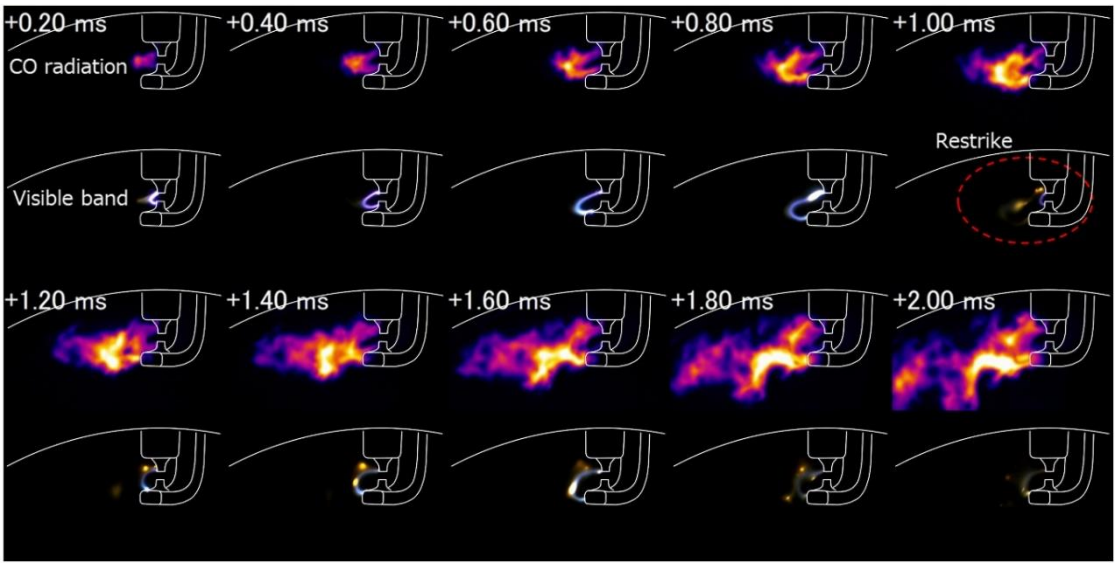

(a) Restrike shortening behavior case

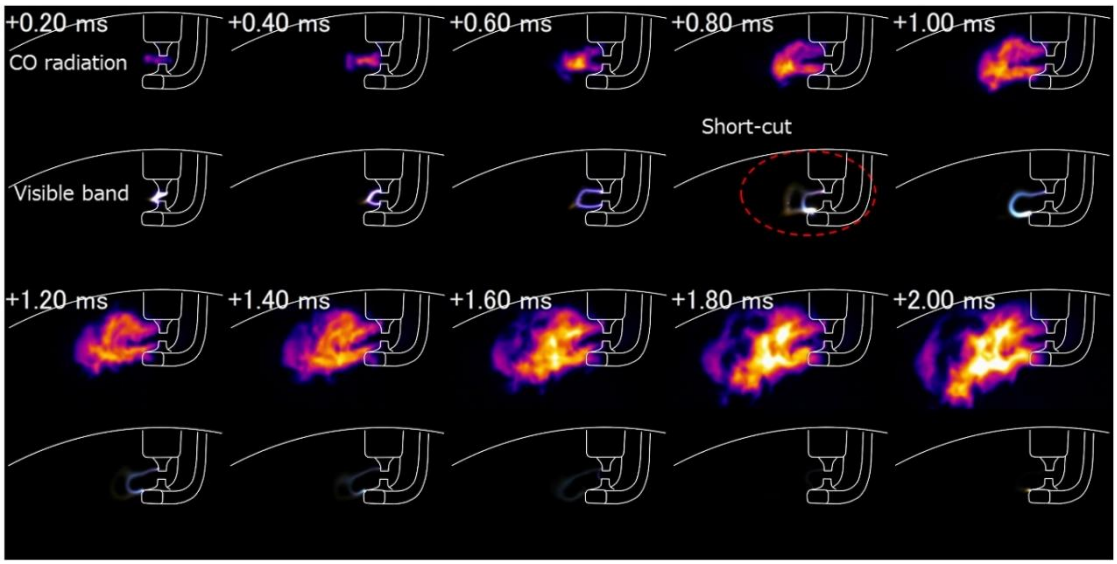

(b) Short-cut shortening behavior case

Figure 2-30 Simultaneous Visualization on different discharge channel shorten behaviors (top: CO radiation images / lower: direct shot images)

In addition, as the combustion was carried out in a small combustion chamber with 60cm^3, small pressure changes can be detected during the ignition period. Therefore, according to the R-W(Rasswei-Withrow) model [18], due to the volume being constant, the pressure changes are only caused by the combustion in the constant volume combustion chamber, the heat release rate consequently can be calculated from the pressure data during the ignition process, and the results are shown in Figure 2-

32. The black line stands for the short-cut case, and the red line stands for the restrike case. Because the short-cut shortening behavior has some benefits to the initial flame overlap and resulted in a large flame area than the restrike shortening behavior, after shortening behaviors had occurred at 1.0ms, the heat release rate between the two cycles began to have a difference. The Short-cut case has a much faster rate than the restrike, which will result in a decrease in the ignition delay.

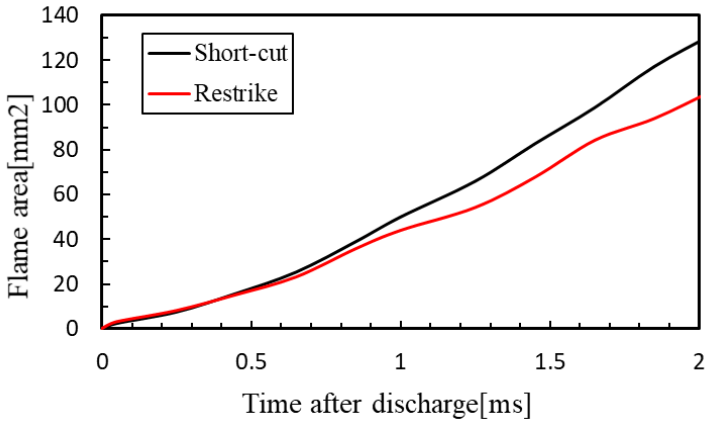

Figure 2-31 Initial flame area of short-cut and restrike cases

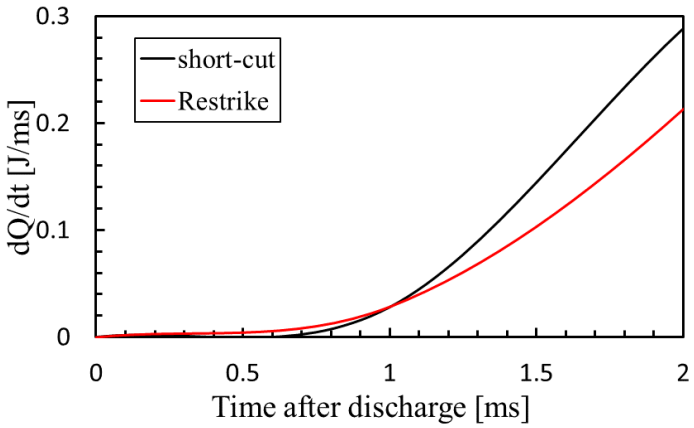

Figure 2-32 Heat release rate of short-cut and restrike cases

2.8 Effect of discharge channel behaviors on ignition delay

This section shows the effect of the discharge channel behaviors on ignition delay. As shown in Figure 2-33, the x-axis is the 1st discharge channel extension length, and the y-axis represents the period from the IG (ignition timing) to the MFB1 (1% mass fraction burned), which was considered to be the ignition delay in this study. Figure 2-33a~c stands for the coil A~ coil C respectively. When comparing all the experimental cases of each coil, black points stand for the short-cut shortening behavior cases, and red points stand for the restrike shortening behavior cases. We can note that the short-cut shortening behavior results in a better ignition delay than the restrike shortening behavior compared to the cases with almost the same 1st discharge channel extension length. The reason can be explained that the initial flame was formed along the discharge channel, and the new initial flame kernel of the short-cut shortening behavior case was formed close to the original flame kernel, which has some benefits to the initial flame development, leading to a higher heat release rate as discussed in the previous section.

Moreover, Figure 2-34 shows the frequency of the two kinds of shorten behaviors after 1st discharge, the black column stands for short-cut behavior, and the red column stands for the restrike behavior. It can be found that short-cut shortening behavior is easier to occur after the end of 1st discharge for all the coils. Higher discharge current coil B and coil C got a higher proportion of the short-cut shortening behavior compared with coil A. Namely, increasing the discharge current results in a higher possibility of short-cut shortening behavior. Discharge duration does not affect the discharge shortening behaviors because of the same proportion of the discharge shortening behaviors for coil B and coil C. It confirmed that discharge current is more influence than the discharge duration on the discharge channel behaviors, including extension and shorten behaviors.

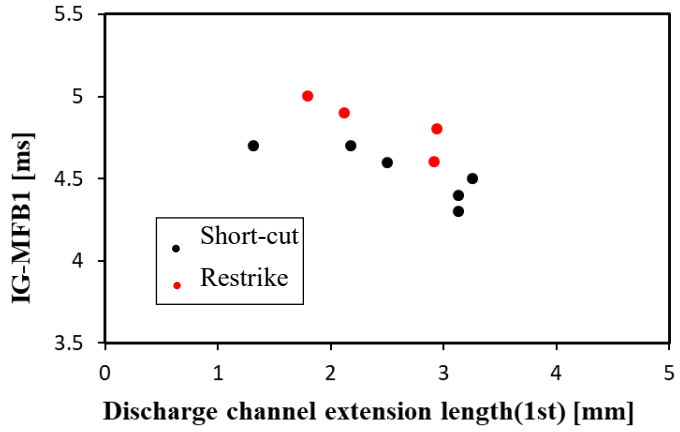

a. Coil A

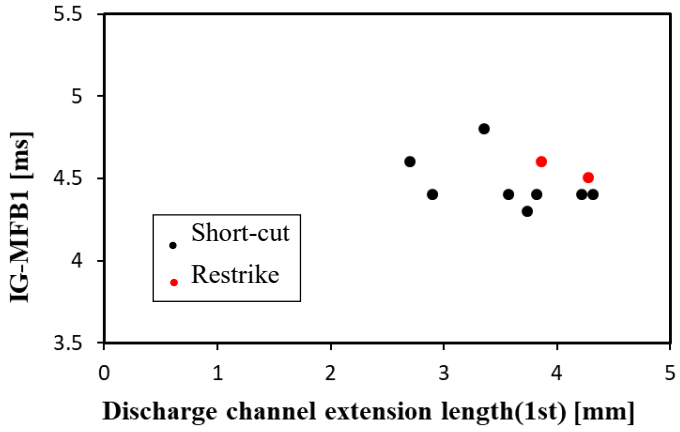

b. Coil B

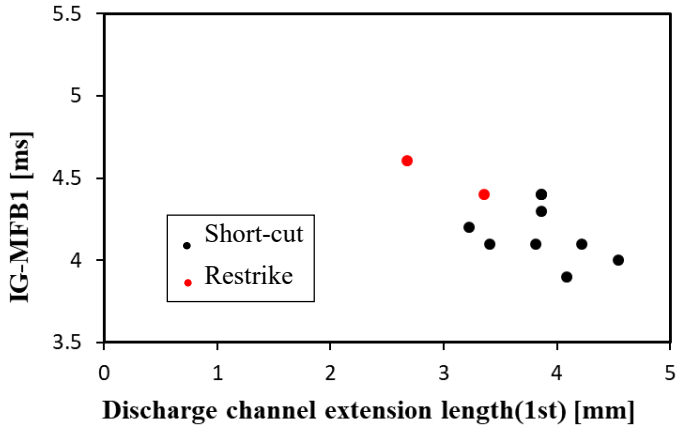

c. Coil C

Figure 2-33 Relationship between discharge channel extension length and ignition delay of all experimental cases

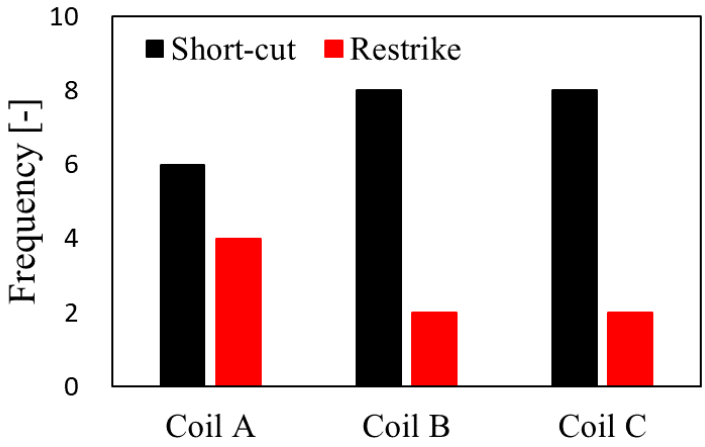

Figure 2-34 The frequency of two kinds of shorten behaviors

2.9 Summary

In this chapter, the weakness of the schlieren photography method had been introduced, which is hard to distinguish between the preheated zone and initial flame. In order to improve the visualization method and get a deeper insight into the process of discharge, a new visualization method, using a high-speed infrared camera (FLIR X6900sc) and a conventional high-speed camera (FASTCAM SA-X) simultaneous, has been set up.

In this chapter, the experiment setup of CVCC has been introduced in detail, including the constant volume combustion chamber, the ignition system, and the simultaneous visualization method. Besides, the effects of discharge current and discharge duration on discharge channel behaviors and initial flame formation have been investigated under the same condition. The key features identified are summarized below:

1. To confirm whether the preheat zone affects the results of infrared images, the test was conducted under both fuel and no fuel conditions. The result has confirmed that the high-speed infrared images can ignore the interference of the preheat zone caused by the discharge channel.

Because the infrared images had hardly any brightness around the spark plug under the no fuel condition, while the discharge channel still formed during the ignition process.

2. Discharge current is the dominant factor that influences the discharge channel behaviors as compared with the discharge duration. The reason can be explained that increasing the discharge current is seen to enlarge the discharge channel extension length and keep the discharge channel extending without shortening, which increases the contact area between the discharge channel and the mixture gas and improves the early flame development during the ignition process.

3. Restrike and short-cut are the two kinds of discharge channel behaviors that occurred in the ignition period under flow conditions. Simultaneous visualization of the discharge channel and initial flame area shows clearly that these two kinds of discharge channel behaviors affect the flame kernel overlap. Because the new flame kernel is closer to the original flame when short-cut behavior occurred, which has some benefits for the flame overlap. Short-cut shortening behavior results in a larger initial flame kernel, and a shorter ignition delay. Therefore, short-cut has some benefits to the flame development and enlarges the early flame during the discharge duration compared to the restrike behavior.

Reference

1. Kim, K., Askari, O. Understanding the effect of capacitive discharge ignition on plasma formation and flame propagation of air–propane mixture. Journal of Energy Resources Technology, (2019). 141(8).12
2. Choe, M. S., Kim, K. S., Choi, D. S. Study on flame propagation characteristics according to new ignition-source in a constant volume combustion chamber. In Defect and Diffusion Forum (2019). Vol. 391, pp. 142-151. Trans Tech Publications Ltd.12
3. Kim, K. S., Lee, K. T., Choe, M. S., Choi, D. S. Understanding of the Spark Effect of Electron Collision by a Capacitive Discharge Ignition in a Constant Volume Combustion Chamber. International Journal of Automotive Technology, (2020), 21(1), 249-257.12
4. Lee, M. J., Hall, M., Ezekoye, O. A., Matthews, R. D. (2005). Voltage, and energy deposition characteristics of spark ignition systems (No. 2005-01-0231). SAE Technical Paper.
5. Yu, S., Tan, Q., Ives, M., Liu, M., Li, L., Chen, X., Zheng, M. (2016). Parametric analysis of ignition circuit components on spark discharge characteristics (No. 2016-01-1011). SAE Technical Paper. DOI: 10.4271/2016-01-1011
6. Shiraishi, Taisuke, Atsushi Teraji, and Yasuo Moriyoshi. "The effects of ignition environment and discharge waveform characteristics on spark channel formation and relationship between the discharge parameters and the EGR combustion limit." SAE International Journal of Engines 9.1 (2016): 171-178.
7. KINOSHITA, Masao; FUYUTO, Takayuki; AKATSUKA, Hiroshi. Measurement of vibrational and rotational temperature in spark-discharge plasma by optical emission spectroscopy: Change in thermal equilibrium characteristics of plasma under air flow. International Journal of Engine Research, 2019, 20.7: 746-757.
8. https://en.wikipedia.org/wiki/Schlieren_photography.
9. Matsumoto, O., et al.: Simultaneous visualization of initial flame and discharge channel during spark ignition process, Transactions of Society of Automotive Engineers of Japan, 49, 6, p. 1150-1155 (2018).
10. E.Mancaruso, B.M.Vaglieco, L.Sequino,: “Using 2d Infrared Imaging for the Analysis of Non-Conventional Fuels Combustion in a Diesel Engine”, SAE Technical Paper, 2015-01-1646
11. OKABE, S., et al. Spark Plug Temperature Measurement Using an IR Camera. Denso Technical Review, 2008, 13.1: 64-70.

12. https://www.flir.com.au/products/x6900sc-mwir/

13. National Institute of Standards and Technology: NIST Chemistry WebBook, NIST Standard Reference Database Number 69, http://webbook.nist.gov/chemistry/ （refer to 2018.03.21）
14. https://www.yumpu.com/pt/document/view/50966710/-fastcam-sa-x-
15. Xiao, D, Fundamental theory of townsend discharge, Gas Discharge and Gas Insulation (2016), pp. 47-88, DOI:10.1007/978-3-662-48041-0_3.
16. Yang, Z., Yu, X., Yu, S., Chen, J., Chen, G., Zheng, M., and Ting, D. S. K, Impacts of Spark Discharge Current and Duration on Flame Development of Lean Mixtures Under Flow Conditions, ASME 2018 Internal Combustion Engine Division Fall Technical Conference (2018), DOI:10.1115/ICEF2018-9771.
17. Kim, J., and Anderson, R. W, Spark anemometry of bulk gas velocity at the plug gap of a firing engine, SAE Transactions, Vol. 104, (1995), pp. 2256-2266.
18. Marcus, K., A specific heat ratio model and compression ratio estimation, Linköping Studies in Science and Technology Thesis, No. 1104 (2004).

Chapter 3 Effects of experimental conditions on the ignition performances

3.1 Coils and different test conditions

After the discussion in chapter 2, the effects of discharge characteristics on the discharge channel behaviors and initial flame formation have been studied under the same condition, this chapter will investigate the ignition performances under different conditions. Figure 3-1 shows the discharge characteristics of three types of ignition coils. This research takes coil A as the standard coil, coil B as the high current coil, and coil C as the high energy coil. The detailed specifications of the coils are shown in table 1. As described in table 1, coil A and coil B have almost the same ignition energy, and coil C is the highest energy one. However, coil C has almost the same discharge duration as coil A, and coil B is much shorter than coil A and coil C. Coil B and coil C had almost the same discharge current which is much higher than coil A.

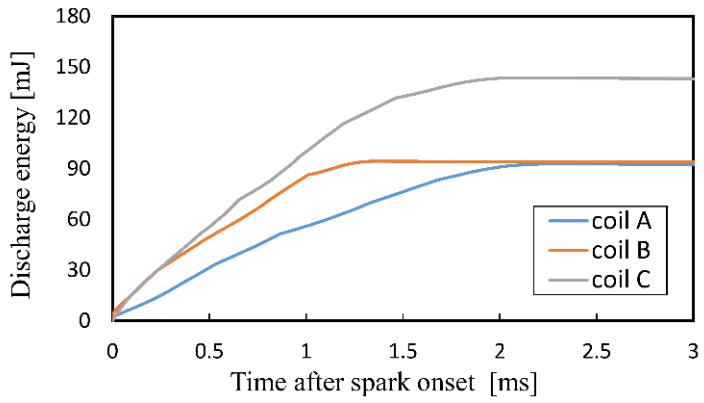

a. Discharge energy

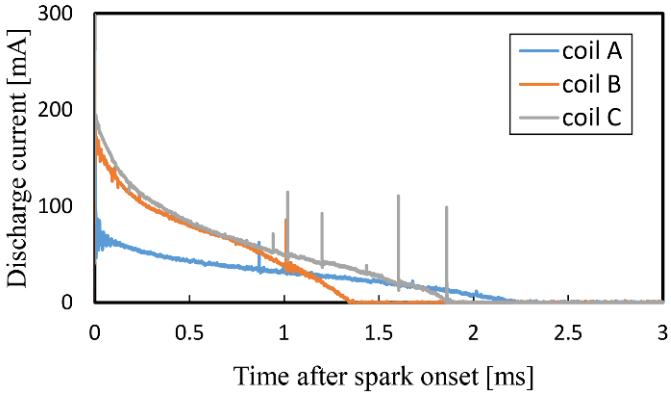

b. Discharge current

Figure 3-1 Discharge characteristics of the ignition coils

The experiments were carried out under three conditions: basic condition, high dilute condition, and high flow condition to determine the suitable discharge strategy under different conditions. Experimental conditions are listed in Table 3-2. The basic condition is the base condition in the three conditions, which has both lower dilution (N_2 dilution 24%) and lower flow velocity (8 m/s). Due to the single variable method, the high diluted condition has a higher dilution (N_2 dilution 28%) than the basic condition, and has the same flow velocity compared with the basic condition; while the high flow condition only has a higher flow velocity (18 m/s) than the basic condition, the N_2 dilution is same with the basic condition.

In addition, the initial condition parameter, such as temperature and pressure, are fixed at 358 K and 400 kPa respective for ensuring the same initial conditions of each test. Each condition of each coil is tested ten times to eliminate the experimental error.

Table 3-1. Detail specifications of the ignition coils

	Coil A	Coil B	Coil C
Discharge current[mA]	65	170	180
Discharge duration[ms]	2.2	1.3	1.9
Ignition energy[mJ]	95.0	95.0	165.0

Table 3-2. Summary of experimental conditions

Conditions	Basic condition	High diluted condition	High flow condition
Nitrogen (N_2) dilution	24%	28%	24%
Mixture composition	C_3H_8:3.06%, O_2:15.29%, N_2:81.65%	C_3H_8:2.90%, O_2:14.49%, N_2:82.61%	C_3H_8:3.06%, O_2:15.29%, N_2:81.65%
Flow velocity	8 m/s	8 m/s	18 m/s
Equivalence ratio	1		
Initial temperature	358K		
Initial pressure	400 kPa		

3.2 Combustion results in different conditions

Figure 3-2 shows the ignition probability of all the coils under different conditions. Ignition probability is the ratio of the successful ignition cases and the total number of experimental cases (10 times). The blue column stands for coil A (standard coil), the orange column denotes coil B (high current coil), and the gray column represents coil C (high energy coil). According to Figure 3-2, it can be observed that three types of coils have the same ignition probability ratio at the basic condition. There is no misfire case under the basic condition for all the coils. However, the differences among the three coils occur when increasing the mixture dilution ratio or enhancing the flow velocity, high current coil B gets the lowest ignition probability when under the high diluted condition compared with other coils, while standard coil A and high energy coil C still have no misfires cases under such condition. When under the high flow condition, standard coil A gets the lowest ignition probability while high energy coil C gets the highest ignition probability. High current coil B is better than the standard coil A. It reveals that the high energy coil C resulted in high-level ignition probability under all the conditions. This means that enhancing the ignition energy can improve the ignition probability remarkably. However, high energy will increase the wear and tear of the spark plug due to the increased discharge current and prolonged discharge duration, thence, coil A and coil B with the same lower ignition energy need to be considered in particular. Standard coil A with a longer discharge duration has a better ignition probability under the high diluted condition. In contrast, high current coil B with

a higher discharge current has a better ignition probability under the high flow condition. Ignition probability can reflect the ignition performance by and large, when comparing results of the basic condition and the high diluted condition, due to the lowest ignition probability ratio of coil B under the high diluted condition, one thing can be found that discharge duration is more important than the discharge current to affect the ignition probability when only in-creasing the mixture dilution ratio; when focusing on the results of the basic condition and high flow condition, one thing can be noted that discharge current becomes the dominant factor compare with discharge duration when enhancing the gas flow velocity since coil A gets the lowest ignition probability.

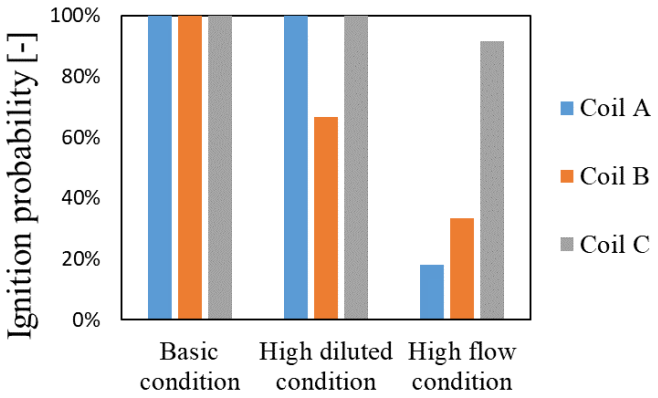

Figure 3-2 Ignition probability of all the conditions

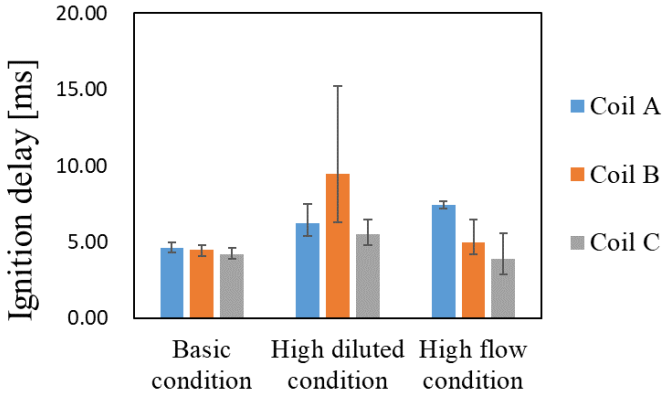

Figure 3-3. Ignition delay of all the conditions

Due to the small internal volume of the combustion chamber, the small pressure changes can be detected by a highly sensitive pressure sensor, and the results of ignition delay are shown in Figure 3-

3. Ignition delay is defined as the period between the start of discharge to the MFB1 (mass fraction burn of 1 percent). It can be found that coil B with a high discharge current results in the longest ignition delay in the high diluted condition, while when in the high flow condition, coil A with the extended discharge duration results in the longest ignition delay. The difference in initial flame formation is largely affected by ignition. Hence, given that coil A has the same ignition energy as coil B, it shows that coil A with extended discharge duration favors more in improving the ignition performance than coil B with higher discharge current under high diluted conditions. Nevertheless, such a result comes to the opposite under high flow velocity conditions, the higher the discharge current is more important under the high flow condition.

According to the R-W(Rasswei-Withrow) model, the pressure changes are only caused by the combustion in the constant volume combustion chamber since the volume is constant in it, the heat release rate consequently can be calculated from the pressure data. Figure 3-4 illustrates the heat release under different conditions of all the experimental cases about three types of coils. As shown in Figure 3-4, combustion time is defined as the period from the start of discharge to the point of peak heat release. The graph of heat release can reflect the combustion speed via the length of combustion time and embodies the combustion stability by the fluctuation of combustion time in all the cases. From Figure 3-4a of the basic condition, all the coils have no significant difference from each other in heat release histories, additionally, the combustion speed and combustion stability have a high level in all the cases; From Figure 3-4b of the high diluted condition, combustion becomes slower and unstable as compared with the basic condition, the timing of the peak heat release point is put off, which means the combustion time is extended. Also, the combustion fluctuation of case-to-case is increased, high current coil B has the slowest combustion case and even has the misfire cases under the high diluted condition. Although standard coil A and high energy coil C have the same ignition probability, coil C combustion cases keep a smaller combustion fluctuation than that of coil A. In Figure 3-4c of the high flow condition, the combustion time of the fastest case of coil C shows slightly shorter compared with the fastest case of coil C under the basic condition, but the combustion fluctuation is increased, which reveals that increasing the flow velocity may improve the combustion speed only when the ignition energy is increased correspondingly. According to these results, one thing should be noticed that increasing the mixture dilution ratio will decrease the combustion speed even increasing the ignition energy cannot reach the combustion speed of low diluted condition, while increasing the flow velocity may improve the combustion speed only if increasing the ignition energy correspondingly. Besides, the combustion stability will decrease no matter increasing the mixture

dilution ratio or the flow velocity, while compared with the low ignition energy coils, increasing the ignition energy can decrease the combustion fluctuation, making the combustion more stable.

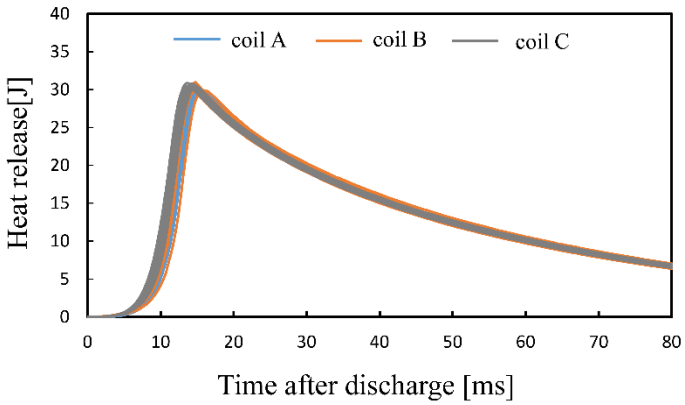

a. Basic condition

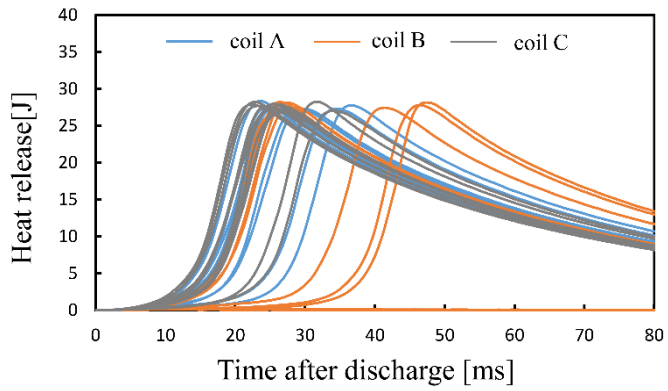

b. High diluted condition

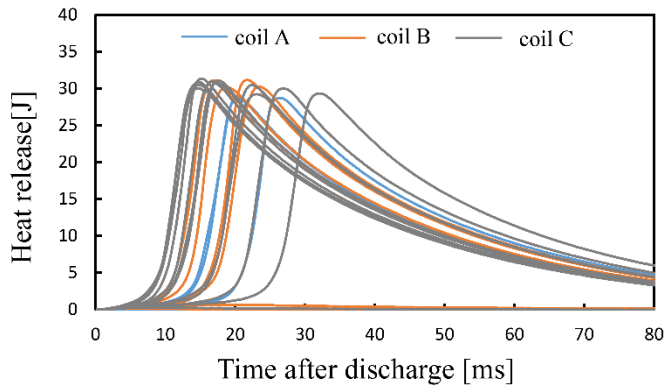

c. High flow condition

Figure 3-4 Heat release under different conditions

As described in combustion results, several interesting results can be found. On the one hand, increasing the mixture dilution ratio will decrease the combustion speed even increasing the ignition energy cannot reach the combustion speed of low diluted condition, when focusing on the same ignition energy coils, prolonging the discharge duration is more important than increasing the discharge current for the ignition performance. On the other hand, increasing the flow velocity may improve the combustion speed only if increasing the ignition energy correspondingly, additionally, if constant the ignition energy, increasing the discharge current has more benefits than prolonging the discharge current for improving the ignition performance.

Since the experiments were carried out in the combustion chamber, the combustion results were mainly affected by the ignition process. Therefore, in order to explain the reason for combustion results, a detailed investigation of simultaneous visualization for the spark discharge channel behaviors and initial flame kernel formation was carried out during the ignition process. The results are shown in the next section.

3.3 Simultaneous visualization results

Figure 3-5a-c shows the simultaneous visualization results under different experimental conditions. Each figure contains three rows of images representing three types of coils, and each row of images includes two kinds of photographs. The top one is the CO radiation images taken by the high-speed infrared camera and the lower one is the direct photographs taken by the normal high-speed camera. The profile of the spark plug was drawn with a white line to show the location of the spark plug.

As shown in Figure 3-5a, high current coil B and high energy coil C have a higher luminance of the discharge channel during the ignition process. Furthermore, after 1.5ms, the initial flame propagates farther than the standard coil A. However, all the coils are holding the initial flame around the spark plug at 2.5ms. It is found that all the coils can form an attached flame kernel after discharge duration under the basic condition. This means all the coils in this study can produce the self-sustained flame after the discharge process so that the flame grows and propagates rapidly. Therefore, the combustion can complete with a shorter duration and high stability.

Under the high diluted condition, according to Figure 3-5b, the initial flame of high current coil

B is detached from the spark plug at 2.5ms, while the standard coil A and high energy coil C can hold the flame attached. Comparing standard coil A with high current coil B, the initial flame of coil B propagates farther than coil A at 1.5ms due to the higher current. However, the propagation distances of the initial flame front are almost the same after 2.0ms, and the rear of the flame moved downstream. Hence, it is more difficult to form the self-sustained flame for coil B under low flow and high diluted conditions, which results in a lower ignition probability and lower combustion stability. On the other hand, from the CO radiation images, the initial flame of high diluted condition develops slower than the basic condition. Even in the high energy coil C, comparing the images of the basic condition and high diluted condition at 2ms, the initial flame of the high diluted condition is smaller than that of the basic condition. This may cause the result that increasing the mixture dilution ratio will decrease the combustion speed even increasing the ignition energy cannot reach the combustion speed of low diluted condition. The reason can be explained that increasing the dilution ratio only has the influence on decreasing the speed of flame kernel formation and flame propagation, shortening the discharge duration results in the initial flame kernel being detached from the spark plug, which contributed to lowering the combustion stability. Due to the little effect on the discharge channel behaviors, the initial flame kernel was smaller than that in the low dilution ratio condition even using the high ignition energy coil C.

When under the high flow condition, comparing the direct photographs at 0.5ms of coil C in Figure 3-5a and Figure 3-5c, it should be noticed that the discharge channel length of the high flow condition is longer than that of the basic condition. That is to say, the discharge channel stretches faster when enhancing the flow velocity. Due to the initial flame being formed along with the discharge channel, a longer discharge channel length results in the initial flame propagating farther. As shown in Figure 3-5c, all the initial flames detach and move downstream at 2.5ms for all the coils, which prevented the initial flame from forming the self-sustained flame. Nevertheless, high current coil B and high energy coil C have a larger flame area at 1.5ms than that of the standard coil A which indicates that high current could ensure the initial flame generates under such enhanced flow conditions. While standard coil A with a lower discharge current results in a smaller initial flame kernel that is even disappeared after the discharge process. On the other hand, the high flow velocity not only lengthens the discharge channel length but also wrinkles the initial flame. As shown in Figure 3-5c of coil A, the luminance of the initial flame is lower than the basic condition (Figure 3-5a). Furthermore, according to Figure 3-5c of coil B, the initial flame starts to detach the spark plug at 1.8ms which is earlier than the high diluted condition (Figure 3-5b). However, the high energy coil C maintains the initial flame

growth well for the higher luminance of the initial flame and holds the initial flame around the spark plug more time compared with low ignition energy coils. Thus, it can be considered that increasing the flow velocity may improve the combustion speed only if increasing the ignition energy correspondingly because the flow intensity has both influence on the discharge channel stretching and flame kernel formation.

The quality of initial flame generation affects the combustion directly, and quantitative analysis of the initial flame helps support the explanation of the combustion results. Therefore, the value of the flame area and the mean luminance are measured to estimate the growth of the initial flame, and the results are shown in the next section.

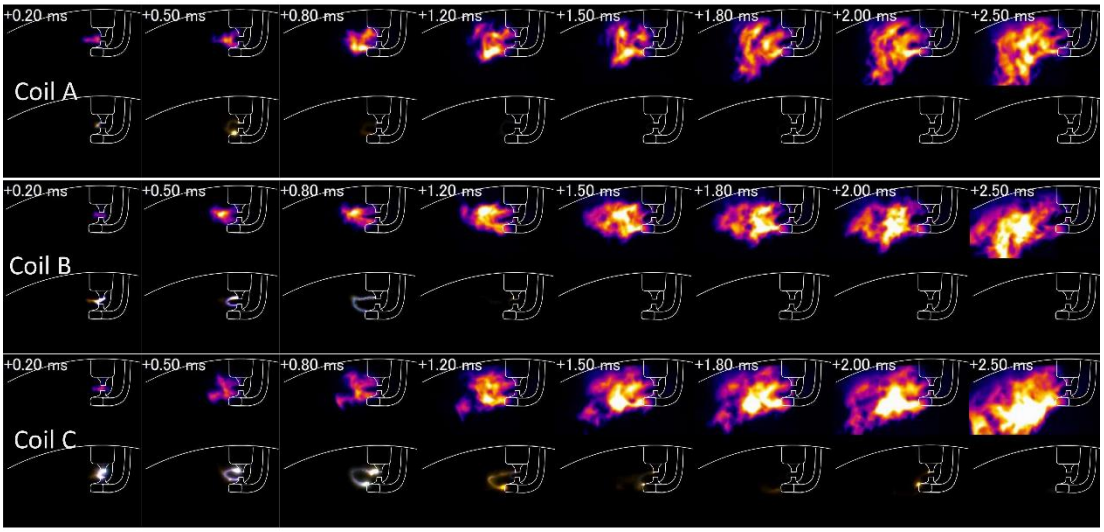

a. Basic condition

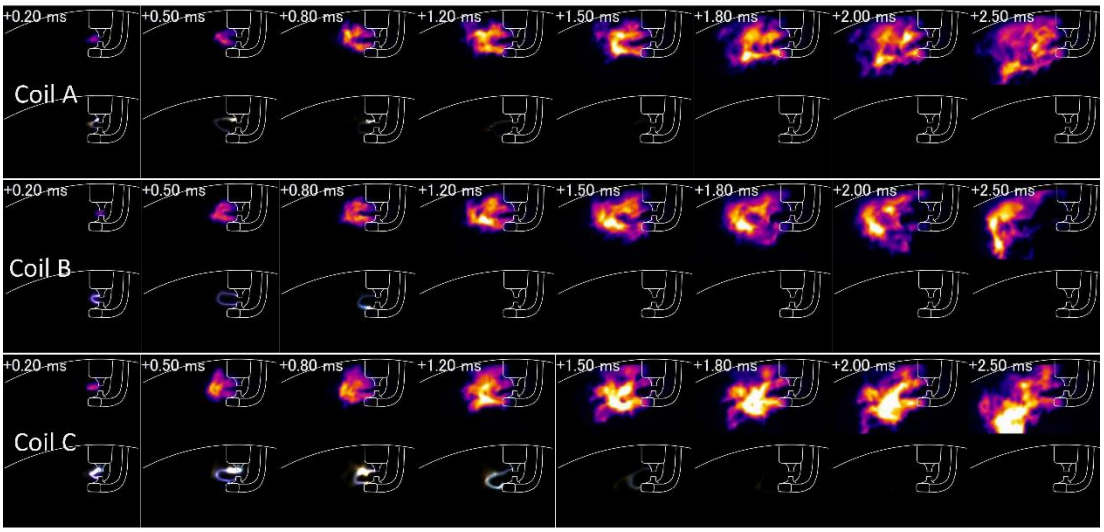

b. High diluted condition

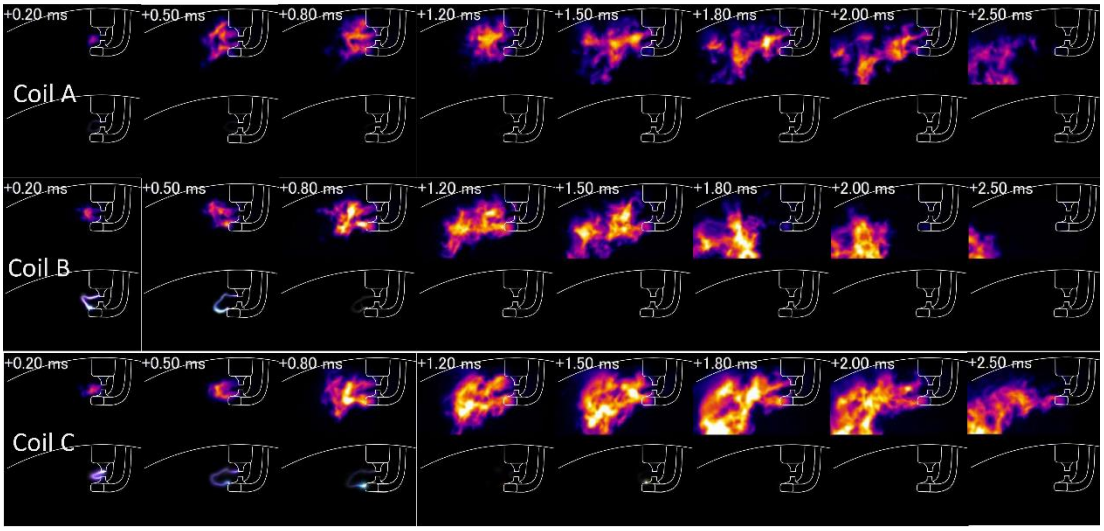

c. High flow condition

Figure 3-5 Simultaneous visualization results of different ignition coils (upper: CO radiation images / lower: direct photographs. Basic condition with the N_2 dilution of 24% and flow velocity of 8m/s, high diluted condition with the N_2 dilution of 28% and flow velocity of 8m/s, and high flow condition with the N_2 dilution of 24% and flow velocity of 18m/s.)

3.4 Quantitative analysis of the flame area and luminance

In order to get a deeper understanding of the initial flame kernel, the initial flame area and initial

flame luminance were quantitatively measured for all experimental cases. The initial flame area was calculated via CO radiation image binarization. As shown in Figure 3-6, firstly, a threshold value was set, then the raw infrared image was binarized and the flame contour could be determined. And the projected initial flame area was achieved by measuring the pixel of the binary image. The average value of the flame area and error bar for all the cases are shown in Figure 3-7a-Figure 3-9a under different conditions. The mean luminance of the initial flame was calculated by the integral luminance value divided by the flame area value, and the results are shown in Figure 3-7b-Figure 3-9b. The blue line stands for the standard coil A, the orange line represents the high current coil B, and the gray line represents the high energy coil C. Both flame area and flame luminance help to evaluate the initial flame generation and reaction intensity.

In order to get a deeper understanding of the initial flame kernel, the initial flame area and initial flame luminance were quantitatively measured for all experimental cases. The initial flame area was calculated via CO radiation image binarization. As shown in Figure 3-6, firstly, a threshold value was set, then the raw infrared image was binarized and the flame contour could be determined. And the projected initial flame area was achieved by measuring the pixel of the binary image. The average value of the flame area and error bar for all the cases are shown in Figure 3-7a-Figure 3-9a under different conditions. The mean luminance of the initial flame was calculated by the integral luminance value divided by the flame area value, and the results are shown in Figure 3-7b-Figure 3-9b. The blue line stands for the standard coil A, the orange line represents the high current coil B, and the gray line represents the high energy coil C. Both flame area and flame luminance help to evaluate the initial flame generation and reaction intensity.

a. Raw infrared image b. Binary image

Figure 3-6 procedure for determining the initial flame area

According to Figure 3-7 of basic condition, high current coil B and high energy coil C generate almost the same flame area because of the same discharge current until 1.5ms. The speed of initial flame growth of high current coil B decrease after 1.5ms, while high energy coil C keeps the high speed until 2ms. Standard coil A has the lowest initial flame growth speed and results in a smaller initial flame size. However, it can keep the growth speed and gets the nearly initial flame size at 2ms compared with coil B. It can be explained that although higher discharge current results in a larger initial flame, the initial flame growth slowed down after the end of the discharge of coil B (discharge duration: 1.3ms). Coil A and coil C keep the speed of initial flame growth because the discharge continues until 2ms. Initial flame luminance indicates the above results more clearly. As shown in Figure 3-7b, the mean luminance of the initial flame for high current coil B decreases immediately after the end of discharge duration at 1.3ms, while coil A and coil C keep increasing until 2ms.

Under the high diluted condition in Figure 3-7, initial flame area growth is slower than in the basic condition. Also, high current coil B firstly has a faster speed of initial flame growth than that of the standard coil A. After the end of the discharge duration of coil B (1.3ms), the growth speed decreases. However, the flame area of coil B is reduced to less than coil A until 2ms under such high diluted conditions. The flame luminance of coil C has the same trend as that of coil B and is less than coil A at 2ms. Therefore, coil B, with the shorter discharge duration, gets the worst ignition performance under such conditions.

As the image results are shown under the high flow condition, the initial flame has out of the view scope after 1ms, so we investigate the flame area and flame luminance before 1ms under such conditions. The results show the initial flame area keeps increasing rapidly until 1ms for all the coils in Figure 3-9, but standard coil A with a lower discharge current has the smallest flame area. Furthermore, the mean luminance of initial flame for standard coil A starts to decrease after 0.5ms, which can infer that the enhanced flow increased the speed of initial flame growth, but this also increased heat transfer between the initial flame kernel and unburned gas. The initial flame kernel generated by the low discharge current will disperse or even be eliminated. Thus, the flame luminance starts to decrease after 0.5ms. So that, coil A with the lower discharge current gets the worst ignition performance under such conditions.

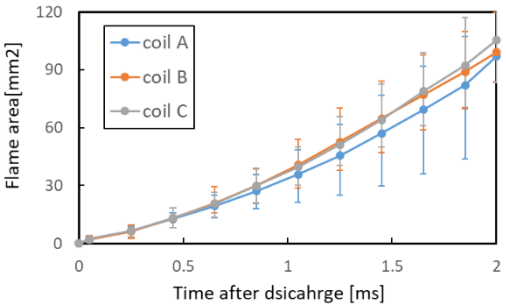

a. Initial flame area

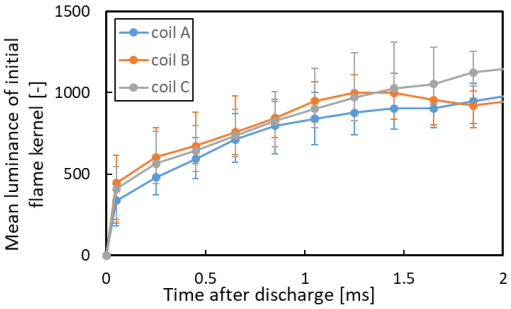

b. Initial flame luminance

Figure 3-7 Basic condition

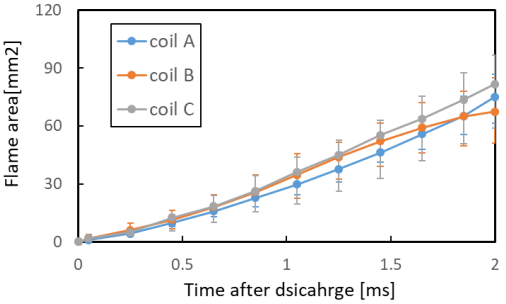

a. Initial flame area

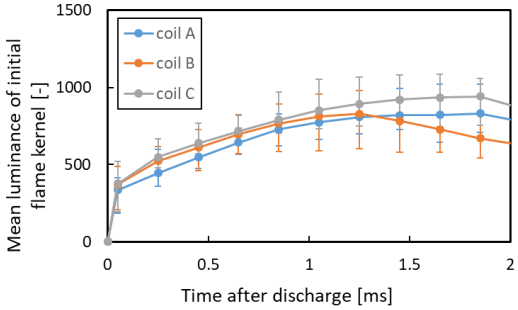

b. Initial flame luminance

Figure 3-8 High diluted condition

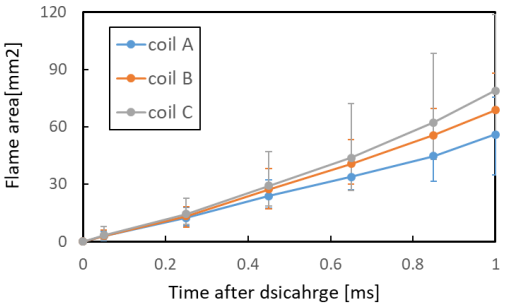

a. Initial flame area

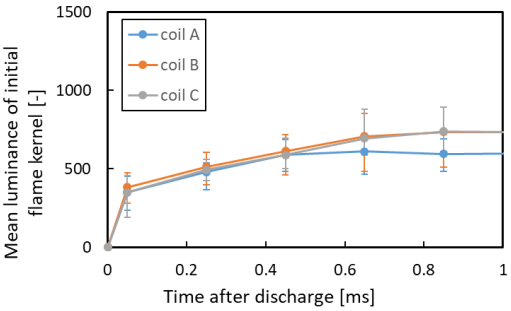

b. Initial flame luminance

Figure 3-9 High flow condition

3.5 Summary

In this chapter, the ignition performance under different experimental conditions has been further analyzed by using different discharge characteristics. The key features identified are summarized below:

1. Under the high diluted and low flow conditions, prolonging the discharge duration has more benefits to improve the ignition performance compared with the high discharge current at the same ignition energy. Because the long discharge duration extends the heating time to the gas mixture, which can keep the initial flame growth speed and form the self-sustained flame by holding the initial flame around the spark plug.

2. When comparing the same ignition energy coils under the enhanced flow condition, discharge current has a significant impact on the ignition performance compared with the discharge duration. The reason can be explained that enhanced flow stretches and wrinkles the initial flame kernel, and may prevent the initial flame from forming the self-sustain flame, the initial flame generated by the low discharge current may easily be quenched under the enhanced flow condition, and high discharge current ensures the initial flame generation and propagation.

Chapter 4 Engine confirmed experiments

4.1 Single cylinder engine

In this study, the engine test is carried out on a single cylinder from the JUKE four-stroke SI gasoline engine, as shown in Figure 4-1 of the intake view and Figure 4-2 of the exhaust view, the intake and exhaust manifold of the engine had been reformed for using the 1st cylinder, during the experiment, only 1st cylinder can be ignited, while for the other three cylinders the fuel injection and ignition are stopped.

The specifications of the engine were given in Table 2-1. The displacement of this engine is 404 cm3, and the compression ratio is 14.1, The bore is 80 mm, the stroke is 81 mm, and the combustion chamber shape is a pent-roof type. The opening and closing times of the engine intake and exhaust valves are controlled by a hydraulic variable valve timing actuator that is controlled by an electronic control unit (ECU), the maximum valve lift is 8.89mm for the intake valve and 8.66mm for the exhaust valve. The fuel injection method is the port injection, a rotary supercharge and a water-cooled intercooler are installed in the intake path, and the supercharge can control the intake pressure by changing the rotation speed. The water-cooled intercooler is also used to control the intake air temperature by changing the water flow rate.

The measuring equipment is described in Figure 4-3. A crank angle detector (Onosokki: CP-7520A) was used to measure the crank angle, and adjust the TDC signal to match the TDC of the piston behavior. A piezoresistive pressure sensor (Kistler: 6041B) was installed around the spark plug to measure in-cylinder pressure. Another two pressure sensors (Kistler: 4049A5SP22) were installed at the inlet of the intake port and the outlet of the exhaust port respective, and the pressure was measured at every 0.1-degree crank angle, the pressure data were recorded by a high-speed data logger (Kistler: KiBox To Go Type 2893). Regarding the temperature related to engine performance, intake air temperature, exhaust temperature, cooling water inlet temperature, cooling water outlet temperature, and oil temperature, were also measured.

In this system, the exhaust gas temperature was reduced to 65°C after through the EGR cooler, and then inducted into the intake mixed with fresh air, the EGR valve was used to control the EGR rate. In order to keep the temperature of the intake air, a part of mixed air was increased the temperature by

the air heater, the throttle control the mixture gas flow, and eventually, the temperature sensor installed at the intake port ensure the temperature of the intake air to 34°C(±0.5°C). The mechanical supercharging was installed to increase the intake airflow and adjust the inlet pressure. The radiator for cooling water was used to constant the cylinder wall at 80°C(±0.5°C). A gas measuring device （MEXA-7100D HORIBA） was used to measure carbon dioxide(CO_2), carbon monoxide(CO), oxygen(O_2), total hydrocarbons(THC), nitric oxide, and nitrogen oxide(NO_X) at both intake and exhaust. The EGR rate was calculated as the ratio between the CO_2 level in the intake and the CO_2 in the exhaust.

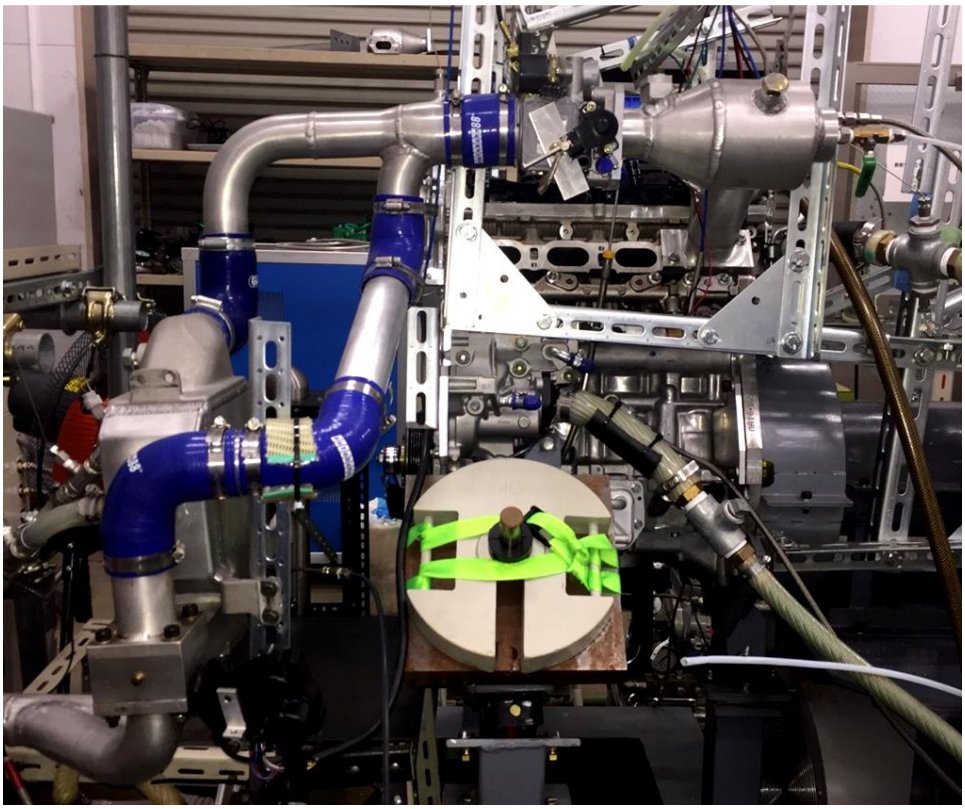

Figure 4-1 Intake side of the engine

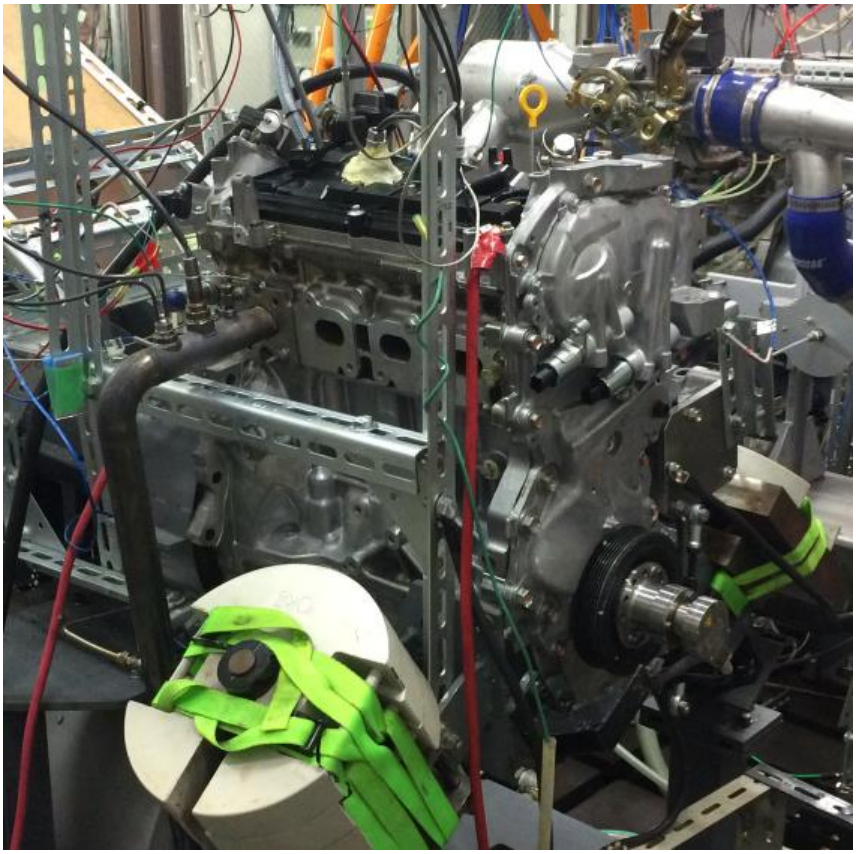

Figure 4-2 Exhaust side of the engine

Table 4-1 Specification of the test engine

Engine Type	4-stroke gasoline engine	
Bore × Stroke	Φ80mm × 81mm	
Displacement	404 cm^3	
Fuel supply System	Port injection	
Compression Ratio	14.1	
Valve Timing(1mm lift)	Intake	11°ATDC
		59°ABDC
	Exhaust	136°ATDC
		4°BTDC
Max Valve Lift	Intake	8.89 mm
	Exhaust	8.66 mm

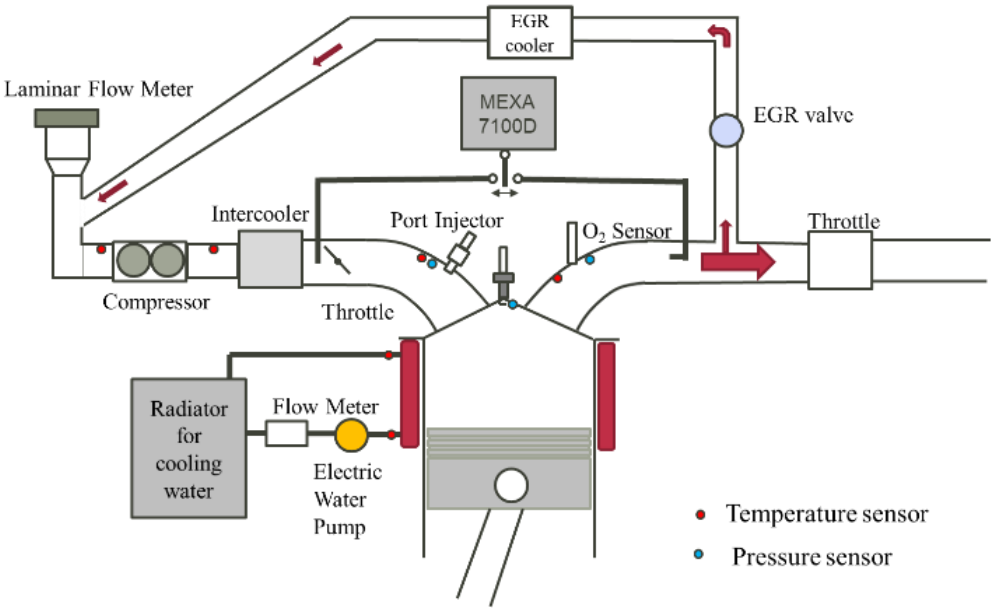

Figure 4-3 Schematic of the measuring equipment for the engine

4.2 High tumble nozzle for improving the flow field

It has been demonstrated in chapter 4, the discharge current has a significant impact on the ignition performance compared with the discharge duration when under high flow conditions. while prolonging the discharge duration has more benefits to improve the ignition performance compared with the high discharge current when under high diluted and low flow conditions.

Figure 4-4 high tumble generation nozzle

In order to confirm the results of CVCC, the experiment has been carried out in a 4-stroke gasoline engine. As shown in Figure 4-4, in order to set up the different flow fields in the engine cylinder, the high tumble nozzle was designed to enhance the flow intensity. Before the engine test, the simulation has been conducted by using the CONVERGE software, Figure 4-5 shows the model of the engine, the nozzle was installed at the intake port, the airflow from the intake manifold can be enhanced, and we set the point around the spark plug for calculating the flow velocity and TKE (turbulence kinetic energy) of the flow. The numerical simulation has been carried out to recognize the flow field both with and without the high tumble nozzle. The results have been shown in Figure 4-6, the left figure is the comparison of flow velocity, and the right figure is the comparison of TKE, in each figure, the orange line stands for the results with the high tumble nozzle, while the blue line is the results without the tumble nozzle. It can be found that the flow velocity with the high tumble nozzle is significate higher than that without the nozzle. Moreover, the turbulence kinetic energy of the high tumble nozzle is almost five times higher than that without the nozzle.

The numerical simulation has demonstrated that the high tumble nozzle can improve the strength of the flow field around the spark plug remarkably.

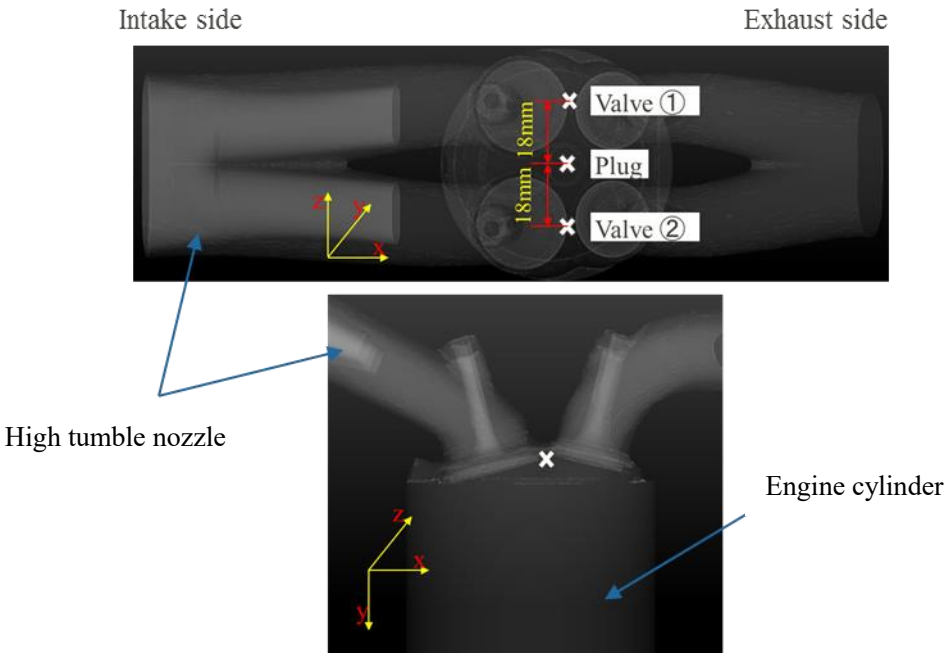

Figure 4-5 The model of numerical simulation

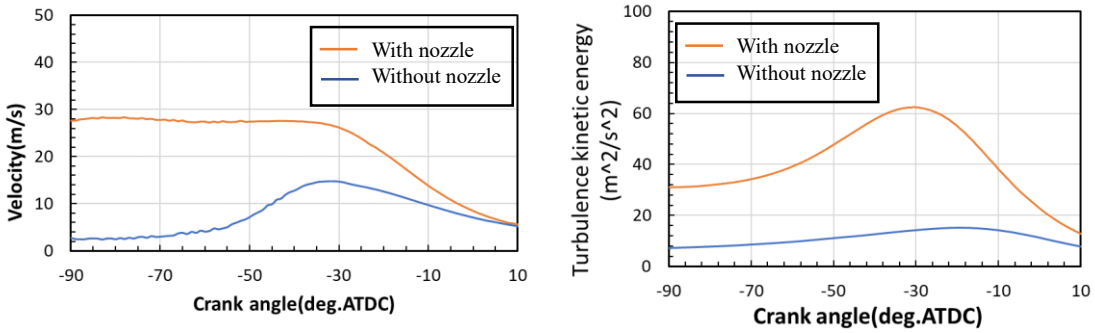

a. Comparison of flow velocity b. Comparison of TKE

Figure 4-6 The numerical simulation results around the spark plug

4.3 EGR experimental conditions

The engine test is intended to confirm the ignition performance of three kinds of discharge strategies in the engine operation, hence, several engine parameters need to be controlled, as shown in Table 5-1 of engine test conditions, the engine speed is constant at 2000 rpm, and the intake temperature is controlled at 34°C. To suppress variation in mixture formation in the cylinder, fuel is supplied using a port-injection system at a flow rate of 0.26 g/s, and the air flow rate is controlled to obtain the stoichiometric air-fuel ratio. The fuel is high-octane gasoline with an octane number of 99.8. The H/C ratio of the fuel is 1.708, and the stoichiometric air-fuel ratio is 14.37. The EGR rate is set from 0% to the EGR limit, the spark timing is changed every two degrees interval from the ignition limit to the combustion limit under each EGR rate condition. The COV of IMEP is used to estimate the engine operation, due to the misfire and partial burning, the combustion is considered unstable and the engine cannot be operating when the COV is excess to 3%. Ignition limit means that the ignition advance degree increased enough to make the knock occur in the cylinder, which also leads to the engine cannot be operated.

The high tumble flow field around the spark plug has been created by using the high tumble nozzle, therefore, the comparison between the high tumble flow and low tumble flow can be confirmed in the engine experimental conditions.

Table 4-2. Summary of experimental conditions of engine test

Engine speed	2000 rpm
Intake temperature	34 °C(±0.5°C)
Coolant temperature	86°C
IMEP	600 kPa
Air-fuel ratio	14.37
EGR rate	0% ~ limit
Spark timing	Ignition limit ~ combustion limit

4.4 The results under different EGR rates

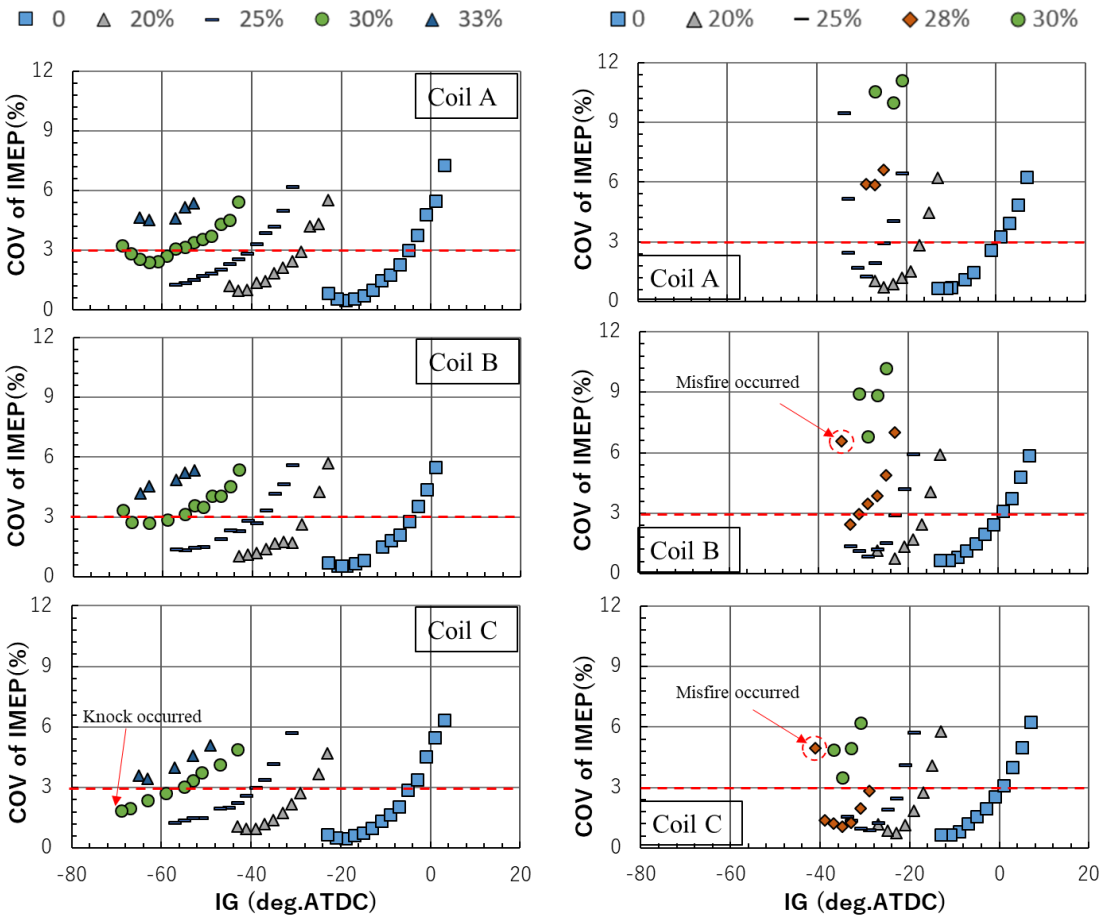

a. Without the high tumble nozzle b. With the high tumble nozzle

Figure 4-7 Engine experimental results on COV of IMEP under different EGR rates

The engine test is carried out on a four-stroke SI gasoline engine to confirm the results in the

constant volume combustion chamber. In this experiment, EGR technology was used in the engine test to evaluate the effect of discharge strategies on combustion performance under engine-like conditions. As depicted in Figure 4-7, all the record data on COV of IMEP were shown with different ignition timing under each EGR rate, the left figure of Figure 4-7a is the results without the high tumble nozzle and Figure 4-7b is the results with the high tumble nozzle. In order to obtain the EGR limit more accurate, EGR rates setup were at different values for the two kinds of flow conditions after the 25% EGR rate, low flow condition (without the high tumble nozzle) was set up at 30%, and 33%, while high flow condition (with the high tumble nozzle) was set up at 28% and 30%. Due to the COV of IMEP can indicate the cycle-to-cycle variations in the in-cylinder combustion, we defined 3% COV of IMEP as the operating limit of the engine condition for investigating the EGR limit.

From Figure 4-7a, when under the low flow condition. There is not much difference in COV of IMEP for three kinds of coils before the EGR rate at 25%, and when investigating the COV of IMEP from the EGR rate of 0% to 25%, it can be found that the COV of IMEP decreased when advancing the ignition timing and the ignition timing cannot be further advanced by the reason of knocking. When increasing the EGR rate to 30%, the difference between three kinds of coils has occurred when comparing the most advanced ignition timing, the COV of IMEP of high energy coil C is under 3% and the ignition timing cannot be further advanced because of the knock occurred. While coil A and coil B exceeded 3% due to the unstable combustion.

From Figure 4-7b, when under the high flow condition. It can be noted that the ignition timing is later than the low flow condition. Misfire occurred and damaged the combustion stability significantly for coil B and coil C at the EGR rate of 28%, however, coil A cannot be operated at the EGR rate of 28%, because the COV of IMEP exceeded 3% for all the ignition timing. This means that the EGR rate of 28% is around the EGR limit for coil B and coil C under such flow conditions, and exceeded the EGR limit for coil A. The reason has been illustrated in the CVCC results, on the one hand, the higher flow increases the speed of the flame generation and propagation, thus, the ignition timing needs to be put off for avoiding the knock. On the other hand, the higher flow wrinkles the flame and extinguishes the initial flame, therefore, the misfire occurred and damaged the combustion stability significantly.

In addition, according to Figure 4-8 of the ignition delay, the results also confirmed that the enhanced flow increases the combustion speed, because the duration of the ignition delay under the high flow condition is much shorter than in the low flow condition.

Therefore, as discussed above, it can be noted that increasing the EGR rate needs to advance the

ignition timing for obtaining the lowest cycle-to-cycle variations, knocking is the obstacle to advancing the ignition timing further when under the low EGR rate conditions; when increasing the EGR rate to the EGR limit, misfire becoming the obstacle to enlarge the ignition advanced timing.

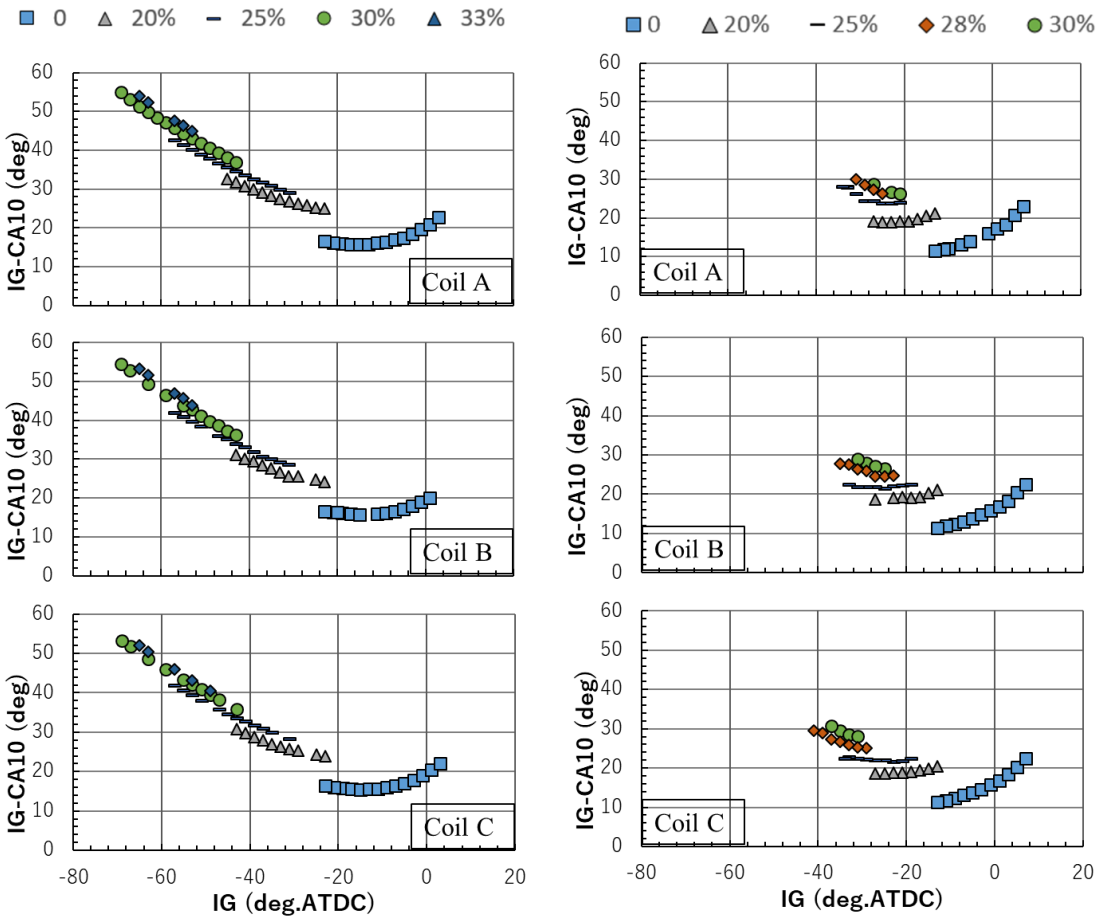

a. Without the high tumble nozzle b. With the high tumble nozzle

Figure 4-8 Engine experimental results on ignition delay under different EGR rates

Figure 4-9 shows the operating range of ignition timing under different EGR rates, as mentioned above, we defined 3% COV of IMEP as the operating limit of the engine condition, and the two operation limits of ignition limit and the combustion limit are determined by varying ignition timing [1]. When advancing the ignition timing, knocking occurred under low EGR rates or misfire occurred under high EGR rates, leading to ignition limit. In contrast, retarding the ignition timing, the flame propagation rate becomes late for the piston speed, leading to incomplete combustion. In general, the

ignition limit induces knockings or misfires, while the combustion limit does increase cycle-to-cycle variations. the EGR limit was determined at the point where the two limits cross each other. As shown in Figure 4-9, both ignition limit and combustion limit of three kinds of coils are almost the same until the EGR rate of 20%, when the EGR rate exceeds 20%, the high energy coil C enlarges the operating range for not only increasing the ignition limit but also increasing the combustion limit, especially around the EGR limit. It can be explained that when under the low EGR dilute conditions, the flame grows relatively fast, so that ignition performance has little influence on the engine combustion performance, thus, these three kinds of ignition coils have no difference on the engine performance. Nevertheless, when under the high EGR dilute conditions, the low combustion temperature slows down the speed of flame growth and development, and the initial flame has a great impact on the flame propagation, as the results have been shown in the CVCC, the coil C results in a bigger initial flame area which is benefits for flame growth and development, thus, coil C has a large operating range than the coil A and coil B by decreasing the cycle-to-cycle variations under the high EGR dilute conditions.

Besides, according to Figure 4-10, the minimum COV of IMEP under different EGR rates has been shown. It revealed the EGR limit for these three kinds of ignition coils, the high energy coil C has the highest EGR limit than coil A and coil B for all the flow conditions. When under the low flow conditions, the difference in EGR limit between coil A and coil B is small, and the minimum COV of IMEP of coil B has slightly higher than that of coil A. However, when under the high flow condition, the EGR limit of coil B is higher than coil A, which has confirmed the results that a high discharge current has more benefits to improve the ignition performance under the enhanced flow conditions.

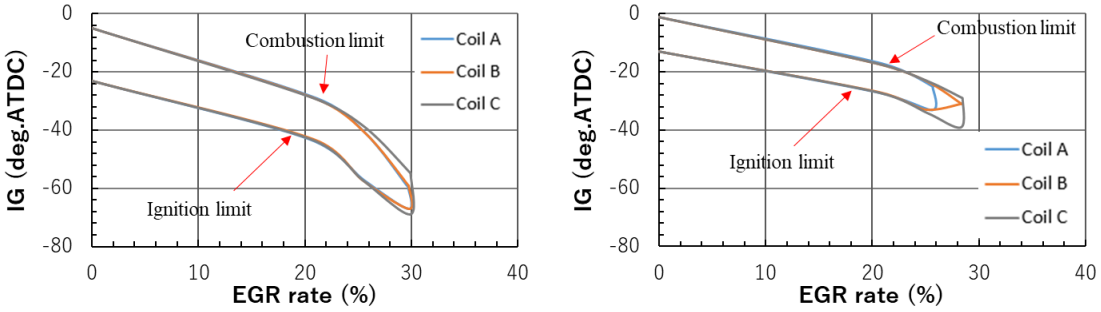

a. Without the high tumble nozzle b. With the high tumble nozzle

Figure 4-9 Operating range of ignition timing under different EGR rates

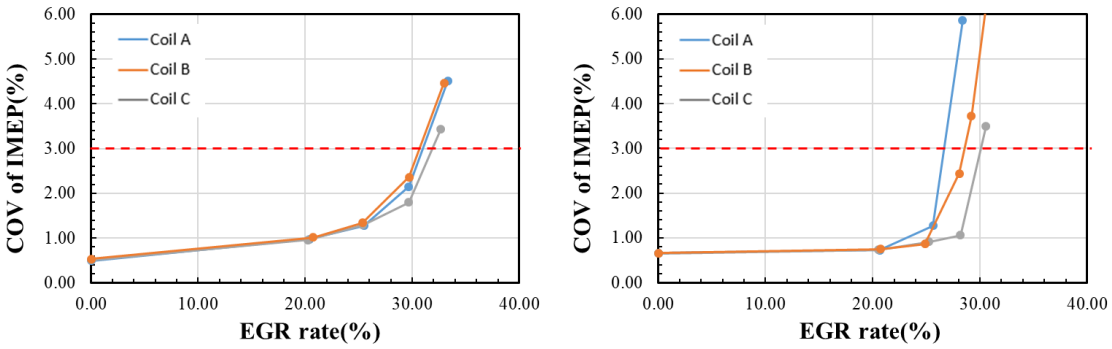

a. Without the high tumble nozzle b. With the high tumble nozzle

Figure 4-10 The minimum COV of IMEP under different EGR rates

4.5 The results around the EGR limit

Figure 4-11 to Figure 4-13 investigated the engine performance around the EGR limit for all the coils under the same ignition timing, we choose the MBT (minimum advance for best torque) of coil B for comparison, the ignition timing is -63 deg ATDC (after the top dead center) of EGR 30% for the low flow condition, and -31 deg ATDC of EGR 28% for the high flow condition.

Figure 4-11 illustrated the in-cylinder pressure of two kinds of flow conditions to depict the overall combustion, the in-cylinder pressure results were averaged from 500 consecutive cycles. As can be observed that coil C has the highest peak in-cylinder pressure for all the flow conditions. Furthermore, the apparent rate of heat release also demonstrated this trend as shown in Figure 4-12, coil C has the fastest heat release rate of maximum 15 J/deg under low flow conditions, and about 17 J/deg under high flow conditions.

When focusing on the same ignition energy coil A and coil B, there is not much difference in the in-cylinder pressure and heat release rate under the low flow conditions, however, according to the Figure 4-13 of all the record cycles of IMEP, the orange points represent the coil B has more cycles lower the 580Kpa, which result in a higher cycle-to-cycle variation and the combustion are more unstable.

When focusing on the same ignition energy coil A and coil B under the high flow condition, coil B with the higher discharge current results in a higher peak in-cylinder pressure, moreover, the heat release rate is also faster and higher than coil A.

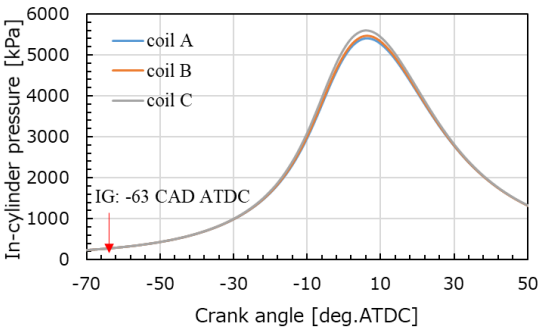

a. Without the high tumble nozzle (low flow condition, EGR rate of 30%)

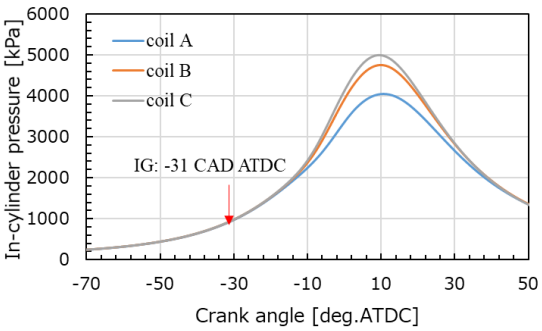

b. With the high tumble nozzle (high flow condition, EGR rate of 28%)

Figure 4-11 The in-cylinder pressure around the EGR limit

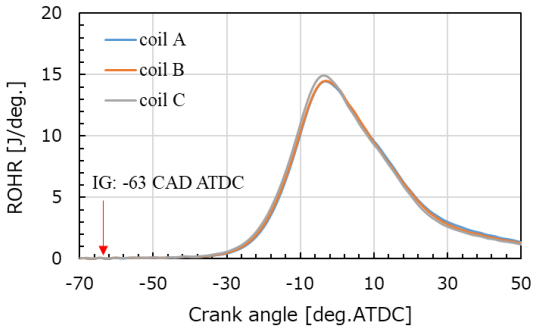

a. Without the high tumble nozzle (low flow condition, EGR rate of 30%)

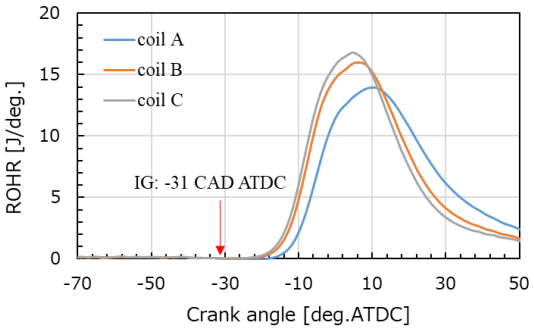

b. With the high tumble nozzle (high flow condition, EGR rate of 28%)

Figure 4-12 The apparent rate of heat release around the EGR limit

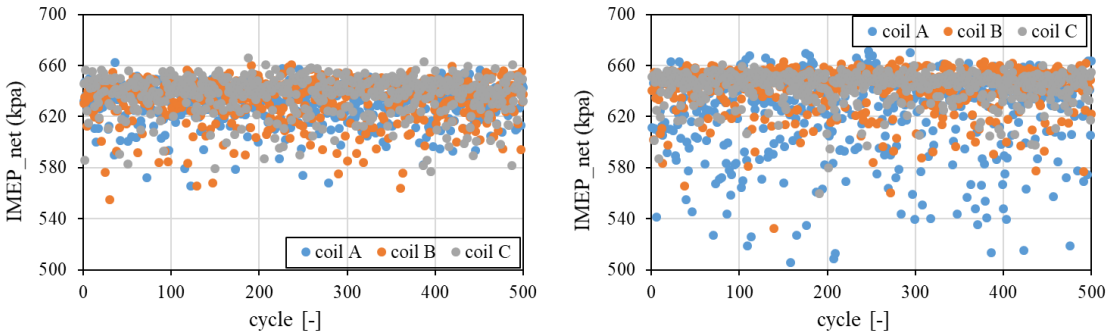

a. Without the high tumble nozzle (low flow condition, EGR rate of 30%)

b. With the high tumble nozzle (high flow condition, EGR rate of 28%)

Figure 4-13 The IMEP of all the 500 record cycles around the EGR limit

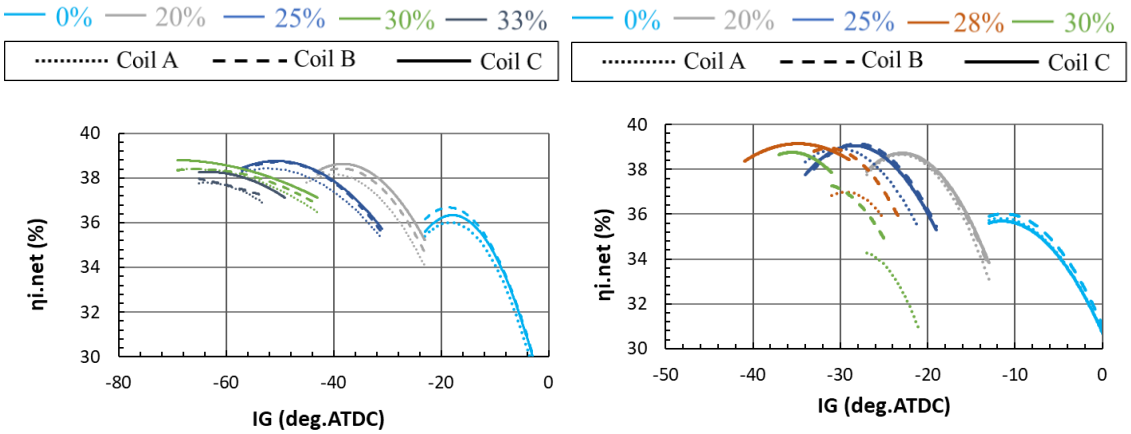

a. Without the high tumble nozzle (low flow condition)

b. With the high tumble nozzle (high flow condition)

Figure 4-14 The thermal efficiency of different EGR rates

Figure 4-14 shows the thermal efficiency under the different EGR rates for those three kinds of ignition coils, different colors stand for the different EGR rates, and different kinds of lines stand for the different ignition coils. it can be found in Figure 4-14, that the highest thermal efficiency occurred at the EGR rate of 30% under the low flow condition, while when under the high flow condition, the highest thermal efficiency occurred at the EGR rate of 28%. It has been demonstrated that the highest thermal efficiency has occurred at the EGR limit. Due to the shorter ignition delay under the high flow condition, the enhanced flow has increased the combustion speed. Thus, coil C with the higher ignition

energy coil has increased the thermal efficiency by around 0.53% when under the high flow condition.

The results confirm that high energy coil C has a better ignition performance for reducing the cycle-to-cycle variations and increasing the in-cylinder pressure and accelerating the heat release under both low and high flow conditions, which has been demonstrated by many researchers [2-5]. Besides, when focusing on the same ignition energy, prolonging the discharge duration has more benefits to improve the engine performance under low flow conditions, because coil A has a lower COV of IMEP and fewer cycles lower the 580Kpa at 30% EGR rate of low flow conditions. By contrast, due to the higher in-cylinder pressure and faster heat release rate of coil B under the high flow conditions, the discharge current plays a more vital role in perfecting the engine performance than the discharge duration.

4.6 Summary

In this chapter, the engine experiment results of three kinds of ignition coils under the two kinds of flow conditions have been analyzed in detail. It has confirmed the results of the CVCC under the real engine conditions, the key features identified are summarized below:

1. Increasing the EGR rate needs to advance the ignition timing for obtaining the lowest cycle-to-cycle variations, knocking is the obstacle to advancing the ignition timing further when under the low EGR rate conditions; when increasing the EGR rate to the EGR limit, misfire becomes the obstacle to enlarging the ignition advanced timing.

2. When focusing on the same ignition energy, prolonging the discharge duration has more benefits to improve the engine performance under low flow conditions, while the discharge current plays a more vital role in perfecting the engine performance than the discharge duration under the high flow condition.

Reference

1. Matsumoto, O. , Kuboyama, T. , Morisyoshi, Y. , Kinusawa, T. et al. A Novel Low Temperature Plasma Ignition System Applied to a GHP Engine. SIA Powertrain 2017.
2. Ogata, K., Kataoka, T., Suzuki, T., Kuboyama, T., Moriyoshi, Y. A high energy ignition system for egr combustion engine (second report). Transactions of Society of Automotive Engineers of Japan, 47(5), 2016.
3. Ogata, K., Kataoka, T., Suzuki, T. A high energy ignition system for egr combustion engine. Transactions of Society of Automotive Engineers of Japan, 47(2), 2016.
4. Jung, D., Sasaki, K., Sugata, K., Matsuda, M., Yokomori, T., Iida, N. Combined effects of spark discharge pattern and tumble level on cycle-to-cycle variations of combustion at lean limits of SI engine operation. SAE technical papers, 2017(March).
5. Jung, D., Sasaki, K., Iida, N. Effects of increased spark discharge energy and enhanced in-cylinder turbulence level on lean limits and cycle-to-cycle variations of combustion for SI engine operation. Applied energy, 205, 1467-1477. 2017.

Chapter 5 Conclusions and Recommendations for Future Works

5.1 Conclusions

In this study, the ignition performance has been studied in detail with different ignition strategies under different conditions, in order to get a deeper insight into the ignition process, a simultaneous visualization method by a high-speed infrared camera (FLIR X6900sc) and a conventional high-speed camera (FASTCAM SA-X) has been set up in CVCC experiment, the discharge channel behaviors and initial flame formation had been investigated fully, furthermore, the influencing factors of conditions, such as flow velocity, local temperature, pressure, and dilute ratio can be separated and controlled in the CVCC, thus, the suitable ignition strategy under different conditions can be studied quantitatively in the CVCC experiments.

In addition, the conditions of the CVCC experiments imitated the engine conditions, the results in CVCC need confirmed in the actual engine conditions, so that, the engine experiment for three kinds of ignition coils under the two kinds of flow conditions have been analyzed in a 4-storke engine. It has confirmed the results of the CVCC under real engine conditions.

The key conclusions identified are summarized in three parts.

1. Simultaneous visualization method

In order to improve the visualization method and get a deeper insight into the process of ignition, a new visualization method, using a high-speed infrared camera (FLIR X6900sc) and a conventional high-speed camera (FASTCAM SA-X) simultaneously, has been set up. Test results have confirmed that the high-speed infrared images can ignore the interference of the preheat zone caused by the discharge channel.

2. Experiment in the CVCC

The CVCC experiment has investigated the effect of discharge characteristics on the discharge channel behaviors during the ignition process. Discharge current is the dominant factor that influences the discharge channel behaviors as compared with the discharge duration. Increasing the discharge

current is seen to enlarge the discharge channel extension length and keep the discharge channel extending without shortening, which increases the contact area between the discharge channel and the mixture gas and improves the early flame development during the ignition process. Restrike and short-cut are the two kinds of discharge channel behaviors that occurred in the ignition period under weak flow conditions. Simultaneous visualization of the discharge channel and initial flame area shows clearly that these two kinds of discharge channel behaviors affect the flame kernel overlap. Short-cut has some benefits to the flame development and enlarges the early flame during the discharge duration compared to the restrike behavior. Furthermore, higher discharge current results in a higher possibility of short-cut shortening behavior after the end of 1st discharge.

In addition, the ignition performance with different coils was also investigated under different conditions. results revealed that increasing the mixture dilution ratio will decrease the speed of initial flame growth, which results in the decreasing of combustion speed even increasing the ignition energy cannot reach the combustion speed of low diluted condition. While increasing the flow velocity may improve the combustion speed only if increasing the ignition energy correspondingly. On the one hand, under the high diluted and low flow conditions, prolonging the discharge duration has more benefits to improving the ignition performance compared with the high discharge current at the same ignition energy. Because the long discharge duration extends the heating time to the gas mixture, which can keep the initial flame growth speed and form the self-sustained flame by holding the initial flame around the spark plug. On the other hand, when comparing the same ignition energy coils under the enhanced flow condition, the discharge current has a significant impact on the ignition performance compared with the discharge duration. The enhanced flow stretches and wrinkles the initial flame kernel, and may prevent the initial flame from forming the self-sustain flame. High discharge current ensures the initial flame generation and propagation.

3. Experiment with the 4-stroke engine

The engine experiment is aimed to confirm the results of CVCC in the actual engine conditions. After the engine experiment under the EGR experimental conditions, it can be found that the EGR rate needs to advance the ignition timing for obtaining the lowest cycle-to-cycle variations, knocking is the obstacle for advancing the ignition timing further when under the low EGR rate conditions; when increasing the EGR rate to the EGR limit, misfire becoming the obstacle to enlarge the ignition advanced timing.

When focusing on the same ignition energy, prolonging the discharge duration has more benefits to

improve the engine performance under low flow conditions, while the discharge current plays a more vital role in perfecting the engine performance than the discharge duration under the high flow condition.

5.2 Recommendations for Future Works

This study has proposed an appropriate method for investigating the ignition, that is by the simultaneous visualization in the CVCC firstly and verified in the engine test bench secondly. The conclusions in this research are based on three kinds of ignition coils, in the future, to further optimize and improve the performance of the ignition system, the more different types of ignition coils, such as two-strikes coil, constant current coil, and multiple discharge coil, are meaningful for further study. In addition, the lean combustion experimental conditions in the engine test are worth carrying out for a better understanding of the ignition performance, and a more detailed and comprehensive analysis is interesting and meaningful.

ACKNOWLEDGEMENT

First and foremost, I would like to sincerely express my deepest gratitude to my primary supervisor Associate Professor Kuboyama, who provided me with constant support and many previous opportunities during my Ph.D. In my study at Chiba University, I have obtained motivation and enthusiasm for engine research due to the key role of Kuboyama. I have also learned a lot from Associate Professor Kuboyama not only academically but also in everyday life.

In addition, similar gratitude is to my secondary supervisor Professor Moriyoshi, who taught me a lot and give me many opinions about my research. Associate Professor Kaneko, Dr. Hokimoto and Dr. Oryoji also taught me a lot and give me a lot of help in my everyday research project. They have a lot of practical experience to help me solve many questions and problems.

I would like to thank Specially Appointed Professor Chen, and Dr. Shen, who help me a lot and taught me a lot of engine research and everyday life experiences. Dr. Li, Dr student Zhong, Wang, and Master student Tan, Zeng also help me a lot during my Ph.D. I also want to thank my friends at Chiba University, Dr. Deng, Zhang, Yan, Zhou, and Wang. Thanks to their friendly help and company.

I would like to thank the Hitachi company and the JSPS KAKENHI Research project to support my research.

Finally, I want to thank my family. There is so much I want to say but so little that can be expressed. They support me all the way regardless of gains and losses. I am proud as a member of my family.

LIST OF RESEARCH WORKS

Published papers

1. Qingchu Chen, Tatsuya KUBOYAMA, Yasuo MORIYOSHI and Kazuhiro ORYOJI, Effect of discharge current and discharge duration on the discharge channel behavior and early flame formation. Mechanical Engineering Journal, Vol.9, No.3, 2022. [DOI: 10.1299/mej.21-00248]

2. Qingchu Chen, Tatsuya Kuboyama, Yasuo MORIYOSHI and Kazuhiro ORYOJI, Study of Discharge Characteristics on Ignition Performance via High-Speed Imaging in a CVCC. applied sciences 2022,12(7),3280. [DOI: doi.org/10.3390/app12073280]

Reference paper

1. Kazuhiro Oryoji, Yoshifumi Uchise, Yoshihiko Akagi, Chen Qingchu, Tatsuya Kuboyama, Yasuo Moriyoshi, In-Cylinder Optical Measurement for Analyzing Control Factor of Ignition Phenomena under Diluted Condition, SAE Technical Paper 2020-01-2048, September 2020. [DOI: doi.org/10.4271/2020-01-2048]

Conference and seminar presentations

1. Qingchu Chen, Tatsuya Kuboyama, Yasuo Moriyoshi, Osamu Matsumoto, Kazuhiro Oryoji. Investigating the impact of discharge characteristics on the discharge plasma behavior and early flame formation of dilute combustion. *31st Internal Combustion Engine Symposium* November 16-18, 2020.

2. Qingchu Chen, Tatsuya Kuboyama, Yasuo Moriyoshi, Osamu Matsumoto, Kazuhiro Oryoji. Effect of Discharge Characteristics on Ignition Performance with Diluted mixture under enhanced flow conditions. *2021 JSAE Annual Congress (Spring).* May 28, 2021.